POLITECNICO DI TORINO

International Business Machines corporation

Master's Degree in

NANOTECHNOLOGIES FOR ICTs

Politecnico di Torino

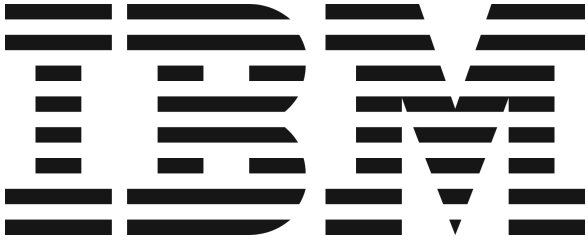

Master's Degree Thesis

Recycling and ring-opening polymerization optimization exploiting new catalysts systems for polyesters and polycarbonates

Supervisor:

Prof. Alessandro CHIADÒ

Co-supervisors:

Dr. James H. HEDRICK

Dr. Nathaniel H. PARK

Candidate:

Riccardo BOSIO

July 2024

A mia madre,

pilastro della mia vita,

che, stoica, ora lotta per la sua,

ch'io possa essere il pilastro che merita.

Abstract

Polymers play a crucial role in modern society, serving diverse applications from packaging and textiles to medical devices and automotive components. The development of biodegradable polymers like polylactide (PLA) and polycarbonates is noteworthy for their sustainable advantages over traditional plastics. These materials can biodegrade and depolymerize under specific conditions, reducing environmental impact and supporting the circular economy through improved recycling and waste management practices. PLA, known as a "bioshopper" material, derived from starch fermentation, is esteemed as one of the greenest polymeric materials. Polycarbonates and PLA are exploited in Theranostics and medical fields. PLA slow biodegradability and biocompatibility make it ideal for drug delivery systems and pharmacokinetic control applications, whereas polytrimethylene carbonate well known biocompatibility made it one of the most exploited polymers in tissue repairing and engineering fields. Understanding its quantitative structure-property relationships (QSPR) is crucial to allow sustainable materials to competitively perform against fossil-fuel-based plastics.

During my internship at IBM Research Almaden, I focused on synthesizing PLA and polycarbonates via ring-opening polymerization (ROP) of related 6-membered closed-ring monomers. This method can utilize organocatalysis, which is particularly appealing for medical applications due to the absence of inorganic contaminants in the final product. This thesis explores the synthesis of these materials using a new

class of organic catalysts known as cyclopropenimines (CPIs), in combination with established (thio)ureas. Additionally, the chlorine salts of cyclopropenium cations were investigated for their potential as phase-transfer catalysts. Comparative studies with well-known catalyst systems and flow chemistry conditions were also conducted. The thermal and recycling properties, as well as the degradation behavior of the polymers synthesized were then evaluated. A still ongoing project aims to find the QSPR of PLA synthesised in automated flow chemistry using a supervised machine learning model. My contribution involved the creation of a large dataset for the ML model, needed to ameliorate its predictive performances.

The ROP of lactides and carbonate monomers, facilitated by the CPI and (thio)urea catalyst system, led to high activity and living behavior with well-controlled dispersity. The correlation between CPI and (thio)urea pKa was found to significantly enhance synthesis performance. For PLA synthesis, the use of a solvent like dichloromethane, which promotes hydrogen bonding, was crucial. The stereo-selectivity of CPI was evidenced by improved thermal properties and wide-angle X-ray scattering (WAXS) analysis of the resulting stereo-block copolymer from racemic lactide mixture synthesis. These findings were recently published in the American Chemical Society's journal, MacroLetters. Attempts to use cyclopropenium cations chlorine salts as phase-transfer catalysts (PTCs) in ROP were unsuccessful, necessitating further investigation to understand the underlying failure mechanism. Thermal experiments and characterizations on the known and new materials investigated their degradation mechanisms, sometimes resulting in ring-closing depolymerization (RCDEP) with significant yields of pristine monomer. RCDEP occurred under non-ideal bulk conditions during isothermal heating without catalysis, confirming these materials' strong potential for chemical recycling.

Acknowledgements

I would like to express my gratitude to Dr. Nathaniel H. Park for providing invaluable knowledge and expertise throughout the experimental activities conducted at IBM Research-Almaden. I would like to extend my gratitude to James H. Hedrick, who, together with Dr. Park, provided invaluable guidance throughout these experimental activities. I am also indebted to the IBM personnel who assisted me during my internship, including Dr. Pedro Arrechea, Dr. Stefano Ambrogio, and numerous others.

I would like to express my gratitude with a special thanks to professor Alessandro Chiadò, who supervised the development of the thesis. I would like to express my gratitude to Politecnico di Torino, its professors, and fellowship students, as well as to all those I met during this experience.

Finally, I would like to thank my family, without whom this would not have been possible, and my closest friend, without whose support and companionship the days would have been less bright.

Table of Contents

List of Tables

List of Figures

Chapter 1

Introduction

1.1 Polymers importance and applications

In today modern society, polymeric materials represent one of the most versatile and common material class, whose application spans in a wide range of fields such as the production of everyday items, from packaging materials [1] to biomedical applications [1–6] such as medical tools or drug delivering [7, 8] and electronic components [1, 6]. The influence of polymers extends from macroscopic applications to nanoscale innovations [5], leading to advancements in drug delivery, tissue engineering [4], and nanotechnology [4, 5, 9].

This material class success is mainly due to the molecular structure of the polymers themselves, formed through means of bonded repeated monomer units, which can be easily engineered and modified in order to deliver unique properties with virtually infinite possible combinations. This design flexibility allowed for their assiduous exploitation, substituting traditional materials and revolutionizing the material science field.

In this context, exploring the importance of polymers extends beyond their purposes and practical applications. The ecological impact of these materials must be considered as well, as modern research seeks sustainable alternatives and biodegradable options. It is esteemed that a quantity exceeding 335 millions tonnes of plastics are produced worldwide annually, whereas in Europe the 26% of plastic waste is landfilled and only the 35% is recycled, with forecasts indicating growing production of plastics amounts in the following years [10]. It is therefore of extreme importance to seek for greener and more environmentally friendly solutions.

This master thesis will deal mainly with green polymers belonging to polyesters and polycarbonates classes. These are versatile classes of synthetic polymers under considerable attention across different industrial domains. The synthesis of these polymers involve different processes. To produce PLA through ring opening polymerization, its lactide monomer unit, is needed. Lactides are usually obtained by the cyclization of

two lactic acid molecules, obtainable from starch crop fermentation [11, 12]. Dicarboxylic acids or diols are required [13] to synthesise carbonate monomer units, whose carbon atoms can be easily substituted, resulting in distinctive chemical composition and an array of tailored properties [14]. Polyesters and polycarbonates studied in this thesis, will present a thermoplastic behaviour [15–17], rendering them amenable to molding and shaping processes. This inherent thermoplastic property, coupled with the diversity of available monomers, contributes to a spectrum of mechanical and thermal properties that can be finely tuned for specific applications.

A comprehensive examination of the synthesis pathways using ring-opening polymerization techniques and the selection of monomeric precursors provides insights into the relationships between structural features and properties in polyesters and polycarbonates. The combination of molecular architecture and processing conditions results in a wide range of properties, including mechanical strength, chemical resistance, and biodegradability. This highlights the inherent versatility of these polymers [4, 18–20].

1.2 Synthesis

1.2.1 Thermodynamics of ring-opening-polymerization

In this master's thesis project, one of our primary objectives was to discover novel intrinsically circular recyclable polymers and to investigate recycling properties of carbonate polymers. To achieve this goal, our approach started with the synthesis of these polymers themselves. The central focus of the thesis lies in investigating carbonate and lactide monomers in order to produce polymers with well defined features in a controlled manner. The chosen monomers possess qualities that make them suitable for ring-opening polymerization (ROP) through the nucleophilic attack of their carbonyl moieties [2, 3]. Figure 1.1 illustrates examples of anionic ROP schemes for the material classes discussed in this thesis. Reaction scheme **(a)** depicts the anionic ROP of polycarbonates, while reaction scheme **(b)** shows the anionic ROP of polyesters, specifically poly-L-lactide (PLLA). In both schemes, the carbonyl group of the carbonate and ester monomers, which undergoes nucleophilic attack to initiate the ring-opening reaction, is highlighted in red.

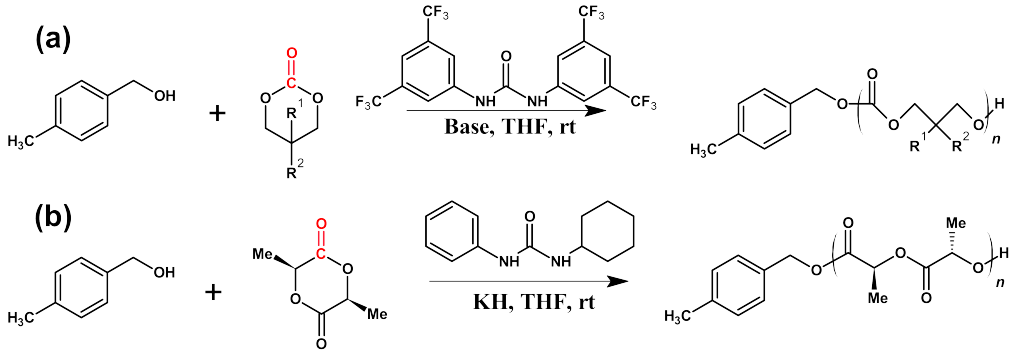

Figure 1.1: Anionic ROP reaction scheme of polycarbonates and PLLA, with alcol, urea and base catalysts system. [21]

To initiate the ROP process, two fundamental conditions must be satisfied: thermodynamic favourability and kinetic feasibility. This requires that the polymerization of

monomeric units is energetically favourable from a thermodynamic point of view, and concurrently that the kinetic pathway of the reaction leading to the final polymeric state, must be viable from an energetic and time point of view.

The reaction kinetic aspect of polymerization will be discussed in detail in the following sections, however, as a preliminary information, it should be kept into account that ROP proceeds by the opening of a cyclic monomer through an initiator compound which then propagates, meaning that other monomer units are added to the growing chain. The general kinetic steps of chain growth polymerization reaction are presented in Figure 1.2.

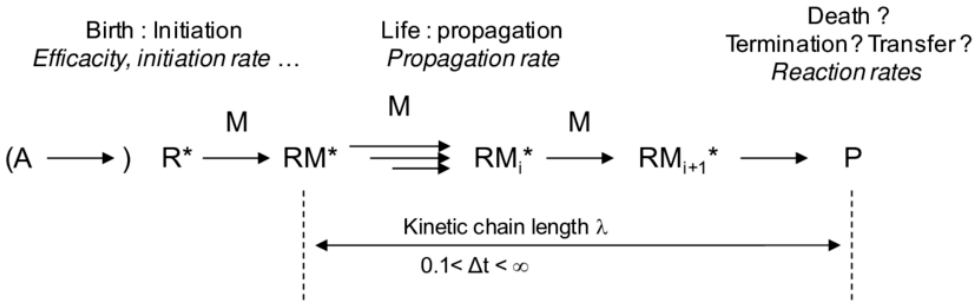

Figure 1.2: General chain growth reaction scheme. [22]

Focusing on the thermodynamics of ROP, the criterion of a given monomer polymerizability is related to its free Gibbs energy of polymerization:

$$\Delta G_p = \Delta H_p - T\Delta S_p \tag{1.1}$$

ΔG_p is the free Gibbs energy of polymerization, meanwhile ΔH_p and ΔS_p are the enthalpy and entropy of polymerization respectively [2, 3, 17, 23].

The ROP is possible only when $\Delta G_p < 0$, and this is dependent on many factors such as the Temperature, the solvent, the monomer-polymer phase, external factors such as pressure, and many others. The enthalpy of polymerization is strictly related to the cyclic monomer ring strain, such that high ring strain will result in high enthalpy values $|\Delta H_p|$. The entropy of polymerization is mainly due to the loss of

free translations degree as the macromolecule chain grows during the polymerization process [2, 10, 23–25].

It would be too naive to consider that the Gibbs energy for a certain polymerization process is independent of the macromolecule that is forming. Indeed, it could be described as a sum of standard Gibbs energy of polymerization plus a term due to both the monomer and both the growing polymer concentrations. This would imply a very complex model in which the Gibbs energy is a time-dependent function of the polymerization process. In particular, it should be taken into account the lowering of the monomer concentration, as well as the dispersity of the molecular weight of the macromolecules growing at a certain time, in the reaction mixture. The following would read, at a given time for a given macromolecule:

$$\Delta G_p = \Delta G_p^0 + RT \ln \frac{[... - m_{i+1}m^*]}{[M][... - m_i m^*]}. \tag{1.2}$$

[2, 23]

Where in the previous equation 1.2, the overall Gibbs polymerization energy is given by the standard term plus the second term containing the gas constant R and the concentration of the growing macromolecule with degree of polymerization $DP_i = i + 1$ divided the concentration of the macromolecule in the process initial state with $DP_i = i$ and the monomer concentration required to add a unit to the macromolecule. The m^* denotes the active end chain monomer unit of the polymer. Considering a sufficiently long macromolecule, the model can be simplified under Flory's assumption, stating that the reactivity of a macromolecule under a polymerization process is independent of its DP_i [2, 23]. Basically, it can be assumed that after a certain number of repeating monomer units of a polymer, the active end-chain monomer unit will be too far away to interact with sufficiently distant monomer units of the polymer, like a sort of near neighbourhood interaction approximation. [2] It is shown experimentally that this behaviour is generally present for polymer chains

of $DP_i \geq 20$. The previous equation 1.2 will therefore simplify:

$$\Delta G_p = \Delta H_p^0 - T(\Delta S_p^0 + R\ln[M]). \tag{1.3}$$

Where it is denoted with ΔH_p^0 and ΔS_p^0 the standard enthalpy and entropy polymerization parameter, respectively [2, 23, 26].

The previous discussion led to a Gibbs free energy of polymerization that is instantaneous and depends on the concentration of the monomer in the reaction mixture. It can be concluded that the polymerization reaction will terminate for thermodynamical reasons when the Gibbs free energy of polymerization reaches the $\Delta G_p = 0$ value, and it is also safe to assume that the ROP will always lead to a certain degree of free monomer unreacted concentration [2, 17]. The latter can be defined as the monomer equilibrium concentration:

$$[M]_{eq} = \exp\left(\frac{\Delta H_p^0}{RT} - \frac{\Delta S_p^0}{R}\right). \tag{1.4}$$

[2, 17, 23, 26]

it can be concluded that the initial monomer concentration $[M]_0$ plays a huge role in the final DP_i that the polymer can reach at equilibrium condition. In particular, the initial monomer concentration has to be greater than the equilibrium one to obtain a polymerization process.

In the early steps of polymerization, the Flory assumption does not hold anymore, therefore for analogous mathematical steps, it would get the expression:

$$[M]eq = \left(\frac{DPn - 1}{DP_n}\right)\exp\left(\frac{\Delta H_p^0}{RT} - \frac{\Delta S_p^0}{R}\right). \tag{1.5}$$

[2]

From the equation 1.1, it is understood that there are four possible cases:

1. $\Delta H_p^0 > 0 \quad \Delta S_p^0 > 0,$

2. $\Delta H_p^0 < 0 \quad \Delta S_p^0 < 0,$

3. $\Delta H_p^0 > 0 \quad \Delta S_p^0 < 0,$

4. $\Delta H_p^0 < 0 \quad \Delta S_p^0 > 0.$

[2, 23]

In case 1, it is obtained that the polymerization is possible if the entropy-related term is greater (in absolute value) than the enthalpy one; vice-versa for case 2. For case 3, the polymerization is never feasible, whereas for case 4, it is always possible, thermodynamically speaking. In particular, it is noticed that in case 1 and 2, the temperature of the polymerization reaction plays an important role in the polymerization Gibbs energy tuning, through the variation of the entropy related term. This will determine the existence of two temperature parameters, the "floor temperature" T_f and the "ceiling temperature" T_c. These parameters are respectively the bottom temperature for a polymerization reaction in case 1 and the upper temperature limit for a polymerization reaction in case 2 to happen. These can be easily defined, under the aforementioned Flory assumption, at equilibrium condition ($\Delta G_p = 0$), from equation 1.3:

$$T_f = \frac{\Delta H_p^0}{\Delta S_p^0 + R \ln[M]_0}; \quad \Delta H_p^0 > 0 \quad \Delta S_p^0 > 0. \tag{1.6}$$

$$T_c = \frac{\Delta H_p^0}{\Delta S_p^0 + R \ln[M]_0}; \quad \Delta H_p^0 < 0 \quad \Delta S_p^0 < 0. \tag{1.7}$$

[2, 3, 23, 24, 26]

The ceiling temperature will be a very important parameter throughout the dissertation of the thesis since its tuning will be a key factor for some carbonate monomers' polymerization, as well as for the resulting polymer depolymerization. It is indeed very easy to assert from equation 1.3 that if it is introduced a perturbation of the temperature with respect to an initial one, at equilibrium, it would get a nonzero Gibbs energy

value for a certain transient time. In particular, the perturbation in temperature will introduce a new contribution related to the perturbation value of the temperature, the entropy and monomer equilibrium concentration, and their dependency with respect to the temperature. In the specific thermodynamic case (2) where both enthalpy and entropy of polymerization are negative, a positive increase of temperature over the equilibrium ceiling temperature would cause a positive free Gibbs energy variation, as stated by equation 1.3. In order to reach thermodynamic equilibrium, the initial monomer equilibrium concentration has to increase to compensate for the new positive contribution of the entropy-related term; thus, the macromolecule resulting from a certain initial monomer concentration will reach lower DP_i with respect to a lower temperature. It is possible to corroborate this from equation 1.4, where it can be seen that the raising of the temperature lowers the negative enthalpy contribution, increasing the equilibrium monomer concentration. The ceiling temperature is a non-unique characterizing parameter of the monomer, and it can be defined with a one-to-one correspondence with respect to the initial monomer concentration $[M]_0$. The literature, however, shows a single value that is often leading to ambiguity, usually referring to a one-molar monomer concentration $[M] = 1M$ or to the maximum ceiling temperature for which the reaction does not occur even with pure monomer. Nowadays, the current IUPAC definition of the ceiling temperature T_c is such that it is defined as "the temperature at or above which the concentration of the monomer at equilibrium with its polymer becomes equal to the initial concentration of the monomer" [3, 27]. The latter specifies that in a closed environment with constant volume and pressure, the polymerization cannot happen at a temperature equal to or greater than the ceiling temperature. It is also possible to express the equilibrium temperature as a function of the molar fraction or conversion of the monomer, which allows the exploring of the monomer concentration at thermodynamic equilibrium for several temperatures:

$$T_{eq} = \left(\frac{\Delta H_p^0}{\Delta S_p^0 + R \ln \left(\frac{n_m}{n_0} \right)} \right). \tag{1.8}$$

[2, 3, 24]

for example when the conversion will be at 50%, the logarithmic argument will be $n_m = n_p = \frac{n_0}{2}$ and equation 1.8 will yield:

$$T_{eq,50\%} = \left(\frac{\Delta H_p^0}{\Delta S_p^0 + Rln(\frac{1}{2})} \right). \tag{1.9}$$

[3]

Further considerations on the ceiling temperature should be made; for example, the dilution of the polymerization system in a solution with respect to the bulk causes a drastic reduction of the ceiling temperature due to an increase in the disorder of the system and thus an increase in the entropy penalty [3, 28]. Conducting a polymerization in a solution allows performing polymerization below the melting temperature of the polymer, but it also modifies drastically the thermodynamic parameters of the process. It should also be taken into account that the solvent interaction with the polymerizing system can lead to further deviation from the bulk thermodynamic parameters [2, 24]. In the experiments performed and described in chapter 2, polymerizations are performed mainly in tetrahydrofuran (THF) due to its high capability of solving a wide spectrum of different polarity chemicals, its relatively inert behaviour, its compatibility with the catalytic system of the ROP, and to compare different results by unvarying the solvent system, reducing variation in the thermodynamic of the system. The latter is also the reason why the experiments were always performed in a 1 M solution of the monomer. Another factor that may influence the thermodynamics of a polarization process is, for example, the substituent that functionalizes a monomer unit. Depending on the position where they are found with respect to the non-substituted monomer unit, they can lead to variation of angle, conformation, or repulsive strain, thus varying the stress of the molecule closed ring

and thus varying the enthalpy contribution. In particular, for the case in which the polymerization reaction shows a ceiling temperature, the higher the strain of the molecule, the higher the negative contribution of the enthalpy of polymerization to the free Gibbs energy of polymerization. The increase of the molecule strain due to a substituted monomer will therefore drive the polymerization equilibrium toward the polymer, lowering the monomer equilibrium concentration and thus increasing the conversion. The substituent size and nature can play a further role, other than the position; it is shown that substituents of different sizes and natures lead to different conversion rates. For example, an increased degree of substitution can lead to an increased rate of cyclization, that in spite of the increased enthalpy contribution, drastically increases the contribution of the entropy [2, 3, 18].

1.2.2 Kinetic of ring-opening polymerization and catalysis

In the previous section 1.2.1 it was discussed the general energetic aspects regarding a polymerization process. The satisfying of the thermodynamic requirements for the feasibility of a polymerization, generally, is not sufficient. There are two main aspects of a polymerization process that have been overlooked up to now, the kinetic pathway that leads from the initial thermodynamic state to the final one and the time the reaction takes to reach it.

The ROP are usually carried in presence of an initiator species which reacts with the monomer to give an active species, which based on thermodynamic, energy barriers and reaction kinetic considerations, propagates by the adding of a monomer active unit to the polymer forming chain, or conversely de-propagates, if these are favourable to the inverse process when a polymer is already existing. Also, the initiation must lead to active monomers that are able to perform propagation in order to sustain the polymerization reaction. The ROPs are indeed carried out in presence of organocatalytic systems or, more in general, in a catalysis system which guarantees

the fulfilment of the ROP prerequisites, acting on polymerization energy barriers and reaction kinetics. [2, 6, 13, 21, 25, 29]

It could happen that a reaction, theoretically favourable from the thermodynamic point of view, considering the Gibbs free energy of the initial and final states, encounters an energetically unfavourable state during the reaction that would lead to its premature ending, namely an energetic barrier. Furthermore, a polymerization has to occur in practical times, and whereas the thermodynamic parameters such as entropy, enthalpy, ceiling temperature etc, deliver information of the polymerization energetic system, nothing is provided in terms of energy barriers, polymerization kinetic (occurring reactions, their reactions rate and more). A striking example is the fact that, following the ceiling temperature definition, the polymerizing system at equilibrium should be "dead", but in reality, there is a number of thermodynamic forbidden monomer to polymer conversion, equal to the reversible process, which happens in time [3].

It is also easy to consider that even if the ROP of a closed ring monomer is energetically favourable, the monomer does not self-polymerize, meaning that the energetic pathway to ring-opening and chain growth polymerization follows an energetic path containing an energy barrier that prevents it. The propagation equilibrium constant, for a particular reaction type in the system is related to its free Gibbs energy of activation:

$$k_p = \frac{k_b T}{h} \exp\left(-\frac{\Delta G_p^{\neq}}{RT}\right) = \frac{k_b T}{h} \exp\left(-\frac{\Delta H_p^{\neq}}{RT} + \frac{\Delta S_p^{\neq}}{R}\right) \tag{1.10}$$

[2, 26]

ROP is usually a prerogative of cyclic monomer units that possess unsaturated carbon bonding, for example the carbonyl groups of lactones, which are targeted by the initiator species to open the ring structure and to lead to the monomer units polymerization. Ideally the perfect catalyst system should lead to a significant lowering

of the kinetic energy pathway of the polymerization, making the reaction feasible in the shortest time possible.

An ideal catalyst system should also simultaneously keep control of the polymeric chain growth during the ROP, consisting of the adding of a monomeric unit at time, contrarily to the step polymerization growth that leads to disperse molecular weight distribution. The ROP shows very often very controlled molecular weight distribution and living polymerization features, offering narrow dispersity (M_w/M_n ratio between the weight average and the number average molecular weight) of the polymers, in contrast with step polymerization and its poor control over the molecular weight distribution. The narrow dispersity that yields ROP is due to its feature that was theoretically highlighted by Flory, for which the number of active propagating polymeric chains contributes significantly to the narrow dispersity outcome. The latter specific chain growth should be conducted with high selectivity for the monomer activation and chain propagation with respects to other detrimental side reaction, in order to meet the living polymerization criteria of a first order kinetics and a linear behaviour between the molecular mass distribution of the polymer and the conversion of the monomer.

In particular the reaction should be devoid of any premature termination, for example due to intra-molecular chain transfer such as cyclization and backbiting (kinetically denoted as k_{cy} and k_{bb}) resulting in premature termination and cyclization of the polymer; possibly devoid of any side-transesterification or also called inter-molecular chain transfer (kinetically denoted as k_{sc}) resulting in chain scrambling of the polymer chain, thus inducing the broadening of the polymer molecular weight distribution, even at low monomer concentration of the system. The resulting living polymerization system should display an invariant number of growing chains that lead to a nearly mono-disperse polymer system [2, 3, 25]. The previous mechanisms of reactions are proposed in Figure 1.3.

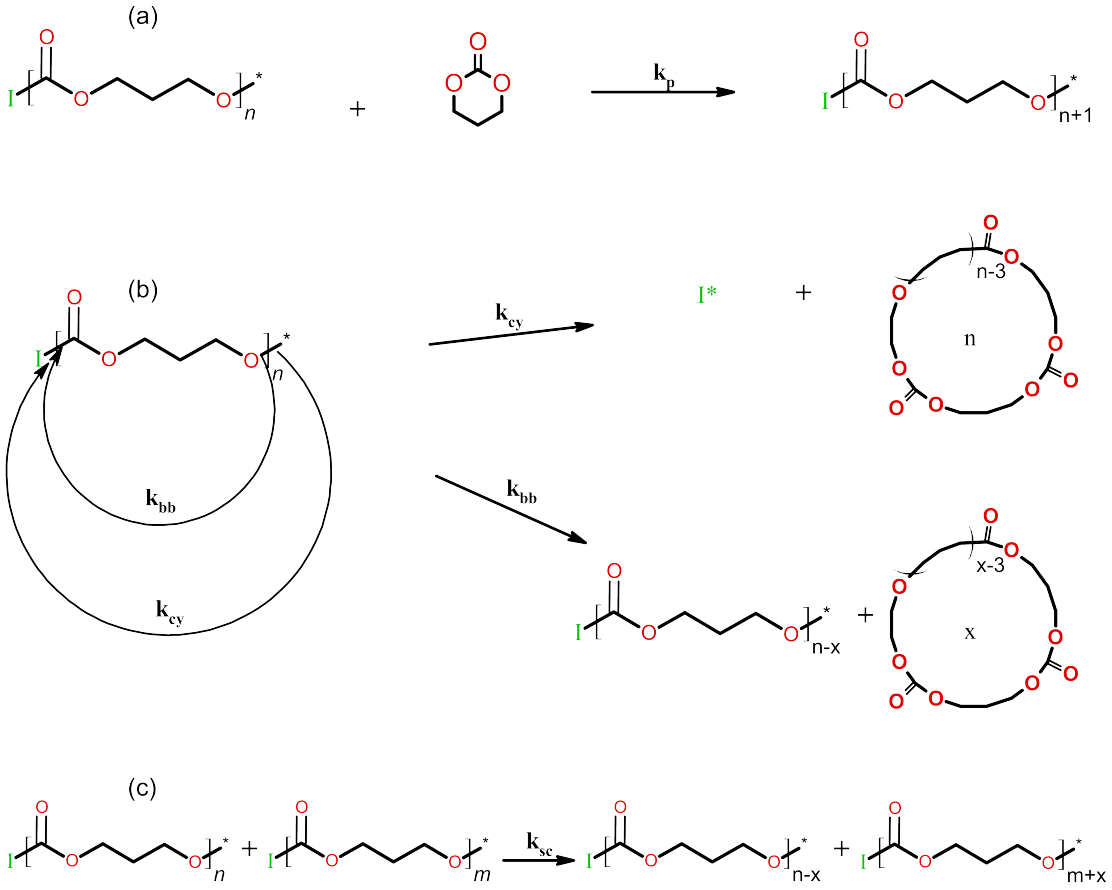

Figure 1.3: Possible reaction schemes: (a) propagation, (b) intramolecular transesterification (cyclization and backbiting) and (c) intermolecular transesterification (scrambling). [2]

To summarize, catalysis ideally allow the polymerization process, increasing its propagation and initiation rate with selectivity over other detrimental side-reactions, through a lowering of the selected energetic pathway that leads from the monomer initial state to the final thermodynamic monomer-polymer equilibrium, providing simultaneously high rate of reaction, high control of molecular weight distribution through selectivity of the catalyst system with respect the monomer meanwhile providing enhanced material properties through stereo-regularity. [1, 2, 6, 13, 21, 25, 29, 30].

It is also interesting to consider the possibility of obtaining kinetically trapped polymers, namely, polymers whose polymerization and depolymerization energetic pathways display an energy state higher than the one of the initial and final thermodynamic energy state, namely an energy barrier. In this way the obtained purified polymer will be trapped in a relative energetic minimum (which may be higher than its monomer unit energy state) making it stable but also easily degradable and even possibly intrinsically chemically recyclable (depolymerization from polymer to monomer) through means of a depolymerization process assisted by relatively small amount of energy [23].

The catalysts systems that are exploited in the further experimental chapters of this thesis, work on the principles of anionic ROP through the exploitation of tested catalysts compound and systems such as metal-alkali alkoxides [6, 13] (K,Na,P) eventually combined with (thio)ureas [6, 13, 21, 25, 29, 31] and alcohol initiators [2, 6, 13, 21, 25]. Alternatively to metal-alkali alkoxide, OROP (organic ROP) was conducted thanks to bases co-catalysts such as the 1,8-diazabicycloundec-7-ene (DBU) [6, 25, 29] and a novel class of organic bases compounds explored during this thesis, called cyclopropenimines (CPI), co-catalysts [21].

The first step to start the ROP is the initiation, through the opening of the monomer ring closed structure. A good performing catalyst system should therefore favour the enthalpy driven opening of the monomer ring and the polymeric chain propagation with respect to any other possible side reaction in order to have a well controlled ROP [2, 3, 25].

Metal transition catalysts system for ROP had a significant impact in achieving the aforementioned results, furthermore the variety of ligand-metal coordination bonds that can be exploited brought the scientific research in this field. Transition metal complexes supported by the functionalization of suitable ligands show high selectivity and even stereoselectivity with great reactivity. In particular Al, Zn, and III

or IV group metals complexes showed ROP of many polyesters with brilliant thermo-chemo-mechanical properties, thanks to their finely tuneable "coordination-insertion" mechanism [2, 6, 25].

Nevertheless, the recently environmental issues, as well as the necessity to obtain metal-free polymers for biomedical and electronic purposes brought the attention of the scientific world to organocatalytic polymerization systems, which improved sensibly in the last 20 years [1, 6]. Polyesters such as lactides or aliphatic polycarbonates exhibit biocompatibility and also biodegradability, therefore the requirement of free of impurity polymers for electronics (for example considering alkali metals particularly corrosive for standard CMOS technology) and biomedical application in which prevalently oligomers are exploited and a 1:20 equivalent of catalyst, in order to reach the targeted DP_i, constitute a great impurity fraction, leading to the research of a greener catalytic system [1, 6, 25].

The first step for a ROP is to activate the initiator or chain-end by the formation of an alkoxide through an alcohol group deprotonation. Other possible way to activate the initiator is through the exploitation of mild bases whose H-bonding with the alcohol, increases the initiator nucleophilicity and its nucleophilic attack mechanism on the monomer. In both ways, the activated chain-end initiator attacks the carbonyl group of the cyclic ester, through a nucleophilic mechanism, in order to mediate the ring-opening of the monomer [2, 6, 13, 25, 29, 30]. (thio)ureas promote an electrophilic attack of the carbonyl oxygen through H-bonding formation, and its exploitation with mild bases such as DBU or CPI, as well as in combination with alkaline metal based alkoxide revealed interesting properties [6, 25, 30] and the formation of urea anions [13, 21, 29]. In particular, the usage of a mild base such as DBU, was shown to be able to perform ROP of PLAs through the activation of the alcohol, but its inert behaviour toward other monomers such as trimethylene carbonate, caprolactone and valerolactone does not allow for polymerization processes as it is not a sufficient

potent nucleophile to enable ring-opening of the monomers, subsequently the alcohol is needed [6].

It is generally preferable to perform catalysis with the aid of a co-catalysts, such as a (thio)urea combined with a base, to perform successful, selective and modestly fast anionic ROP reactions with better performances [6, 25, 29]. The combination of the DBU-alcohol system with (thio)urea was shown to significantly increase the reactivity of the process, introducing the electrophilic attack of the (thio)urea on the carbonyl group oxygen, by its two hydrogen bonding formed by the hydrogen bonded to the nitrogen atoms of the (thio)urea group. In this way it can happen the nucleophilic attack of the monomer through the activation of the alcohol chain end due to the mild base and a direct catalytic process due to the (thio)urea. The simultaneous process further lowers the energetic path of the initiation and propagation, thus increasing its selectivity through the well designed (thio)urea molecule recognition of the monomer [6, 25, 29]. The trimethylene carbonate ROP kinetic pathway, due to this catalysis system is proposed in Figure 1.4, in which the activation of the alcohol **(A-1)** thanks to the base **(DBU)**, which acts as initiator species and nucleophilically attacks the carbonyl group of the monomer is visible. The urea offering selectivity due to the created hydrogen bondings toward the monomer carbonyl groups, is also present. After the ring-opening reaction, the urea translates its hydrogen bondings along the activated monomer reaching the chain end to add further monomer units, thus performing the propagation of the chain as visible in the right side of the picture.

A new class of ureas were proposed by Waymouth et al. [29], where the sulphur atom was replaced with an oxygen. This new class is reported to be less acidic and therefore the anions of this compounds related class show a more pronounced basicity which is a crucial factor for the H-bonding activation of the alcohol for nucleophile attack. These ureas allowed to keep the advantage of selectivity and stereoregularity of (thio)ureas combined with a higher reaction propagation constant. Therefore, it

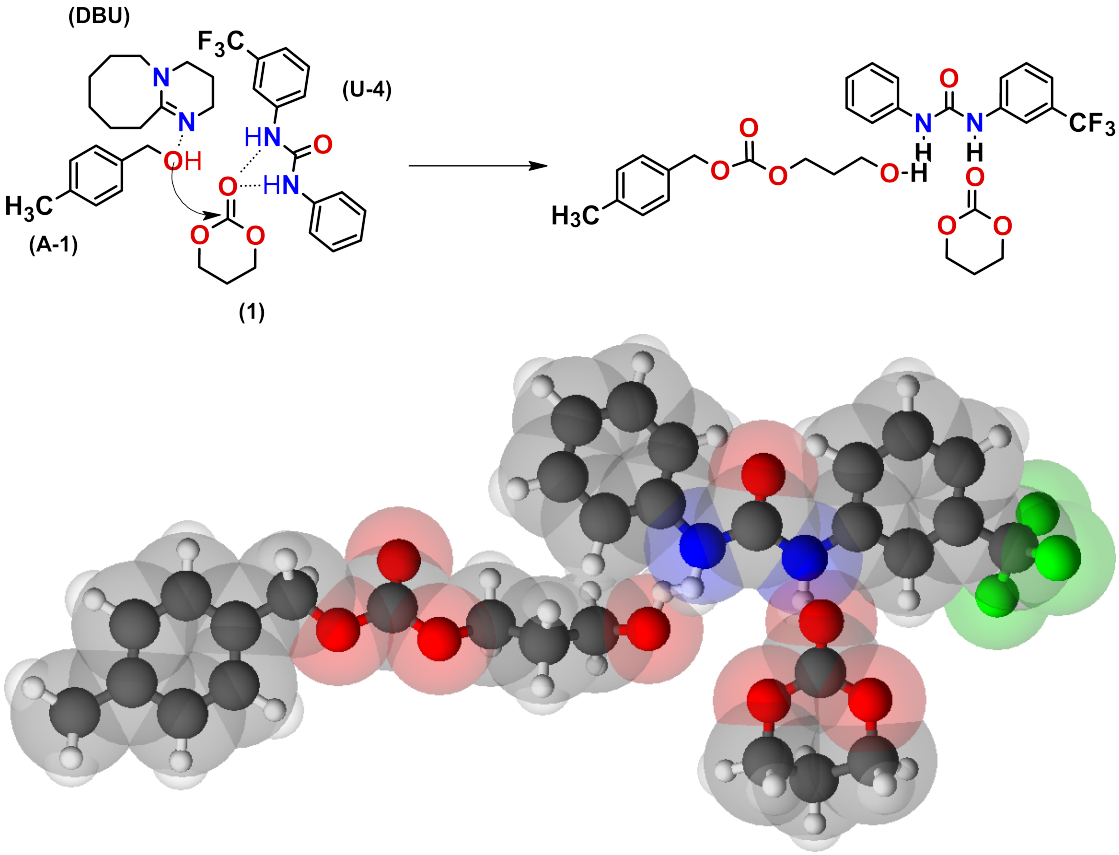

Figure 1.4: OROP propagation pathway for poly(**1**), catalysed with alcohol **(A-1)**, urea **(U-4)** and **(DBU)** [29].

allows for the exploitation of an organic catalyst system such as DBU or CPI combined with these ureas, with competitive performance with respect to inorganic catalysts systems [21, 29].

Alkali metal alkoxide such as the ones generating from the deprotonation of KOH or NaOH, provided a strong nucleophilic initiation thanks to the presence of the alkali metal counter-ion, which in turn provided very fast initiation and propagation but poor selectivity, reflecting in broad dispersity regarding lactones ROP. Also, the $KOCH_3$ stand-alone lactide polymerization resulted in broad dispersity and epimerization, reflecting the poor stereoselectivity of the catalyst. The combination of alkali metal alkoxide and ureas was shown to deliver fast and selective ROP with

great stereoregularity. In particular, the diaryl-ureas can be functionalized with CF_3 substituent on their aryl groups. These substituents are electron withdrawing, thus reducing the base behaviour of the molecule. This allows an easy modification of the catalyst that reduce or increase the nucleophilic behaviour of the alcohol, attacking the monomer, with increased nucleophilicity due to the basicity of the urea, leading to a higher rate but also less molecular weight distribution control at high conversion [13, 29].

The mechanism of initiation and propagation was revealed to consists in the creation of a complex in which the ureas deprotonates thanks to the alkali metals strong base, where the alkali metal acts as a counter-ion for the formed urea anion forming a reaction complex, H-bonded with the alcohol. The urea anion, with its counter-ion, electrophilically attack the carbonyl group of the monomer meanwhile, the activated alcohol through its enhanced basicity, thanks to its alkoxide creation, is H-bonded to the urea anion and attacks the monomer nucleophilically with enhanced performances as well, allowing the ROP [29].

The complex created through monomer H-bond with the catalyst complex, makes the system even more energetically favourable in terms of Gibbs free energy. In the further steps, the urea anions H-bonds translates along the newly added monomer unit, which allows propagation when reaching the chain end, by making the polymer active and amenable for further ROP, allowing chain growth with great thermodynamic favourability.

Thus, the process allows for the strong and fast initiation similarly to the one delivered by the nucleophilic attack due to the alkali metal alkoxide presence, but with the combination of the urea electrophilic attack, through which both the reducing of the energetic pathway of propagation and molecular supra-recognition lead to high selectivity, stereo-selectivity and fast propagation process of the ROP [13].

The proposed catalyst systems were developed in the last 15 years and optimized,

today further researches are developing tri-motif activation mechanism catalysts with new molecule similar to the diaryl-ureas, such as 2,2'-bisindole. This catalyst system showed a tri-mechanism activation path that lowers the free Gibbs energy of activation further, nearly doubling it, with respect to the usual urea-alkali alkoxide base system. The alkali metal counterion create the 2,2'-bisindole anion that acts like the urea, in terms of its H-bonding activation motifs both toward the alkoxide, that attack nucleophilically the monomer, and both toward the monomer itself, plus the alkali cation directly interacts with the monomer closed ring unit, such that the 2,2'-bisindole can restore its neutrality and further attack the monomer unit for ROP [30].

Another type of catalysts are the Phase transfer catalysts, which adds to the normal catalysts function the facilitating of the reaction in a heterogeneous system with immiscible phases, generally operating catalysis through the transferring (usually) of an anionic species from the liquid or solid phase to the organic. The advantages are many, comprising the less dependence on expensive organic solvents, the possible exploitation of simple bases such a KOH, possible enhancement of reactivities and many more, depending on the specific application. PTC usually are restricted to ammonium or phosphonium compound, but their synthesis is often complicated and poses a serious barrier. Tris(dialkylamino)-cyclopropenium (TDAC) salts were proposed as possible PTC alternative to those previously mentioned [32]. Their ability to sustain the characteristic basicity and nucleophilic operating environment was tested, showing stability toward detrimental side reaction as hydrolysis and ring-opening [11, 32]. The choice of this class of compounds mainly relays on their particular aspect for which they are the smallest molecule known to satisfy the Huckles requirement of aromaticity which makes them stable in spite of the high stress of the ring. Cyclopropenium activation was shown to be useful to enable alcohol nucleophilic substitution and furthermore its Brønsted basicity was proven making it theoretically available as alcohol initiator for the nucleophile attack of the monomer in a ROP

process. Cyclopropenium ions were found to be a new class of strong super bases, due to the stability of the aromatic conjugate acid [11]. As previously discussed, it is known that the higher basicity of the activating compound corresponds to a higher nucleophilic behaviour of the activated alcohol, making them particularly suitable for ROP of lactones or carbonate monomers [11].

1.2.3 Flow chemistry

Flow chemistry is an intriguing field, proven to be suitable for anionic ROP of cyclic lactones and carbonates, with particular advantages over batch ROP reactions [33].

Obvious advantages lie in the fact that flow polymerization through small tubular reactors allows for higher thermal exchange due to increased surface-to-volume ratio resulting from size scaling. This enables better control over hazardous exothermic reactions, with more efficient mixing of reactants leading to shorter residence times (RT) [34]. RT is defined as the time for a fluid to traverse and exit a reactor from its injection in the reactor itself, whereas RTD is its time distribution referred to a fluid simultaneously injected. Additionally, flow chemistry includes the possibility of scaling the reaction by increasing the reaction time, employing larger reservoir as well as conducting parallel reactions, enhancing throughput for industrial applications. Flow chemistry enables generally safer handling of toxic and hazardous chemicals and the possibility to simplify multi-block co-polymerization without the need for intermediate purification and functionalization steps. This is achieved by simply sequentially adding monomers in the reactors or performing a catalyst switching [33, 35–38].

Co-polymerization can be performed in flow chemistry, leading to decreased costs compared to batch processes, allowing the exploitation of more complex, niche and cheaper materials [33].

The high control during ROP process over small residence time, through the control of the inlet flow rate of the reactants, allows reproducible and controlled reactions that

can be quenched in time with a precision degree not achievable in batch conditions [39, 40]. This leads to the possibility of exploiting highly active catalysts such as metal alkali oxides, resulting in finely narrow controlled molecular weight distribution through rapid quenching, controlled by the RT, upon reaching high conversion. This also avoids polymers in reaction mixtures to undergo backbiting, scrambling, and other side-reactions that do not permit polymerization living behaviour in batch conditions [33, 37, 38].

ROP and OROP have been observed for polyesters [41–43] and polycarbonates [44, 45]. Sterically hindered strong bases such as metal alkali oxides have been shown to be good catalysts in continuous flow reactions for those materials. These sterically hindered bases are indeed shown to be slow initiators in batch conditions that lead to broad dispersity. For example, L-lactide polymerization in potassium tert-butoxide resulted in $Đ > 1.4$ broad polymer and 83% conversion of the initial monomer after 22 hours, when the reaction is performed in batch. In continuous flow, the same reaction delivered a conversion of 86% and dispersity $Đ = 1.11$ with a RT of 38 ms [37]. This is because the catalyst system has a slow initiation rate of polymerization compared to the propagation rate. The combination with an alcohol allows the possibility to form primary alkoxide that acts as an efficient initiating species, due to the high pK_a of the potassium tert-butoxide conjugate acid. Given the metal alkali oxide strong base, a primary alkoxide easily forms, ensuring the initiation of the polymerization process. Furthermore, its propagation rate is higher with respect to the base's initiation. The previous, combined with higher mixing efficiency, short RT, controllable RT and RTD, enables controlled and fast polymerization processes that would not be possible to achieve in batch for the same catalyst system [37].

The possible combination of the previous catalyst system with urea anions further enhances the control and rate of the reaction. In particular, the possibility to functionalize these anions with electron-withdrawing moieties such as -CF_3 groups can

tune their basicity and their subsequent activation of the alcohol and therefore the initiation rate, leading to three orders of magnitude difference between the different substituted types of ureas [29].

Urea anions are suitable for the creation of block-copolymers in flow reactors, in which the sequential adding of monomers with different reactivity can be counterbalanced by introducing less reactive urea anions, giving high control to chain propagation. However, some limitations in block sequencing occur, as the urea anions should be introduced from the most basic to the most acidic in order to obtain, at each step, a proton transfer that quenches the most active urea. Therefore, the co-monomers should also follow the complementary trend in terms of their reactivity, limiting the repetition of the block units [38].

Fluid dynamics is another matter that should not be overlooked when considering flow polymerization. These reactions usually occur in a μ-fluidic regime for the previous related scalability advantages. Therefore, the fluid usually flows under laminar flow, namely its Reynolds number is $Re < 2000$. Considering the incompressible fluid Navier-Stokes equation, namely a solenoidal flow in which the internal viscosity can be neglected, assuming also that the gravitational force is applied vertically to the horizontal flow:

$$\rho_m \frac{D\bar{U}}{Dt} = -\overline{\nabla} P^* + \eta \nabla^2 U. \tag{1.11}$$

The previous equation contains the mass density ρ_m, the material derivative of the flow velocity with respect to time $\frac{D\bar{U}}{Dt}$, the gradient of the pressure term, in which the gravitational term is also included $P^* = P - \rho_m \bar{g}$ and finally it is present the viscosity multiplied by the Laplacian of the velocity of the flow $\eta \nabla^2 U$, a term related to the external forces of the fluid. In flow chemistry reactions, it is usual to have pressure-driven flow, also called "Poiseuille flow." It can be further assumed a uniform pressure gradient

$$\frac{dP}{dx} = -k \qquad k := \text{constant}.$$

After a certain transient time, the flow will reach a steady-state condition, and far from the edges of the tubular structure, the flow obeys the following equation (assuming a $\hat{x}$ directional flow):

$$\frac{\partial^2 U_x}{\partial y^2} = -\frac{k}{\eta}. \tag{1.12}$$

Imposing the no-slip condition at the top and bottom of the tubular section (assuming a 2D section of the tubular in which the micro-flow is happening), namely it is imposed the velocity of the flow $U_x = 0$ at $y = 0;\ y = h$, it is finally found the solution:

$$U_x = -\frac{k}{2\eta}y^2; \qquad U_{\max}(y = \frac{h}{2}) = \frac{h^2 k}{8\eta}. \tag{1.13}$$

The latter equation shows a parabolic velocity profile of the fluid, in which the fluid should be ideally still at the fluid interface with the surface of the tubular reactor. However, due to non-idealities such as the possibility to compress fluid, non-perfect horizontal flow, approximations like the lack of diffusion terms, and many more, the latter dissertation only provides a qualitative behaviour of the flow [46].

It is evident that this will cause a broad RTD with consequences on the molecular weight distribution control. Therefore, different strategies have been adopted, in particular to enhance mixing in order to obtain homogeneous RT and mixing of the different reactants. Examples are many, such as droplet flow, where droplets are allowed to flow instead of using continuous flow. In this way, tubular friction allows the fluid to continuously circulate from its surface to its inner section. Static mixers involve the insertion of static obstacles in the micro-tubular reactor to provide temporarily turbulent flow with $Re > 2000$ and increase mixing, as well as Dean Flow, which exploits curves to produce perturbations of the flow. Each technique is more suitable for particular scopes. Droplets flow may be hard to implement as the compressibility of the fluid may influence it by volume, pressure, and temperature changes altering the mechanism of the flow. Static mixer performances instead are dependent on the flow rate and fluid viscosity, causing pressure drop and may be designed for specific parameters of a desired flow [33, 47–50].

Finally, despite all the efforts of computational chemistry, accurately predicting the outcome of polymerization reactions remains challenging, and trial and error approaches are still crucial. Flow chemistry allows the production of polymer libraries with great control, particularly if it is possibly automated.

1.3 Recyclability

1.3.1 Recycling strategies

Plastics production results in an amount exceeding the annual 335 million tonnes of materials [10], with forecasts that point out a drastic increase of production in the following years. The great success of this family of materials is due to its cost-effective, durability, versatility, and so forth. It is esteemed that 4.8 to 12.7 million tonnes of plastics are entering the ocean every year and most of the remaining plastics are landfilled or incinerated [1, 51]. The need for a sustainable (meaning that the rate of natural resource consumption must be lower than the reservoir regeneration rate) circular closed-loop life cycles of plastics material is evidently necessary.

In particular, this thesis will focus on recycling strategies for polyesters and polycarbonates, which are promising material in this field for several reasons. Polyesters such as PLAs are ranked the highest in the GDM (green design metric) which takes into account all the steps of a polymer life, from its resource to its end of use, on the other hand other metrics, like LCA (life cycle assessment), value this polymer on a middle level, since this model focus also on the environmental impact of the feedstock production, such as agriculture and natural chemical reaction steps like fermentation. PLA is indeed a starch bio-derived polymer, retrievable from crops like corn, and therefore sustainable in the strict definition of the word [52]. Both polyesters and polycarbonates belong to a family of renewable and degradable polymers, leading a lot of attention to these classes of polymers. These properties are due both from their bio-derived feedstocks and both from the fact that their ester and carbonate linkage in their aliphatic backbone can be easily decomposed by natural microorganisms [1, 53]. PLA is indeed the bio-shopper most exploited material.

The aforementioned classes of polymers show important thermodynamic properties for recycling. The advances in catalysis for the monomer and their relative polymers

synthesis deliver greener (in particular for polymer synthesis) systems, with high efficiency and low cost. Esters and carbonate monomers, in their ring closed version, are able to undergo ROP and therefore chain-growth polymerization, with living behaviour and high degree of control over molecular weight distribution, with high yield, green routes and mild reaction conditions, unlike step-growth processes. The latter makes these classes of polymers suitable for biomedical application, also because of their easy tailoring. The possibility of these materials to undergo ROP, allows also the possibility of chemical recycling through pyrolysis, namely a thermal assisted depolymerization process, in which these polymers perform their unzipping (the converse process of chain-growth) yielding pristine monomer units [54–56] from the initial polymer with great control and selectivity, even though quite often, catalysts and solvents are needed to achieve selective results with high yields and milder conditions [57]. The interest of this recycling procedure is that the monomers can be recycled into virgin polymers with renewed performances, unlike mechanical recycling and melting cycles recycling procedures [10].

1.3.2 Ring-closing depolymerization

From previous sections 1.2.1 and 1.2.2 it was discussed the thermodynamic and kinetic aspects of ROP of cyclic esters and carbonates, in particular regarding the six membered ring monomer belonging to these classes. Dainton-Irvin equation 1.7 is a measuring quantity of the balance of monomer and polymer equilibrium in a ROP reaction, giving insightful information about the thermodynamic of the system and its polymerization feasibility [2, 3, 58].

At the basis of chemical recycling, there should be the fulfilment of its thermodynamics requirements, since the ceiling temperature is the temperature of a given polymerizing system for which the reaction equilibrium is such that the monomer concentration is equal to the initial one. Consequently, the depolymerization reaction

for polymers exhibiting ceiling temperatures, should take place at temperature equal or greater than the ceiling one. It has been demonstrated the depolymerization of AOMEC (2-allyloxymethyl-2-ethyltrimethylene carbonate), a six-membered ring carbonate monomer by Olsén et al., in the same anionic environment in which the polymerization reaction took place (solvent and catalyst consisting of an organic base and an alcohol), simply switching to a temperature higher than the ceiling one [58].

A first thermodynamical limit for a polymer to achieve RCDEP (Ring closing depolymerization) is that the ceiling temperature must be low enough to avoid the reaching of the onset degradation temperature T_d (the temperature for which 5% or alternatively 10% of the material, in weight, is degraded) [23]. Monomer such as six membered ring carbonates and esters are particularly interesting for chemical recycling. Their thermodynamic parameters feature a highly enthalpy driven ROP due to the stress induced by their closed ring configuration, but also a large entropy penalty with temperature, leading to modest ceiling temperatures and easiness of polymerization and depolymerization with low energy input [3, 10, 23, 24, 58].

Consistently with the previous discussion, thermodynamic requirements are not enough to guarantee the depolymerization process to happen, and its kinetic aspects must be carefully considered. In a recent work by Plummers et al., out of 63 monomers undergoing ROP and subsequently undergoing depolymerization procedures, only three were found to be able to perform bulk solely thermal assisted depolymerization, namely, without assists of solvent and catalysts [10]. However, the latter were performed at temperature higher than $300\,\mathrm{K}$ with respect to the ceiling temperature, whereas a specimen able to undergo thermal assisted depolymerization with lower temperature difference with respect to the ceiling one yielded modest monomer recovery up to the 71% [10]. Nevertheless, the ability of a system to perform thermal bulk depolymerization, namely the worst condition in which this procedure can happen, is a great indicator of the polymer ability to be chemically recycled. The dead system, namely the quenched

and purified polymer, is usually a "kinetically trapped" system that ensures the thermal stability at temperature $T > T_c$. The resulting polymer is indeed a metastable system that is not anymore in a monomer-polymer equilibrium state and its re-activation requires energy to satisfy the overcoming of its own energy of depropagation barrier related to the kinetic aspects of the reaction. Thus two fundamental aspects must be taken into account when looking for ICPs, (1) the monomer design to ensure such kinetic trapping and ideal T_c value, such that the material can be easily polymerized and depolymerized with minimal input energy and with a good trade-off for thermal stability; (2) The catalysts design to lower the kinetic barrier as much as possible lowering the polymerization and depolymerization energy path of the system. The catalyst should also provide the highest possible degree of selectivity, therefore avoiding epimerization and unwanted side reactions, resulting in the retrieving of a different monomer. Finally the catalyst system should possibly ensure a green route through organic catalysts choice [3, 10, 23].

Regarding the monomer design a possible strategy to favour RCDEP is the Thorpe-Ingold effect, namely the phenomenon for which the ring-closure reaction and more generally cyclization are favoured by higher degree of substitution due to their steric hindrance, with particular regard to the di-methyl group [3, 10]. The presence of heteroatoms also influences the RCDEP, in the same manner it influences the ROP, their position in the closed ring is extremely relevant and their effect is strictly related to the induced or removed stress, which changes the enthalpy thermodynamic value and the driving force of ROP or RCDEP [3, 10].

Regarding the catalyst system, the ideal system is found to be similar to the one described in the synthesis, it must be highly selective, devoid of side reaction, epimerization and atacticity, it must show fast depropagation rate and great lowering of the energy barrier and finally to be possibly green. However, the depolymerizing catalysts system often is necessarily different from the one exploited during ROP.

The main reason is that the condition under which the two reactions are performed are usually different. Depolymerization of these polymers are performed at higher temperature,in solution with carefully chosen solvents or bulk, possibly differing to the synthesis conditions of the polymer and other possible variation in the reaction environment [10]. The latter exclusively depend on the ability of the system to undergo depolymerization and by its purpose, indeed there are many cases in literature in which the same catalyst system is used both for the ROP and RCDEP [1, 58].

To pose an example, if a material is at its end of use and needs to be recycled through chemical recycling, it is obvious that the best choice of the reaction environment is the one that requires minimal energy input [10, 23]. This could generally be an environment at the lowest temperature greater than T_c, that allows the catalysts system to depolymerize the material, maybe exploiting a solvent such that the dilution increases the entropy of polymerization and further decreases the ceiling temperature [3]. The solvent to be employed in depolymerization processes must be carefully studied in terms of its polarity difference with respect to the polymer, in order to obtain the best enthalpy (due to stress increase or reduction by the solvent), which can be modified with the solvent polarity and entropy (due to lower or greater solubility of polymerization) of polymerization trade-off [24]. The increase of entropy thermodynamic parameter can also be interpreted as a lowering of the monomer concentration resulting in lower ceiling temperature from Irving-Dainton equation [2, 3, 24].

Depolymerization procedure do not serve only as a mere strategy for recycling, but it can be exploited as a synthesis path for functionalized ring closed monomers. The possibility to functionalize the polymer and then recover its functionalized monomer unit through RCDEP poses as an alternative synthesis pathway, especially to those monomers whose functionalization is quite cumbersome [58].

1.4 Accelerated discovery

1.4.1 Automated flow chemistry

In the fields of chemistry and materials science, there is a growing interest in automating laboratories for high-throughput study purposes. This field divides into combinatorial chemistry (investigates solvent, materials, etc.), high throughput screening (HTS) for biological and bio-activity of materials and high throughput experimentation (HTE) which mainly deal with optimization of processes due to physical parameter variations (temperature, pressure, concentration, etc.).

This field could be applied for accelerated discovery of new materials, drugs, bio-material, catalysts systems, optimal reaction condition parameter, and to any "design-make-test-analyse" experiment. The advantages of an automated laboratory, with a particular eye upon flow chemistry, are many, the increasing of throughput (due to parallel automated tasks) lead to easiness in polymer library synthesis, crucial to develop quantitative structure-property relationship (QSPR) model, the speeding up of experimental steps, the increasing of reproducibility, increasing safety and lowering of the carbon footprint [4, 5].

The inherent programmatic aspect of chemical reactions well suits the possibility to software program the automation of flow chemistry reactions. It has been reported by Park et al. [38] the creation of homopolymer and block-co-polymer libraries, where in the first case, PLLA from DP 10 to 50 with repeating unit increment of 1 was reported, whereas the 100 AB di-block-co-polymer poly-(VL)-block-poly-(L-LA) was reported with blocks increment steps of repeating units of 4 with an overall synthesis process of 9 minutes.

Challenges to overcome appears as well, in particular in order to obtain an automated close-loop laboratory. The automation of sample characterization, precipitation

and purification is particularly problematic, constituting a bottle-neck in the experimental work-flow, requiring intensive time-consuming manually batch performed work. Other limitations for example are related to the environment in which the experiment should take place, ROP experiments often require N_2 inert atmosphere to avoid lowering of the molecular weight of polymers and side-reactions. Despite the proposing of strategies to perform it in open air for specific cases, it is still a problem to be addressed to achieve full close-loop automation [4].

Automating chemical reactions in the laboratory using software to control hardware components is inherently intuitive due to the procedural nature of chemical processes. The laboratory can be automated by the platform approach, which divides the laboratory in 5 conceptual main parts, the receptionist, the coordinator, the planner, the librarian and the executor. The receptionist is the interface between the human operator and the laboratory robot, through a GUI or even aided by chat or voice-bot. The coordinator instead is the centre of the automated laboratory, capable of I/O operation and able to manage the workflow, connecting the different parts of the system. It will read and re-write data from the librarian, which are usually exchanged in terms of variables, file or database management. The coordinator-planner interaction instead will manage the experiment priority and choose which are to be executed and in which order. Finally, the coordinator-executor interaction manages the experiment setup and realization both for physical and computational experiments [5].

The computational experiments recently boosted through the implementation of machine learning (ML) and artificial intelligence (AI) combined with simulation model and theory such as density functional theory (DFT) [4, 5, 9].

An alternative proposed solution to the platform-based approach is based on dynamical knowledge graph. This exploits agents which are automated software able to act toward achieving their objective [5]. The dynamic knowledge graph contains both agents and data, based on semantic ontology, which are structured

framework to represent data and explaining its underlying concepts, relationships and properties, enhancing interoperability and making them both human and machine comprehensible. One of the main problems among data structure is indeed the lack of a data sharing standard. Agents and data will create a digital twin of the real lab, through data reading from the real lab equipment, able to perform optimization of the experiment if needed, for example invoking the design of experiment (DoE) agent and changing some experiment related parameter, and subsequently perform the modified experiment by the executing agent. The modularized nature of this approach allows easy integration of new components [5]. The goal ultimately relies in an automation of the chemistry lab thanks to AI and ML, granting the possibility to human researcher to focus on data interpretation and design of new experiments and boosting the discovery of new material [4, 5].

1.4.2 Models for Material Design

The increasing amount of accessible data has enabled the possibility to exploit AI and ML with great efficiency and results. In the polymer field, ML datasets are still not as developed, and recent efforts are employed to reach the same technology maturity as in the case of small molecules [4, 9, 18–20].

AI and ML are key techniques for material data-driven design, aiming to reduce the number of experiments, identify the most promising candidates for target properties through rapid screening, and optimize experiments in a computationally efficient manner [4, 18–20].

The most challenging part in developing a ML model for predictive purposes in the polymer and material science field is the scarcity of datasets and the low fidelity of most of the data, which are often not open-access. Furthermore, the lack of a standard data representation is quite challenging [4, 5, 9, 18–20]. SMILES have been extensively used for small molecules, whereas efforts in the polymer field have been

made to convert data into machine-readable numeric formats through fingerprinting (conversion of material, structure and property into binary data, often in matrix form) or graph-based data and GNN (graph neural networks) [4, 18–20]. However, a solution to encode all material information into machine-readable data is still a major challenge. The combinatorial-sequence nature of polymers introduces an incredibly large search field, with 10^{15} possible combinations for sizes up to 50 repeating units [19].

Different mathematical regression models are possible, from linear regression, which is easily understandable and interpretable, to Gaussian process regression and the more promising neural networks (NN). Linear regression is more adequate for small datasets (<10,000) due to its robustness and ability to provide uncertainties for search space exploration and subsequent Bayesian optimization (BO). NN, on the other hand, can work efficiently with large datasets, requiring lower computational efforts. GNNs are reported to allow self-acquisition and processing of data for further ML model creation through supervised techniques (where the input and output results are known to train the model) [18, 20].

ML models aim to substitute computationally costly and time-consuming simulations. For example, they have the potential to replace molecular dynamics (MD) and Monte Carlo (MC) simulations for computing secondary level quantities, with the ultimate goal of replacing first-level simulations like DFT for retrieving charge density, electronic wave functions, and energy levels, such as predicting the potential form of the system with attention to the exchange-correlation term [18]. Synergistic approaches between computational simulations and ML predictive models offer great advantages, exploiting the former for forward design and optimization and the latter for rapid inverse design and finding the best synthesis conditions [4, 20].

There are many application examples of AI and ML models in the polymer field. For instance, the discovery of copolymer ^{19}F MRI agents with imaging sensitivities

higher than those of previously reported materials, was achieved by combining ML-assisted material research with automated-flow laboratories [9]. ML inverse problems were successful in finding new QSPRs for polymer design in high energy capacitor applications and biodegradable high T_c polymers [18].

Many other examples are available in literature, and the development of more robust ML models, together with the development of closed-loop automated laboratories for high-throughput screening, could solve the critical challenges of these fields and potentially lead to a revolution in material science soon.

Chapter 2

Aim of the work

The principal objective of this research, developed during my internship at IBM Almaden-Research, is to investigate and evaluate innovative strategies for the synthesis and recycling of polyesters and polycarbonates. In particular, the catalytic systems based on cyclopropenimines (CPIs) for the ring-opening polymerisation (ROP) of cyclic carbonate and polyester monomers were initially examined. This investigation aims to create sustainable and high-performance materials through means of novel highly performing organocatalyst systems.

In order to replace plastics derived from fossil fuels with with materials that are recyclable and less environmentally harmful, the alternative candidates must firstly be equally performant. It is therefore important to synthesise these materials in order to evaluate their potential use and provide them with the necessary properties for their intended application. Consequently, a significant proportion of research is dedicated to the synthesis of PLA and polycarbonates, due to their biodegradability and potential for biomedical applications. The synthesis experiments are designed to produce polymers with precise control over molecular weight and distribution, aiming for narrow dispersities which are of great importance for application-specific properties. In the case of PLA, the novel catalyst systems investigated also provide stereoregularity under low temperature conditions.

Cyclopropenimines represent a novel class of organic bases that are known for their high basicity and stability, which make them promising candidates for the catalysis of ROP. This study compares the performances of CPIs based catalyst systems against traditional catalytic systems, such as metal-alkoxides and other well-established organocatalysts, under different conditions. Key reaction parameters, including the choice of co-catalysts (such as (thio)ureas), solvents, and reaction times, are varied to determine their impact on polymerization efficiency and polymer properties.

Cyclopropenium ions were also investigated as a possible class of compounds suitable to perform PTC, in order to enhance the performances of aqueous bases,

including for example alkali metal bases, in organic solvents. The cyclopropenium ions were employed in their chloride salt form, and PLA syntheses starting from lactide monomer units were performed using a wide range of catalyst systems, varying the presence of urea and cyclopropenium salts. This included combinations where both, either one, or neither of the aforementioned components were present. This approach was taken for each aqueous base compound in order to assert the impact of the investigated PTC catalyst on the performance of the overall catalyst system.

Advanced analytical techniques including nuclear magnetic resonance (NMR), gel permeation chromatography (GPC), differential scanning calorimetry (DSC) and thermogravimetric analysis combined in-situ with mass spectroscopy analysis (TGA-MS) are employed to characterize the thermal and structural properties of the synthesized polymers, as well as the polymerization reaction figure of merits, such as monomer to polymer conversion. These analyses provide insights into the relationship between the conditions of polymerization and the resulting polymer properties. These includes thermal properties and molecular weight distribution, which in turns affects thermal, mechanical and degradation properties of the polymers.

Thermal ring-closing depolymerization (RCDEP) experiments were conducted under several different conditions in order to deliver chemical recycling of certain polycarbonates, converting them into their monomer units. These experiments were conducted exploiting DSC, TGA-MS and heating tools such as ceramics hot-plates. Additionally, Degradation experiments were conducted to further investigate the polycarbonates degradation mechanisms. These were performed using DSC and TGA-MS designed experiments, exploiting nuclear magnetic resonance (NMR) analysis for characterization of the experiment resulting sample.

Furthermore, the study seeks to develop a quantitative understanding of the structure-property relationships (QSPR) of synthesised PLA under automated flow reaction conditions. This involves the creation of extensive datasets to support

the development of a machine learning predictive model that can predict polymer properties based on synthesis parameters. Such predictive models are instrumental in accelerating the discovery and optimization of new polymeric materials. My contribution to this research was to perform DSC analysis on a set of polymers to deliver the learning model with information about the synthesis conditions and the resulting polymer thermal properties.

The overall goal of this thesis is to optimize the polymerization processes for CPIs, to produce highly performing polyesters and polycarbonates, to enhance their practical applications in a range of fields, including medical devices, drug delivery systems, and sustainable packaging materials and to perform thermal assisted degradation experiments of the resulting polymers in order to investigate which novel material could offer the best trade-off in terms of performances and recyclability. Furthermore, the developing of a learning model that aims at further deepen the human knowledge in this field may potentially accelerate the discovery of these materials by uncovering hidden QSPR between synthesis conditions and resulting polymer properties. By establishing a robust framework for the use of CPIs in ROP, delivering high performance polylactides and by conducting the investigation of degradation and thermal property obtained polycarbonates, this research aims to contribute to the development of environmentally friendly and high-performance polymers.

Chapter 3

Experiments and materials

3.1 Carbonate synthesis for recyclable polymers

3.1.1 Materials

As already mentioned in the introduction, materials under study and therefore exploited for experiments belong to the classes of polyesters and polycarbonates, obtained through ROP of their cyclic 6-member monomers. Herein a list of these chemicals in Figure 3.1 along with a list of the co-catalysts exploited for their polymerization in Figure 3.2 is presented for future references.

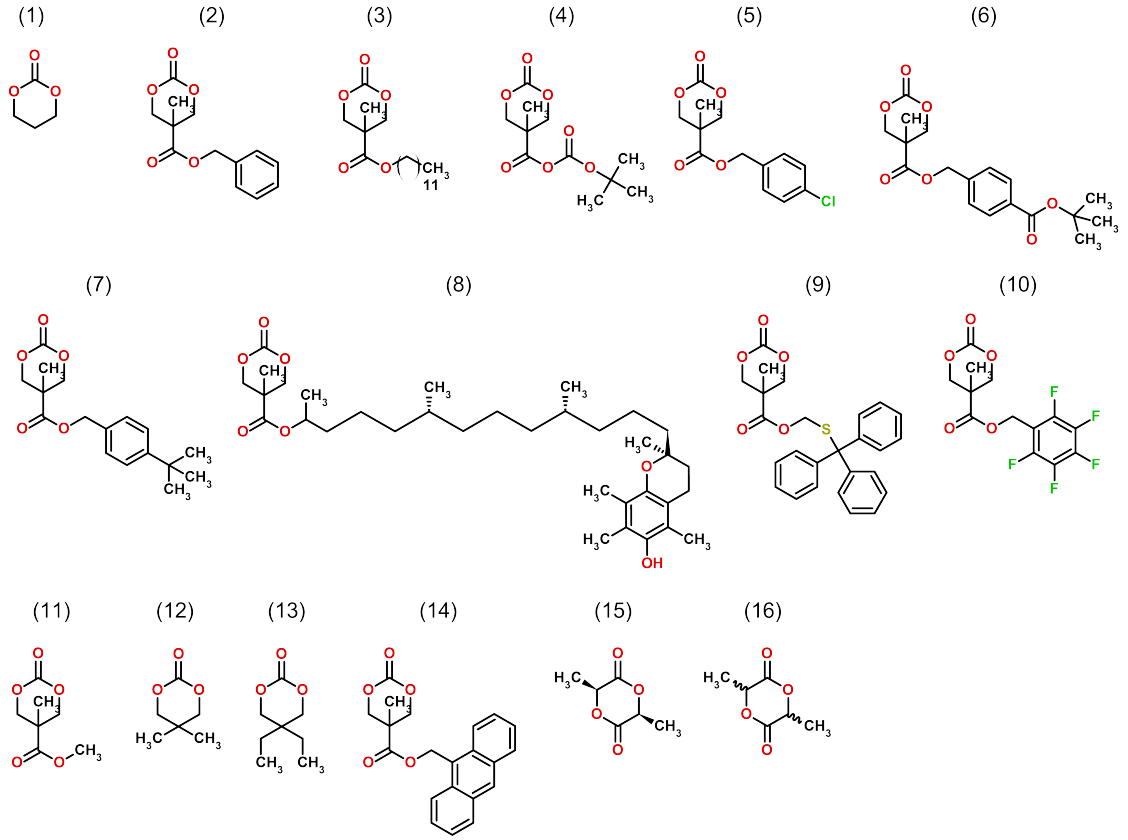

Figure 3.1: List of monomers used during this study.

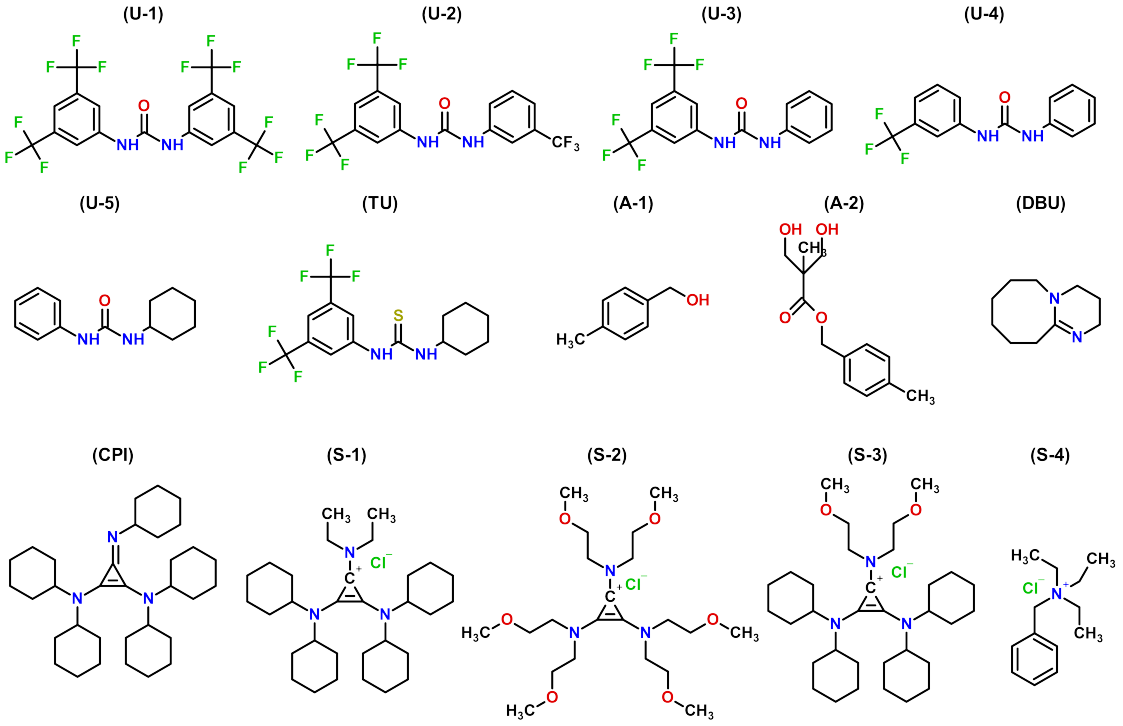

Figure 3.2: List of co-catalysts used during this study.

3.1.2 Batch polymerization experiments

Batch polymerization experiments setup

The Ring-Opening Polymerization (ROP) of carbonate monomers was meticulously executed within a nitrogen-filled glovebox environment, filtered through an HEPA filter. The setup is depicted in Figure 3.3. The experimental procedure unfolded through a series of sequential steps adhering to established protocols.

Figure 3.3: Nitrogen filled glove-box.

The initial phase involved placing 2 DRAM and 4 DRAM (7.5 mL and 14.78 mL glass vials) inside an oven maintained at 180 °C. Accompanied by molecular sieves and magnetic stir bars, these vials were prepared for subsequent deployment within the glovebox. This transition occurred after a cooling interval within the glovebox antechamber following vacuum treatment. The vacuum treatment served a dual purpose: further desiccation after the oven temperature treatment and elimination of potential impurities. For precise measurement and administration of liquid compounds within the range of 1 to roughly 100 microliters, glass comparably scaled volume capacities syringes were favoured. Conversely, plastic syringes of varying capacities (1 mL, 3 mL, 5 mL, and 10 mL) were employed for swift and efficient handling of stock solutions. These syringes were used to transfer of monomer stock solutions to catalyst solutions, catalysing the onset of the ROP process. The same vacuum treatment was

applied to both syringes and molecular sieves in tandem with glass vials within the glovebox antechamber. Introduction of additional items into the glovebox necessitated their preliminary placement within the glovebox antechamber as well. To accelerate purification and mitigate oxygen and non-inert atmospheric gas contamination, a threefold N_2 refill and evacuation procedure ensued following an appropriate vacuum exposure period. This rigorous regimen was instrumental in achieving contaminant eradication.

Chemical compounds underwent NMR analysis to assess their chemical integrity and viability. Any discrepancies observed in the NMR spectra necessitated re-crystallization and further NMR analysis to verify the correct outcome. Following this analysis, the compounds returned to the glovebox through the previously mentioned decontamination protocol via the antechamber.

Batch polymerization experiments procedure

Initiating the procedure, a 2 or 4 DRAM vial (7,393 and 14,787 mL glass vials capped with teflon caps) was assigned an experiment number and designated as the "monomer" stock solution vial. The same nomenclature was applied to the 4 DRAM catalyst stock solution vial, while a 2 DRAM vial was dedicated to the quench. Each monomer and catalyst stock solution vial housed a single stir bar. The weighing process commenced, prioritizing the monomer stock solution. Depending on the intended polymer's purpose, the polymerization process could be initiated using the initiator combined with the monomer or catalyst stock solution. The choice affected conversion rates and control over the reaction.

The procedure entailed the following steps for accurate compound measurement: Taring the glovebox scale with the monomer stock solution vial containing the stir bar, adding the initiator and subsequently the monomer with a metallic spatula, measuring the desired quantity, and adjusting if necessary. The same process applied

to the catalyst solution. When the initiator was combined with the catalyst stock solution, the sequence was initiator, re-taring the scale, base catalyst weighing, and urea co-catalyst measurement. Benzoic acid for the quench stock solution followed this sequence. The spatula was consistently cleaned between weighing steps to prevent cross-contamination. Generally, when adding compounds to a stock solution, the compound orders to be added was defined from the least weight amount related compound to the highest. It is more probable to commit important relative weighing errors for small quantities, therefore this method allowed for adjusting the weight if excess quantity were introduced and also to eventually discard less material if the error was not reparable.

The monomer was always weighed before the catalyst to maintain a controlled, monomodal molecular weight distribution, avoiding contamination that would earlier start the polymerization of the monomer. The same principle applied to the quench component (benzoic acid), which could compromise the entire polymerization reaction if it contaminated the monomer or catalyst stock solution.

In case of liquid phase catalyst, it was added to its stock related vial through volume measurement thanks to the syringes.

The final step involved using appropriately sized disposable syringes to efficiently and rapidly pour the solvent in the several vials. The molecular sieves were previously introduced in the solvent, if needed, to get rid of possible moisture. The vials containing the dissolved stock solutions are stirred upon homogeneity and after that other clean syringes are exploited to withdraw the solutions. The timer was started after the monomer solution was poured into the catalyst solution (or vice versa). All the solution exploited a quantitative of solvent balanced between the catalyst and monomer stock solutions in order to deliver a monomer $[M]_0$ = 1 M solution. Stirring typically operated at 1200 rpm or an optimized velocity to prevent bubble formation and spilling to ensure maximal reaction efficacy, increasing conversion, control over

the molecular weight distribution and degree of polymerization of the polymer. Upon reaching the designated reaction time, the quench solution was added to the mixture, stirred briefly, and the entire assembly was carefully removed from the glove-box through the antechamber. This included both the polymer product and disposable tools (napkins, syringes, vials, etc.).

Finally, the obtained polymer is precipitated and centrifuged in a three-fold way in order to ensure a good degree of purification from catalysts, monomers and unwanted contaminants. The purified polymer is then let under-vacuum with desiccants in order to deprive it from solvents and moisture.

Batch polymerizations materials and examples

Entry 1 of table 4.4 and table 4.3, was obtained from **(1)** trimethylene carbonate (1,3-dioxan-2-one) polymerization. The carbonate monomer polymerization was performed with the **(A-1)** initiator and **(DBU)** with Urea **(U-2)** catalyst system.

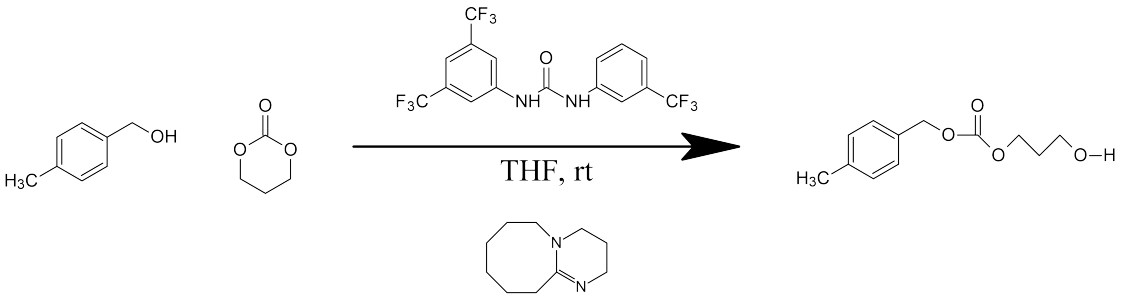

Figure 3.4: Entry 1 of table 4.4, polymerization reaction scheme.

The reaction process commenced by preparing a monomer stock solution, combining **(1)** with **(A-1)** (4-methyl-benzyl-alcohol) as the alcohol initiator with a 1:50 ratio. The catalyst solution was formulated, blending **(U-2)** and **(DBU)** in a 2.5:1:50 ratio, respectively. The stock solutions were dissolved with tetrahydrofuran (THF) serving as the solvent and forming a $[M]_0$ = 1 M solution, when the catalyst and monomer stock solution were mixed starting the reaction. To conclude the polymerization process,

the reaction was quenched with benzoic acid, effectively terminating further polymer growth, at 3 minutes from synthesis process start.

Entry 2-7 of table 4.3 and table 4.4 were realised under the same procedure with different amount of monomer, and therefore catalysts and solvent, but with same ratios and initial monomer concentration of the reaction mixture.

Entry 2 from table 4.3 and table 4.4 was obtained with **(9)** (1 g, 2.162 mmol, 50 equiv.), **(DBU)** (16.78 µL, 0.108 mmol, 2.5 equiv.), **(U-2)** (45.1 mg, 0.108 mmol, 2.5 equiv.), **(A-1)** (5.28 mg, 0.043 mmol, 1 equiv.) and THF as solvent (1,895 µL). The reaction was quenched after 90 s.

Entry 3 from table 4.3 and table 4.4 was obtained with **(6)** (1 g, 2.955 mmol, 50 equiv.), **(DBU)** (22.91 µL, 0.148 mmol, 2.5 equiv.), **(U-2)** (61.6 mg, 0.148 mmol, 2.5 equiv.), **(A-1)** (7.2 mg, 0.059 mmol, 1 equiv.) and THF as solvent (1,864 µL). The reaction was quenched after 90 s.

Entry 4 from table 4.3 and table 4.4 was obtained with **(10)** (1 g, 3.264 mmol, 50 equiv.), **(DBU)** (25.3 µL, 0.163 mmol, 2.5 equiv.), **(U-2)** (68.1 mg, 0.163 mmol, 2.5 equiv.), **(A-1)** (8 mg, 0.065 mmol, 1 equiv.) and THF as solvent (2,163 µL). The reaction was quenched after 90 s.

Entry 5 from table 4.3 and table 4.4 was obtained with **(11)** (700 mg, 4.089 mmol, 50 equiv.), **(DBU)** (31.7 µL, 0.205 mmol, 2.5 equiv.), **(U-2)** (85.3 mg, 0.205 mmol, 2.5 equiv.), **(A-1)** (10 mg, 0.082 mmol, 1 equiv.) and THF as solvent (3,260 µL). The reaction was quenched after 90 s.

Entry 6 from table 4.3 and table 4.4 was obtained with **(3)** (700 mg, 2.131 mmol, 50 equiv.), **(DBU)** (16.52 µL, 0.107 mmol, 2.5 equiv.), **(U-2)** (44.4 mg, 0.107 mmol, 2.5 equiv.), **(A-1)** (5.2 mg, 0.0426 mmol, 1 equiv.) and THF as solvent (1,350 µL). The reaction was quenched after 90 s.

Entry 7 from table 4.3 and table 4.4 was obtained with **(2)** (300 mg, 1.921 mmol, 50 equiv.), **(DBU)** (14.9 µL, 0.097 mmol, 2.5 equiv.), **(U-2)** (40 mg, 0.097 mmol, 2.5 equiv.),

(A-1) (4.7 mg, 0.038 mmol, 1 equiv.) and THF as solvent (1,562 µL). The reaction was quenched after 90 s.

(3) polymerization was also conducted with potassium methoxide ($KOCH_3$) alkali metal base and Urea **(U-4)** catalyst system, presented as entry 8 of table 4.3 and table 4.4.

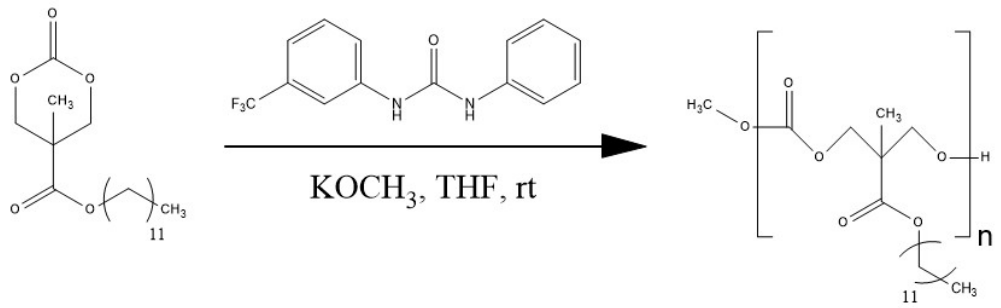

Figure 3.5: Entry 8 of table 4.3 and table 4.4 polymerization reaction scheme.

The polymerization of **(3)** (dodecyl 5-methyl-2-oxo-1,3-dioxane-5-carboxylate) was performed utilizing **(3)** (300 mg, 0.913 mmol, 50 equiv.), **(U-4)** (10.2 mg, 0.0365 mmol, 2 equiv.), $KOCH_3$: (1.3 mg, 0.0183 mmol, 1 equiv.) and THF as solvent (602 µL). Both monomer and catalyst stock solutions were dissolved in tetrahydrofuran, serving as the solvent, as well as the benzoic acid stock solution, chosen as a quenching agent. The reaction commenced upon mixing of the well dissolved monomer and catalyst stock solutions after stirring. The reaction was quenched after 15 s yielding the desired polymer.

3.1.3 Low-temperature polymerization

Experimental setup and procedure

Considering the section 3.1.2, the preparation phase differs because of some important details needed to carry the polymerization reaction in a low temperature environment. First of all, a specialized low-temperature vial is employed. It features a penetrable

sealing lid to allow chemical introduction meanwhile preventing air infiltration, in order to keep a nitrogen inert atmosphere. These vials are introduced into the glove-box in Figure 3.3 following the decontamination procedure described in the aforementioned section 3.1.2. A Dewar flask is then loaded with ice and placed on top of a magnetic stirrer outside the glove-box.

The reaction procedure follows the one of the section 3.1.2, where the ready catalyst stock solution is found in the low temperature specific designed vial, whereas the monomer stock solution is placed in 2 DRAM vial whose lid featuring a syringe penetrable sealing lid. Once the stock solutions are prepared, they are transferred outside the glove-box and the catalyst stock solution is placed in the ice bath together with the monomer stock solution vial. The long low temperature designed vial is designed to plunge deep in the coolant to maximize the thermal exchange to refrigerate. After waiting enough time to ensure that the low temperature for both stock solutions is reached, the monomer solution is then introduced into the catalyst vial, with a syringe. The reaction proceeds until few drops of hydrochloric acid quenched it.

Low temperature polymerization materials

Entry 10 of table 4.3 and table 4.4 was synthesised from **(13)** exploiting potassium methoxide ($KOCH_3$) and urea **(U-4)** with a ratio 50:1:2 respectively.

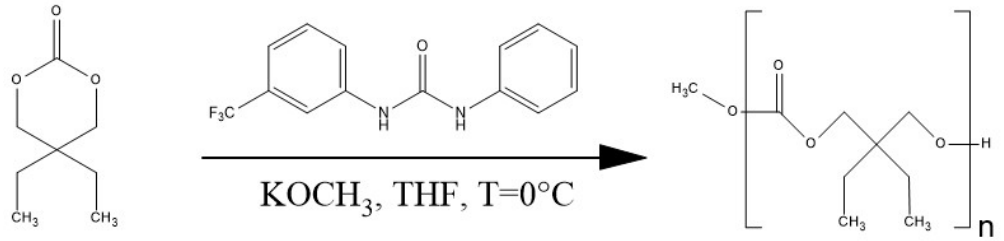

Figure 3.7: Entry 10 of table 4.3 and table 4.4 low temperature polymerization reaction scheme.

(13) (300 mg, 1.896 mmol, 50 equiv.) was dissolved in 1 mL of THF, meanwhile

Figure 3.6: Dewar flask on magnetic plate, with clamps to hold the low temperature vial.

the $KOCH_3$ base (2.66 mg, 0.038 mmol, 1 equiv.) and **(U-4)** (21.2 mg, 0.076 mmol, 2 equiv.) are added to catalyst stock vial and dissolved in 573 µL of THF.

The reaction is then conducted following the previous section, describing the low temperature-polymerization procedure. HCl was add in few drops as a quenching agent to the final 1 M polymerization reaction solution, after 2 hours from the polymerization process begin.

Similarly, poly**(12)**, presented in entry 9 of table 4.3 and table 4.4 was synthesised with the same catalyst system, catalysts to monomer ratio and procedure, in a unknown quantity by an IBM researcher.

Poly**(14)** synthesis, shown in table 4.3 was attempted with **(14)** (300 mg, 0.856 mmol, 50 equiv.), $KOCH_3$ base (1.2 mg, 0.017 mmol, 1 equiv.) and **(U-4)** (9.6 mg, 0.034 mmol,

2 equiv.) and 1,190 µL of THF.

3.1.4 Flow-polymerization

To conduct the flow-polymerization experiment, four disposable 5mL syringes were introduced into the nitrogen-filled glove-box. Two of these syringes were only filled with THF, while the remaining the third syringe was loaded with the monomer stock solution and the remaining one with catalyst stock solution following the section 3.1.2 procedure. The experimental setup included the Pump 33 DDS (Dual Drive System) Syringe Pump from Harvard Apparatus shown in Figure 3.8, a syringe dual pump apparatus. The pumps were configured to provide a flow rate of $0.25\,\mathrm{mL\,s^{-1}}$ from each syringe outlet.

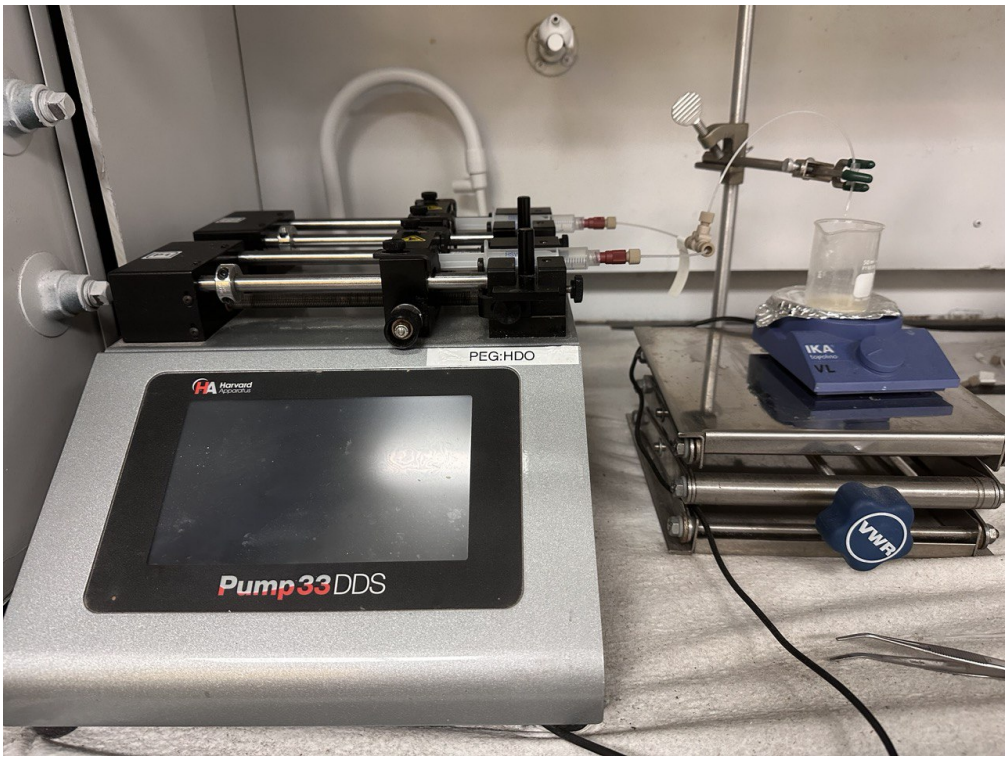

Figure 3.8: Pump 33 DDS (Dual Drive System) Syringe Pump from Harvard Apparatus with syringes stock, flow reactor circuit and quench containing beaker.

The flow circuit was assembled by connecting two input inlets to the syringes, linked to tubes with a diameter of 0.5 mm and a length of 10 cm each. The outlets of the two syringe tubes were merged using a T-mixer, resulting in a single outlet connected to a tube with a diameter of 1 mm and a length of 20 cm. As a result, the final flow rate at the outlet of the system was $0.5\,mL\,s^{-1}$. A beaker containing benzoic acid was positioned at the end of the flow reactor outlet for quenching the final solution, with an additional beaker placed nearby.

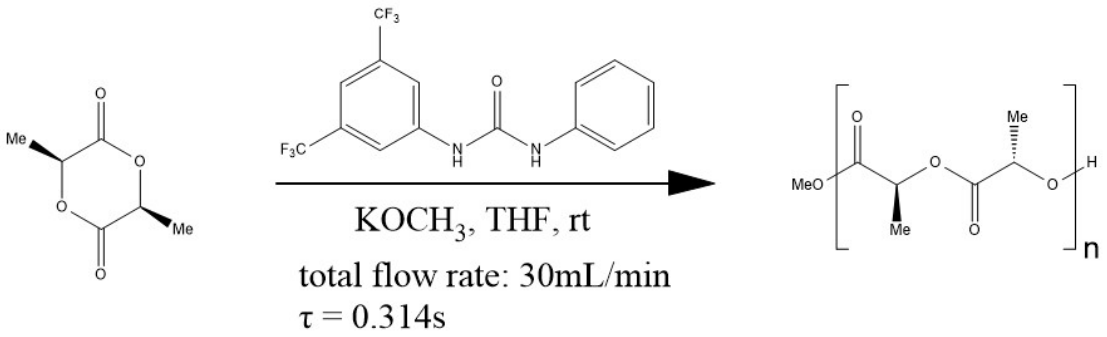

Figure 3.9: L-LA **(15)** polymerization in flow chemistry

The monomer stock solution consisted of 5 mmol of L-LA (L-Lactide) monomer **(15)** (720 mg) and 4.3 mL of THF. The catalyst stock solution contained 0.6 mmol of **(U-3)** (209 mg), combined with 0.2 mmol of $KOCH_3$ (14 mg) and 4.85 mL of THF.

With the stock solutions ready and positioned in the syringes, they were moved out of the nitrogen-filled glove-box. Initially, the two THF-filled syringes were placed in the syringe holder, and a preliminary run was initiated after calibrating the machine to ensure proper alignment, desired outlet flow rate and cleaning of the flow reactor. The resulting output was collected in an empty secondary beaker and disposed of in a designated chemical waste container.

Subsequently, the syringes containing the catalyst and monomer stock solutions were substituted into the syringe holder. The emptied beaker was once again positioned under the outlet, and the flow reaction was initiated. Nearly instantly with a couple

of seconds of delay, the beaker was swiftly replaced with another containing 250 mg of benzoic acid and 2 mL of THF as a quenching solution, ensuring minimal contamination from the previous run. A residence time of $t_r = 0.314$ s ensured that the exclusion of the initial drops from the final polymerization mixture, minimized contamination.

Within a 20-second interval, the reservoir of stock solutions was depleted, successfully concluding the reaction.

3.2 Cyclopropenimines catalysis

3.2.1 Experimental setup

The experimental setup and procedure is equal (except materials differences) to section 3.1.2 setup and procedure, in particular 4-methyl-benzyl-alcohol **(A-1)** or benzyl 2,2-bis(methylol)propionate **(A-2)** were used as initiators in a 50:1 = $[M_0]$: $[I_0]$, whereas concerning the catalyst system, 1-N,1-N,2-N,2-N-tetracyclohexyl-3-cyclohexyliminocyclopropene-1,2-diamine **(CPI)** was used as base together with (thio)ureas with a 50:1 = $[M_0]$: **[(CPI)]** and 50:2.5 or 50:2 = $[M_0]$: [(T)urea] monomer to catalysts initial concentrations ratios. Solvents such as THF or CH_2Cl_2 were exploited to obtain a monomer 1 M reaction solution concentration.

3.2.2 Material quantities and polymerization example

Entry 1 of table 4.1 polymerization was conducted with **(1)** (100mg, 0.98 mmol, 50 equiv.) which was combined with **(A-1)** (2.4 mg, 0.02 mmol, 1 equiv.) in the monomer stock vial. The catalyst stock vial contained a blending **(U-1)** (24.3 mg, 0.0490 mmol, 2.5 equiv.) and **(CPI)** (9.7 mg, 0.0196 mmol, 1 equiv.).

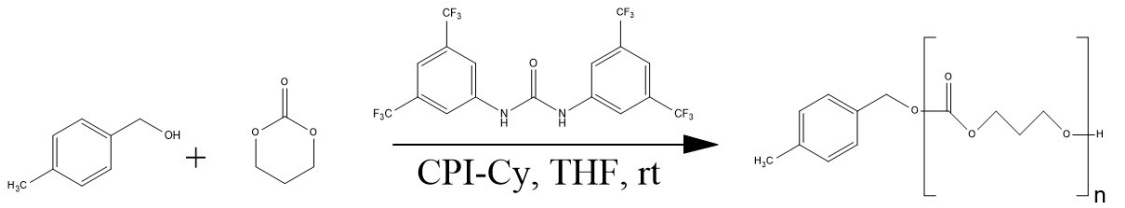

Figure 3.10: Entry 1 of table 4.1 polymerization reaction scheme (CPI-Cy refers to **(CPI)**).

The stock vial compound was dissolved in solutions with Tetrahydrofuran (944 µL), employed as the solvent. The reaction started upon pouring the catalyst stock solution into the monomer stock solution, which was quenched after 5 minutes with benzoic

acid.

Entry 2 of table 4.1 followed an equal procedure to the one described above but **(U-4)** (14.3 mg, 0.0490 mmol, 2.5 equiv.) was exploited in place of **(U-1)**, and an overall 954 µL of THF was exploited.

Similarly, entry 3 of table 4.1 was polymerized thanks to monomer **(2)** (150mg, 0.6 mmol, 50 equiv.) combined with **(A-1)** (1.5 mg, 0.012 mmol, 1 equiv.) in the monomer stock vial. The catalyst stock vial contained a blending **(U-1)** (14.9 mg, 0.03 mmol, 2.5 equiv.) and **(CPI)** (5.9 mg, 0.012 mmol, 1 equiv.).

In this case and for all the following cases regarding this section, the "Reverse adding" has been performed, namely the pouring of the monomer solution in the catalyst solution to start the polymerization reaction. 577 µL of THF to obtain a 1 M reaction solution were exploited. The reaction was quenched after 1 minute with benzoic acid in dissolved in THF.

Entry 4, 5, 9 and 10 of table 4.1 were polymerized similarly to entry 3 of table 4.1. In case of entry 4, **(U-4)** (8.8 mg, 0.030 mmol, 2.5 equiv.) substituted **(U-1)**, and exploited 583 µL of THF as solvent. In case of entry 5, **(TU)** (11.3 mg, 0.030 mmol, 2.5 equiv.) substituted **(U-1)**, and exploited 580 µL of THF as solvent, the reaction was quenched after 40 minutes. In case of entry 9, THF was substituted with dichloromethane (CH_2Cl_2) in the same volume and the reaction was quenched after 30 s. In case of entry 10, the difference with the synthesis of entry 3 consists in the replacement of **(A-1)** with **(A-2)** (2.7 mg, 0.012 mmol, 1 equiv.), the urea **(U-1)** reduction to (11.9 mg, 0.024 mmol, 2 equiv.) and 577 µL of THF were exploited. The reaction was quenched after 30 s.

Entry 6 of table 4.1 was polymerized thanks to monomer **(2)** (150mg, 0.457 mmol, 50 equiv.) combined with **(A-1)** (1.1 mg, 0.009 mmol, 1 equiv.) in the monomer stock vial. The catalyst stock vial contained a blending of **(U-1)** (11.3 mg, 0.023 mmol, 2.5 equiv.) and **(CPI)** (4.5 mg, 0.009 mmol, 1 equiv.), 580 µL of THF were exploited. The

reaction was quenched after 30 s.

Entries 7 of table 4.1, 8 of table 4.1 and 11 of table 4.4 were synthesised in the same manner of entry 6 of table 4.1 with minor differences. In the case of entry 7, THF was substituted with CH_2Cl_2, whereas for entry 8 of table 4.1 and 11 of table 4.4, **(A-2)** (2 mg, 0.009 mmol, 1 equiv.) substituted **(A-1)**, the urea **(U-1)** was reduced to (9.1 mg, 0.018 mmol, 2 equiv.) and 440 µL of THF were exploited. The reaction was quenched after 30 s.

Entry 11 of table 4.1 was synthesised with **(4)** (100mg, 0.365 mmol, 50 equiv.) in the monomer stock vial. The catalyst stock vial contained a blending of **(A-2)** (1.6 mg, 0.007 mmol, 1 equiv.) with **(U-1)** (9 mg, 0.0182 mmol, 2.5 equiv.) and **(CPI)** (3.6 mg, 0.0073 mmol, 1 equiv.). THF in 351 µL overall quantity was exploited to dissolve the stock vials compounds. The reaction was quenched after 5 minutes and the polymer was precipitated in Heptane.

Entry 12 of table 4.1 was synthesised with **(5)** (100mg, 0.335 mmol, 50 equiv.) in the monomer stock vial. The catalyst stock vial contained a blending of **(A-2)** (1.5 mg, 0.007 mmol, 1 equiv.) with **(U-1)** (8.3 mg, 0.017 mmol, 2.5 equiv.) and **(CPI)** (3.3 mg, 0.007 mmol, 1 equiv.). THF in 322 µL overall quantity was exploited to dissolve the stock vials compounds. The reaction was quenched after 30 s.

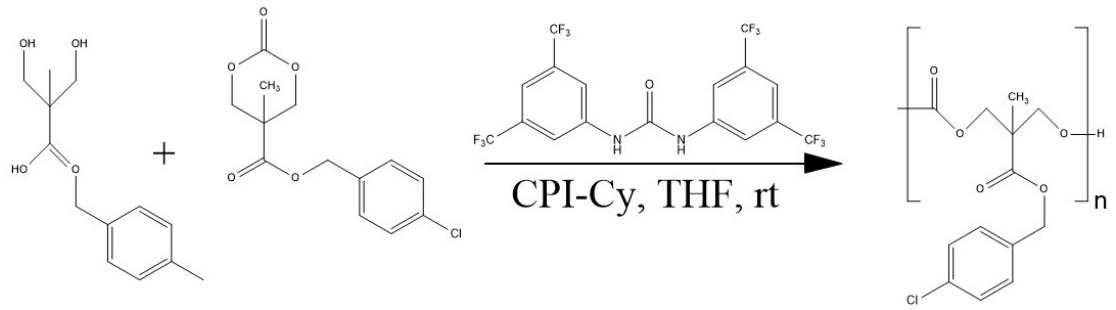

Figure 3.11: Entry 12 of table 4.1 polymerization reaction scheme (CPI-Cy refers to **(CPI)**).

Entry 12 of table 4.1 was synthesised with **(5)** (100mg, 0.335 mmol, 50 equiv.) in the

monomer stock vial. The catalyst stock vial contained a blending of **(A-2)** (1.5 mg, 0.007 mmol, 1 equiv.) with **(U-1)** (8.3 mg, 0.017 mmol, 2.5 equiv.) and **(CPI)** (3.3 mg, 0.007 mmol, 1 equiv.). THF in 322 µL overall quantity was exploited to dissolve the stock vials compounds. The reaction was quenched after 30 s.

Entry 13 of table 4.1 was synthesised with **(6)** (100mg, 0.2854 mmol, 50 equiv.) in the monomer stock vial. The catalyst stock vial contained a blending of **(A-2)** (1.3 mg, 0.0057 mmol, 1 equiv.) with **(U-1)** (7.1 mg, 0.0142 mmol, 2.5 equiv.) and **(CPI)** (2.8 mg, 0.0057 mmol, 1 equiv.). THF in 275 µL overall quantity was exploited to dissolve the stock vials compounds. The reaction was quenched after 30 s.

Entry 14 of table 4.1 and 12 of table 4.4 was synthesised with **(7)** (100mg, 0.3264 mmol, 50 equiv.) in the monomer stock vial. The catalyst stock vial contained a blending of **(A-2)** (1.5 mg, 0.0065 mmol, 1 equiv.) with **(U-1)** (8.1 mg, 0.0163 mmol, 2.5 equiv.) and **(CPI)** (3.2 mg, 0.0065 mmol, 1 equiv.). THF in 314 µL overall quantity was exploited to dissolve the stock vials compounds. The reaction was quenched after 30 s.

Entry 15 of table 4.1 was synthesised with **(8)** (200mg, 0.34 mmol, 50 equiv.) in the monomer stock vial. The catalyst stock vial contained a blending of **(A-1)** (0.8 mg, 0.0068 mmol, 1 equiv.) with **(U-1)** (6.7 mg, 0.0135 mmol, 2 equiv.) and **(CPI)** (3.4 mg, 0.0068 mmol, 1 equiv.). THF in 438 µL was exploited to dissolve the stock vials compounds and obtain a 0.75M monomer solution. The reaction was quenched after 30 s. Entry 16 of table 4.1 and 13 of table 4.4 was synthesised similarly to the previous entry 15 of table 4.1, but the quantity were increased to **(8)** (1.472 g, 2.5 mmol and 50 equiv.) and consequently the catalysts quantities, keeping the same ratios as in the case of entry 15. THF was exploited in 3.21 mL and the reaction mixture was quenched in 10 minutes.

3.3 TAC experiments

3.3.1 Experimental setup and procedure

The experimental setup is similar, once again, to the one in section 3.1.2. A PTFE 0.2 µm filter is introduced in the glovebox as well. Unlike experimental procedure section 3.1.2, once the catalyst stock vial solution is prepared (made of the base and eventually the urea with or without combination with the salt) it is filtered. The filtering is performed by purging the solution into a 1 mL plastic syringe with a PTFE filter attached to its end. The filtered solution is collected in a new vial. The reaction is then performed following the procedure described in section 2.1.1, as well as the following steps (quenching, analysis, purification etc.).

TAC polymerization experiments

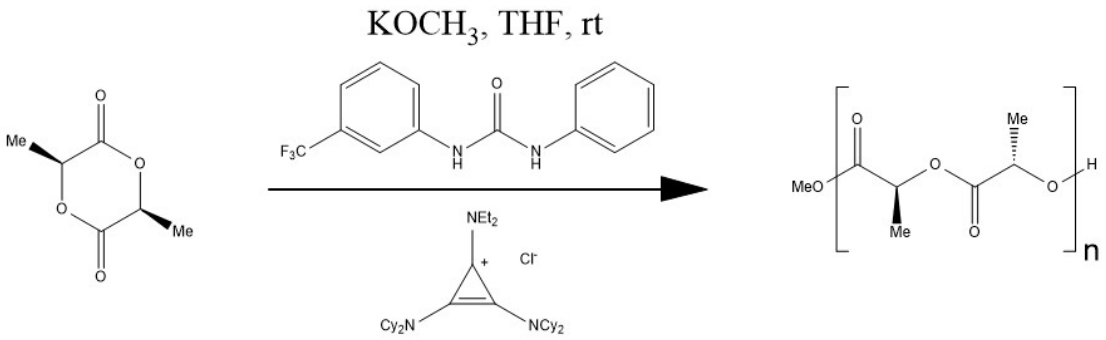

Figure 3.12: Entry 1 of table 4.5 synthesised with potassium methoxide, **(S-1)** salt and **(U-4)**. Polymerization reaction scheme.

Entry 1 of table 4.5 was synthesised from **(15)** (200 mg, 1.387 mmol, 50 equiv.) dissolved in THF, consisting of the monomer stock solution; The catalyst stock solution was realised with $KOCH_3$ (1.9 mg, 0.028 mmol, 1 equiv.), **(U-4)** (19.4 mg, 0.069 mmol, 2.5 equiv.) dissolved in THF, stirred and then it was added the **(S-1)** (14 mg, 0.028 mmol, 1 equiv.). After stirring and filtering the catalyst stock solution, the reaction was set to

begin by mixing the monomer stock solution with the catalyst one, an overall 1,152 µL of THF was exploited, the reaction was quenched after 20 s. Entry 2 of table 4.5, followed the same process and materials of entry 1, with exception for the absence of **(S-1)** and exploiting an overall 1,166 µL of THF.

Entry 3 of table 4.5 was synthesised from **(15)** (200 mg, 1.387 mmol, 50 equiv.) dissolved in THF, consisting of the monomer stock solution; The catalyst stock solution was realised with KH base (1.1 mg, 0.028 mmol, 1 equiv.), **(U-5)** (14.7 mg, 0.069 mmol, 2.5 equiv.), **(A-1)** (3.4 mg, 0.028 mmol, 1 equiv.) dissolved in THF, stirred and then it was added the **(S-1)** (14 mg, 0.028 mmol, 1 equiv.). After stirring and filtering the catalyst stock solution, the reaction was set to begin by mixing the monomer stock solution with the catalyst one, an overall 1,155 µL of THF was exploited, the reaction was quenched after 30 s. Entry 4 of table 4.5 was synthesised in equal manner to entry 3, without the adding of the salt **(S-1)** and with an overall 1,169 µL of THF.

Entry 5 of table 4.5 was synthesised from **(15)** (100 mg, 0.694 mmol, 50 equiv.) dissolved in THF, consisting of the monomer stock solution; The catalyst stock solution was realised with Lithium tert-butoxide (LiOtbut) base (1.1 mg, 0.014 mmol, 1 equiv.), **(U-5)** (7.4 mg, 0.035 mmol, 2.5 equiv.), **(A-1)** (1.7 mg, 0.014 mmol, 1 equiv.) dissolved in THF, stirred and then it was added the **(S-1)** (7 mg, 0.014 mmol, 1 equiv.). After stirring and filtering the catalyst stock solution, the reaction was set to begin by mixing the monomer stock solution with the catalyst one, an overall 578 µL of THF was exploited, the reaction was quenched after 30 s. Entries 6-8 of table 4.5 were synthesised in equal manner to entry 3, with minor difference. Entry 6 was synthesised without the adding of the salt **(S-1)** and with an overall 584 µL of THF. Entry 7 synthesis was attempted without the adding of the urea **(U-5)** and with an overall 584 µL of THF. Finally, entry 8 was synthesised without the adding of both **(S-1)** and **(U-5)** with 591 µL of THF.

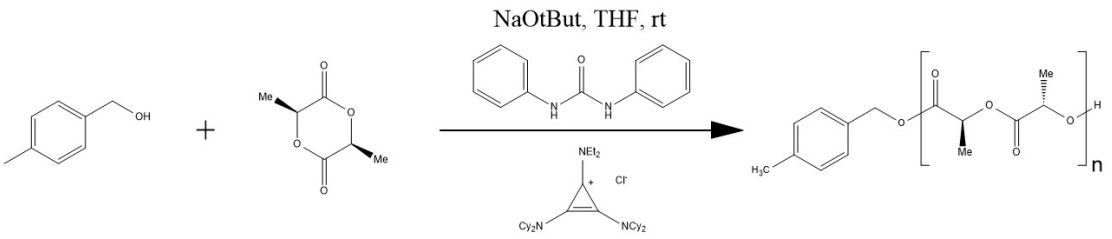

Figure 3.13: Entry 8 of table 4.5 synthesised with NaOtbut, **(S-1)** salt and **(U-*5*)** polymerization reaction scheme.

Entry 9 of table 4.5 was synthesised from **(*15*)** (150 mg, 1.041 mmol, 50 equiv.) dissolved in THF, consisting of the monomer stock solution; The catalyst stock solution was realised with Sodium tert-butoxide (NaOtbut) base (2 mg, 0.021 mmol, 1 equiv.), **(U-*5*)** (11 mg, 0.052 mmol, 2.5 equiv.), **(A-1)** (2.5 mg, 0.021 mmol, 1 equiv.) dissolved in THF, stirred and then it was added the **(S-1)** (10.5 mg, 0.021 mmol, 1 equiv.). After stirring and filtering the catalyst stock solution, the reaction was set to begin by mixing the monomer stock solution with the catalyst one, an overall 865 µL of THF was exploited, the reaction was quenched after 30 s. Entries 10-12 of table 4.5 were synthesised in equal manner to entry 9, with minor difference. Entry 10 was synthesised without the adding of the salt **(S-1)** and with an overall 875 µL of THF. Entry 11 synthesis was attempted without the adding of the urea **(U-*5*)** and with an overall 876 µL of THF. Finally, entry 12 was synthesised without the adding of both **(S-1)** and **(U-*5*)**, with 886 µL of THF. Entries 13-16 of table 4.5 synthesis attempts were performed in the same manner of entries 9-12 of table 4.5 synthesis attempts, with the replacement of the NaOtbut base with Potassium tert-butoxide (KOtbut, 2.3 mg, 0.021 mmol, 1 equiv.).

Entry 17 of table 4.5 was synthesised from **(*15*)** (300 mg, 2.082 mmol, 50 equiv.) dissolved in THF, consisting of the monomer stock solution; The catalyst stock solution was realised with LiOtbut base (3.3 mg, 0.042 mmol, 1 equiv.), **(U-*5*)** (22 mg, 0.104 mmol, 2.5 equiv.), **(A-1)** (5.1 mg, 0.042 mmol, 1 equiv.) dissolved in THF, stirred and

then it was added the **(S-4)** (8 mg, 0.035 mmol, 0.84 equiv.). After stirring and filtering the catalyst stock solution, the reaction was set to begin by mixing the monomer stock solution with the catalyst one, an overall 2,043 µL of THF was exploited, the reaction was quenched after 30 s. Entry 18 of table 4.5 was synthesised in the same manner, without the exploitation of **(U-*5*)** and an overall 2,043 µL of THF were employed. Entries 19-20 of table 4.5 were synthesised exactly in the same manner of entries 17-18 of table 4.5 but NaOtbut (4 mg, 0.042 mmol, 1 equiv.) replaced the LiOtbut.

Finally, entry 21 of table 4.5 was synthesised from **(15)** (300 mg, 2.082 mmol, 50 equiv.) dissolved in THF, consisting of the monomer stock solution; The catalyst stock solution was realised with LiOtbut base (3.3 mg, 0.042 mmol, 1 equiv.), **(U-*5*)** (22.1 mg, 0.104 mmol, 2.5 equiv.), **(A-1)** (5.1 mg, 0.042 mmol, 1 equiv.) dissolved in THF, stirred and then it was added the **(S-3)** (23.5 mg, 0.042 mmol, 1 equiv.). After stirring and filtering the catalyst stock solution, the reaction was set to begin by mixing the monomer stock solution with the catalyst one, an overall 2,027 µL of THF was exploited, the reaction was quenched after 30 s.

3.4 Thermal experiments

3.4.1 General DSC experimental setup and procedure

The vast majority of the thermal experiments were conducted through means of a differential scanning calorimetry (DSC) Perkin Elmer 8500 machine shown in Figure 3.14. The samples were prepared following a procedure through which an aluminium pan, was tared on an electronically balanced tare, filled with $\tilde{1}$ mg of sample, covered with an aluminium lid and then clamped together with a mechanical clamping tool. The sample weight is measured and registered during the operation. Once the sample is ready, the thermal experiment can start. The DSC machine is turned on, as well as its cooling system to refrigerate the reservoir in order to keep fine precision of the heat flux measurements and temperature control of the furnace during the run. The sample is placed in the sample holder, an appropriate program for the thermal analysis is set up, that will define the number of heating, cooling and isothermal cycles and steps, heating and cooling rates, maximum temperature to achieve during the analysis at each cycle and all the relevant parameters. The sample weight is entered as a data while creating the sample list in the software (containing the sample position to be used), in order to normalize the quantities such as the enthalpy of fusion with respect to the weight. The double furnaces are placed under a $20\,\mathrm{mL\,min^{-1}}$ Nitrogen stream. The sample and reference pan (an empty pan used as reference) are loaded inside the furnace and then capped with the appropriate lids. Once all these steps are performed the thermal experiments starts following the thermal program described in the appropriate method file for the sample.

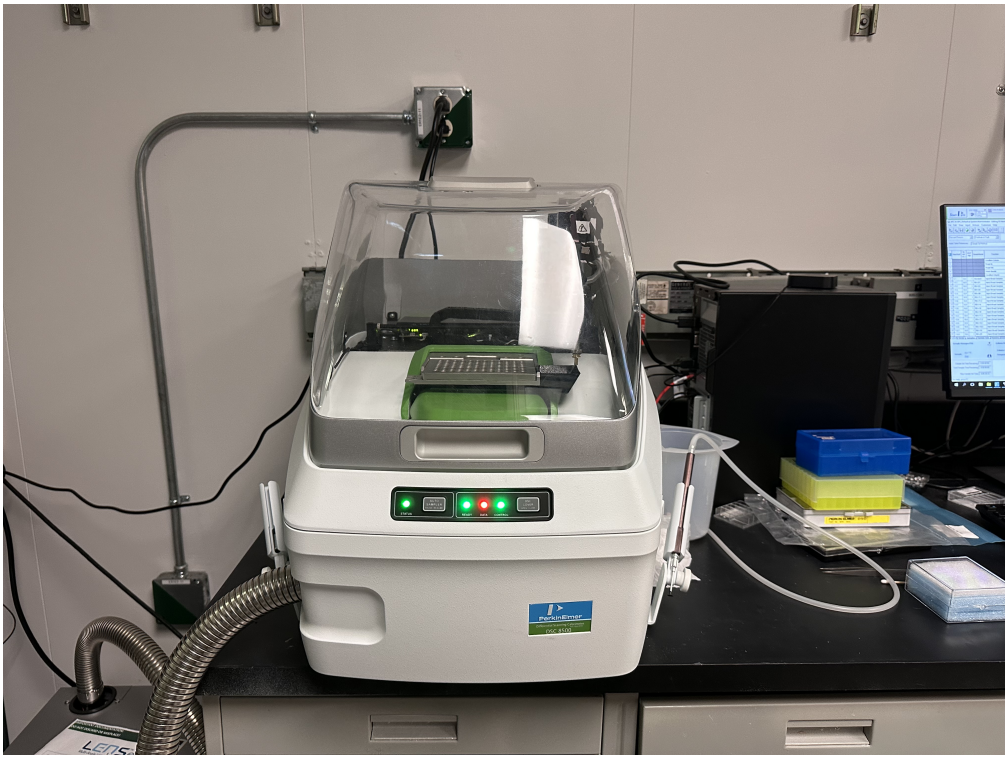

Figure 3.14: DSC 8500 Perkin Elmer machine.

3.4.2 DSC analysis of PLLA: data set creation for supervised ML predictive model training

A large number of PLLA (poly**(15)**) was polymerized through means of an automated flow chemistry synthesis system, varying synthesis parameter such as reactor circuit geometry and flow rate. Parallel synthesis reactions lead to a high-throughput synthesis of PLLA library. Thermal analyses of the samples were performed following the setup and procedure of section 3.4.1, using a heating rate of 20 °C min^{-1} and a temperature range from 20 °C to 175-185 °C. The cooling cycle was operated as follow: Cooling cycle: 185-175 °C to 20 °C at 20 °C min^{-1}, hold for 1 min at 20 °C, then the re-heating cycle was performed from 20 °C to 175-185 °C at 5 °C min^{-1}.

3.4.3 DSC analysis for CPI catalysts system made polymer

DSC was performed on DSC Perkin Elmer 8500 machine or Q-2000 DSC (TA Instruments). Relevant samples (regarding the PLA, whose thermal properties were under main focus of the study), were analysed with the Q-2000 DSC instrument. In the last case, samples were enclosed in aluminium pans and measurements carried out under N_2 atmosphere (50 mL min^{-1} flow rate) using a heating rate of 10 °C min^{-1} and a temperature range from 20 °C to 220 °C. The cooling cycle was operated as follow: Cooling cycle: 220 °C to 175 °C at 1 °C min^{-1}, hold for 30 min at 175 °C, 175 °C to 150 °C at 3 °C min^{-1} and 150 °C to RT at 10 °C min^{-1}. Other samples were analysed by the DSC Perkin Elmer 8500 instrument with the same setup and procedure described in section 3.1.2. In case of PLA samples, the optimized thermal analysis program is the same previously described for the Q-2000 DSC instrument. In the case of carbonate polymers, the analysis thermal cycles were operated firstly performing the following heating cycle: heating rate of 20 °C min^{-1} and a temperature range from -50 °C to 150 °C. The cooling cycle was operated as follow: 150 °C to -50 °C at 10 °C min^{-1}, hold for 1 min at -50 °C, then reheating in equal condition to the first heating cycle, followed by a ballistic cool-down.

3.4.4 Thermal assisted RCDEP and thermal degradation.

In order to investigate the degradability and recyclability of the synthesized polymers, thermally assisted RCDEP and experiments were performed.

RCDEP and thermal degradation through DSC and isothermal heating experiments

following the procedure and setup of section 3.4.1 DSC samples were prepared. In this case an amount of 0.5 mg of polymer is used to avoid excessive pressure development inside the DSC pan. Each target polymer was exploited to prepare three samples,

one containing the polymer only, one with the only adding of **(DBU)** and another one with the only adding of CPI. The two were added in a 10% quantity in weight (with respect to the polymer). Subsequently the DSC experiment was started, a single heating cycle: heating rate of 20 °C min^{-1} and a varying temperature range from 20 °C to 250/300/350/400 °C depending on the sample.

Another experiment consisted of setting up a sample of bulk polymer, and a sample of bulk polymer (or alternatively with the addition of CPI in a 10% quantity in weight, with respect to the polymer) in a 2 or 4 DRAM glass vial, which was introduced in the glove-box antechamber to fill it with Nitrogen atmosphere. The vial was subsequently placed on a Corning™ PC-220 Pyroceram™ Hot Plate Stirrer, 480°C, Glass Ceramic shown in Figure 3.15. The experiment was performed placing the vials on the heater hot plate for 12 hours at heating level 4 or 5, corresponding to 170 and 230 °C respectively.

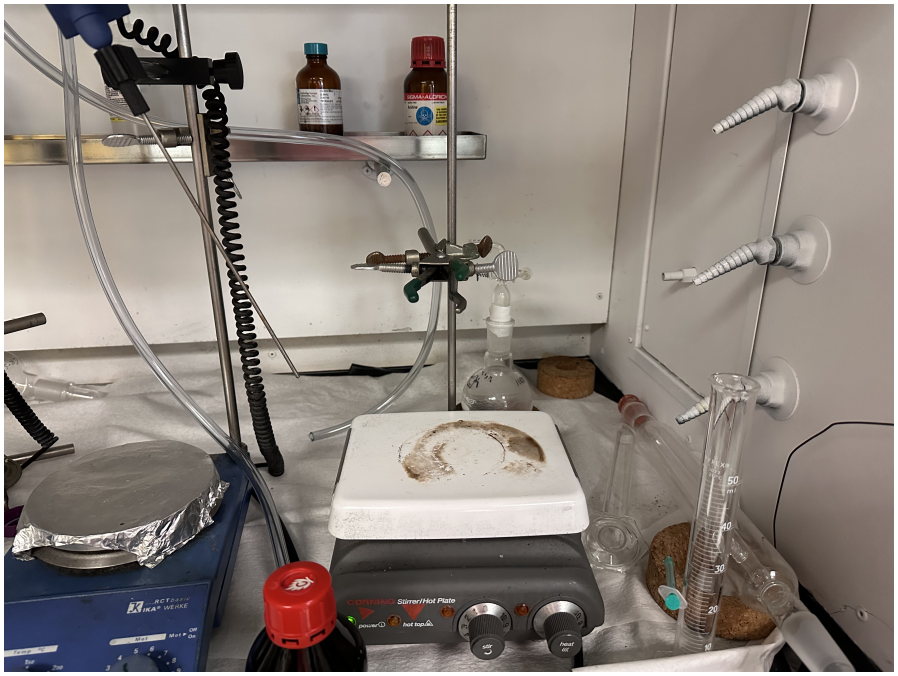

Figure 3.15: Corning™ PC-220 Pyroceram™ Hot Plate Stirrer.

Both for DSC experiments and Hotplate ones, NMR analyses of the samples were performed with setup and procedure describer in section 3.5.2.

3.4.5 TGA for recyclable materials

Decomposition Thermal experiments and analysis were run on a AutoTGA 2950HR V5.4A machine to perform Thermogravimetric analysis, shown in Figure 3.16. Appropriate pan (aluminium or platinum depending on the experiment temperatures) were filled with the sample, registering the weight similarly to the DSC analysis case, the sample pan is not capped and placed on a sample holder, that will allow the sample to volatilize during the analysis and to perform a real time mass variation and Mass spectra analysis during the experiment, giving further insight of how the material reacts and decompose in temperature under both an air or nitrogen environment. The analyses were conducted to explore the decomposition mechanism of the several polymers. In particular the polycarbonates were analysed, which are derivatives of the trimethylene carbonate **(1)**, through means of its functionalization.

Figure 3.16: AutoTGA 2950HR V5.4A machine for TGA-MS analysis.

3.5 Characterization setup and process

3.5.1 Purification of the polymer

The polymerization mixture is extracted with a Pasteur pipette and added to a plastic centrifuge tube filled with methanol (or another liquid). This process leads to the precipitation of the polymer. The tube is then stirred on a vortex plate and subjected to a three-fold process consisting of a centrifuging cycle at 4400 rpm for 20 minutes, 10 to 20 mL of superficial solution discarding and methanol refilling.

At the last centrifuging cycle, most of the solvent is discarded, the residual material along with the precipitated polymer at the tube's bottom is cautiously dried. The final drying process is performed initially with a nitrogen stream through the Schlenk line, then once the polymer is dried enough, it can be performed within a vacuum glass desiccator containing desiccants or within a controlled temperature vacuum oven, combining vacuum suction and slightly higher temperature to eliminate solvents from the polymers. The drying process usually lasts at least 24 hours.

3.5.2 NMR analysis

All the NMR analysis were performed with a 400 MHz Bruker Avance NMR instrument shown in Figure 3.17

Figure 3.17: 400 MHz Bruker Avance NMR instrument.

Monomer to polymer conversion estimation

A small 2 DRAM vial labelled as the "crude" sample is utilized. It is filled with a small portion of the quenched reaction solution and then gently dried using a nitrogen stream from the hood Schlenk line or the glove-box vacuum anti-chamber.

Once the crude sample is partially dried and briefly subjected to vacuum conditions either within a vacuum glass desiccator or the glove-box anti-chamber, the sample is ready for Nuclear Magnetic Resonance (NMR).

For NMR analysis, a Pasteur pipette is employed to extract a small amount of the crude sample, which is then carefully introduced into an NMR glass tube. A second pipette is used to withdraw the NMR solvent (typically $CDCl_3$, i.e., deuterated chloroform) and introduced into the first pipette. This facilitates the transfer of

the crude sample into the NMR glass tube, where it dissolves. Alternatively, the NMR solvent is directly poured into the vial and the dissolved unpurified mixture is withdrawn and poured in the NMR tube. The NMR tube is subsequently capped, tagged, and gently manipulated to ensure any residual sample along the tube's interior is collected and dissolved.

After this, the NMR tube is equipped with an NMR tube adapter, and the solvent level is verified and adjusted if needed. The NMR sample is placed within the NMR machine's sample holder, and the analysis is set up usually involving proton NMR (^{1}H-NMR) analysis. Analysing the crude sample through an ^{1}H-NMR analysis allows for an estimation of the ratio between the polymer and monomer within the final solution, thereby determining the monomer's percentage conversion into polymer (alternatively ^{13}C-NMR is also available).

Purified and dried polymer analysis: determining DP and molecular compound structure

The purified and dried polymer is weighted and poured into the NMR tube in a 20 to 40 mg weight quantity. Proceeding as in the conversion estimation case, dissolution of the compound in the NMR tube is performed through means of the adequate NMR solvent.

NMR (^{1}H-NMR and sometimes ^{13}C-NMR) analysis are conducted. This step aims to determine the degree of polymerization, recognizing moieties of the alcohol initiating species and computing the ratio of repeating units quantity with respect to the one of the alcohol to estimate the polymerization average degree of the polymer. In order to verify that the correct compound formation has happened, integration of the detected peaks, shifts value, as well as peaks shape due to spin-spin coupling are carefully analysed.

3.5.3 GPC analysis setup and procedure

GPC measurements were performed using a Waters Advanced Polymer Chromatography (APC) equipped with a Waters 410 differential refractometer shown in Figure 3.18. The set of columns consisted of three Waters ACQUITY APCTMAQ (pore sizes: 450/200/125, dp: 2.5 µm). THF was used as the eluent at a flow rate of 0.75 mL min^{-1} at 25 °C. The APC system was calibrated with polystyrene standards and elution time shifts checked by a 13 kDa PS (polystyrene) standard injected with each sample set.

Figure 3.18: Waters Advanced Polymer Chromatography (APC) equipped with a Waters 410 differential refractometer for GPC analysis.

If aliquots were extracted during the reaction for monitoring purposes, the crude aliquot samples may also require GPC analysis. Unlike the NMR case, these samples do not necessitate drying. They are extracted from the running polymerization mixture, quenched and placed within a small 2 DRAM glass vial, labelled with the crude sample name and quenching time.

For GPC analysis, an amount of 5 mg per milliliter of solvent (typically THF) is weighted and added to the vial. The specific GPC solvent is added, and the solution is vigorously mixed to ensure full dissolving before being withdrawn and filtered using a Pasteur glass pipette and a plastic syringe fitted with a 0.2 µm PTFE filter. The filtered solution is transferred to a specially designed GPC sample holder vial, and the analysis is configured through the machine's software.

The same treatment is performed for the post precipitation and purification obtained polymer, where the sample is withdrawn before fully drying the purified polymer.

Chapter 4

Results and discussion

4.1 Cyclopropenimines catalysis

In OROP (organic ring-opening polymerization) and in particular in anionic reaction processes, organic bases paired with ureas and alcohol chain-end or initiator are a well tested catalyst system. CPIs (Cyclopropenimines) were targeted as a promising compound class to serve as bases to promote OROP. CPIs are found to be accessible, soluble, stable, tunable, and inexpensive bases. Their tunability can be easily performed through the pendant group functionalization, attached to the imino nitrogen atom bonded to the cyclopropene ring. In the following section, my internship work related to the study of the possible exploitation of this new catalyst system, leading to a scientific publication [21] is presented. In particular, in the following section a wide range of polylactides and polycarbonates materials, comprised of their synthesis results are displayed, furthermore, the same compounds synthesis are presented under different catalyst systems for comparison. To continue, analysis through DSC and GPC measurements of PLLA samples, realised by Stanford university collaborators, will be reported and discussed.

4.1.1 Polycarbonates synthesis and comparison with other catalyst systems

A wide range of carbonate monomers exploited to synthesise their related polymer under several different catalysts systems and conditions are reported below in table 4.3. Initial experiments were performed in order to find the best catalyst system featuring **(CPI)**, comprising the choice of the urea co-catalyst, solvent and reaction time. Two different ureas: **(U-1)**, **(U-4)** and a thiourea **(TU)** were exploited separately on the same system in order to compare their catalyst activity when combined with **(CPI)** and **(A-1)**.

(1) also known as TMC is notoriously exploited in medicine through its homopolymer PTMC (and possibly in a block-co-polymer configuration), for example it has been exploited to create cell sheet scaffolds for cells seeding [59].

(1) was polymerized both with **(U-1)** and the less acidic **(U-4)** (entries 1 and 2 respectively, of table 4.1). The resulting PTMC highlighted the importance of well matching the conjugate acid of the **(CPI)** base and urea pK_a, in agreement with literature [60]. Indeed, the pK_a of **(U-1)** = 13.8 and the pK_a of (CPI-H+) = 14.7 [21], slightly promoting an anionic ROP, whereas for **(U-4)** it would promote a cooperative ROP system given is far less acidic behaviour, with not as well matched pK_a as in the first case. PTMC synthesised with **(U-1)** resulted in 97.7% monomer conversion compared to 83.4% with **(U-4)**, after 5 minutes. Furthermore, the dispersity index indicated an equal result of narrow $Đ$ = 1.04 (the molecular weight distribution of entry 1 from table 4.1 is shown in Figure 1), which indicates also that the **(U-1)** system is more selective given the higher degree of conversion that usually leads to a broadening of the molecular weight distribution. The polymerization degree was found to be comparable to the target one (47 vs 50 for entry 1 of of table 4.1 and 45 vs 50 for entry 2 of table 4.1). This result is of great importance since polymer for biomedical applications require the narrowest molecular weight distribution possible and usually also low degree of polymerization.

(2) was synthesised under the same catalyst systems with the further addition of the new **(CPI)** and **(TU)** catalyst system (entries 3 for **(U-1)**, 4 for **(U-4)** and 5 for **(TU)** of table 4.1), confirming the same trend found in PTMC for the two ureas. The thiourea catalyst system provided (as expected) a reduction of the catalyst activity with respect to the two ureas, requiring 40 minutes to reach the same conversion that the other two co-catalyst made possible to be reached in 30 s. However, the **(CPI)**-**(TU)** based catalyst system provided superior selectivity leading to lower $Đ$ and nearly perfect mono-modality of the molecular weight distribution (shown in Figure 2).

The bi-modality resulting for the poly**(2)** is a critical issue and it was found also for poly**(3)** (entry 6 in table 4.1, shown in Figure 3). ^{1}H-NMR analysis of the monomer unit highlighted some impurity traces. Re-crystallization was performed to enhance the purity of the monomers. Re-performing the synthesis with re-crystallized monomer, however, did not lead to a different result.

The performing of "reverse-addition" (monomer stock-solution pouring into the catalyst stock solution to start the reaction) slightly ameliorate the results, the chain-growth of the polymer sequentially adds one monomer unit at the time, therefore it is more important to start the reaction through a non uniform adding of the monomer stock solution (due to the pouring of the monomer stock solution in the catalyst one through syringe pumping) rather than the catalyst one. In this way the catalyst molecules can initiate the reaction simultaneously and perform chain-growth with the feeding of monomer stock solution in time, avoiding different initiation in time which potentially leads to broad molecular weight distribution.

The problem was further solved either by promoting H-bonding, to enhance the ureas co-catalyst activity and therefore selectivity of the catalyst system, with an organic non-competitive solvent such as dichloromethane (CH_2Cl_2) rather than THF, since solvents with lower donor number enhance H-bonding interactions [61], the result is shown in entry 7 of table 4.1 (and in Figure 4). Another solution consisted in the exploitation of **(A-2)** diol as initiator (entry 8 in table 4.1), the hypothesis was that at high conversion, step-growth mechanisms may appear and leading to bi-modality due to premature termination of the growing chain, confirmed by the mono-modality of molecular weight distribution (shown in Figure 5) resulting by the exploitation of a diol initiator. The same methods were applied in case of **(2)** and the results are represented in entries 9 and 10 of table 4.1.

Monomers **(4)**,**(5)**, **(6)**, and **(7)** were further polymerized exploiting the optimized catalyst system consisting of the diol alcohol initiator **(A-2)** combined with **(CPI)** and

(U-1), in THF and with "reverse-addition". The results are reported for entries 11, 12, 13 and 14 respectively, in table 4.1. The system led to high conversion in short reaction times and narrow dispersity indexes, except for entry 11 from table 4.1 exhibiting a broad mono-modal molecular weight distribution.

A particular mention needs to be made for monomer **(8)** which presents vitamin-E as substituent. It was synthesised at room temperature, even if based on Thorpe-Ingold effect, a low ceiling temperature and thermodynamic inhibition of polymerization were expected, due to its propensity to cyclization [3]. In particular, entry 15 in table 4.1 shows conversion of 86% in 30 s with a $Đ$ = 1.09, however a reaction was performed for longer time and listed as entry 16 in table 4.1 and entry 14 of table 4.4, delivering a $Đ$ = 1.14 which has been reached after 10 minutes, with conversion reaching ~100% after 1 minute, showing the high selectivity of the catalyst system. ^{1}H-NMR spectra of entries 15 and 16 reaction mixture are available in Figures 11, 9 and 10. In Figure 10 is highlighted the monomer doublets peaks, 2H at $\delta = 4.97$ ppm shift and 2H at $\delta = 4.38$ ppm shift, whereas the same protons of the monomer ring closed unit, are found in the open linear chain polymer, composing the 4H at $\delta = 4.52$ ppm shifted singlet peak. Finally, the ^{1}H-NMR spectrum of the quenched reaction mixture aliquot, after 1 minute, is shown in Figure 12 where a nearly full conversion is already visible.

A series of monomers where polymerized with different catalyst systems which were already studied and reported in literature, such as the combination of an alcohol with **(DBU)** organic base and **(U-2)** in solution with THF as organic solvent. Another exploited system is the combination of $KOCH_3$ alkoxide strong base with **(U-4)** in THF as solvent.

A first comparison can be made between PTMC obtained with **(CPI)** in entry 1 of table 4.1 and entry 1 of table 4.3 obtained with **(DBU)** and **(U-2)**, although the reaction time are not the same, the **(CPI)** catalyst system retained a narrower molecular weight distribution at nearly full conversion, exhibiting higher selectivity. The livingness of

Entry	Monomer	Initiator	Urea	Solvent	Time(s)	Conv.(^{1}H-NMR)	$Đ$ (GPC)	DP (^{1}H-NMR)
1	**(1)**	**(A-1)**	**(U-1)**	THF	5 mins	97.7%	1.04	47
2	**(1)**	**(A-1)**	**(U-4)**	THF	5 mins	83.4%	1.04	45
3	**(2)**	**(A-1)**	**(U-1)**	THF	60	96.1%	1.14	57
4	**(2)**	**(A-1)**	**(U-4)**	THF	60	91%	1.18	51
5	**(2)**	**(A-1)**	**(TU)**	THF	40 mins	95%	1.08	53
6	**(3)**	**(A-1)**	**(U-1)**	THF	30	91.2%	1.06	60
7	**(3)**	**(A-1)**	**(U-1)**	CH_2Cl_2	30	92.3%	1.07	51
8	**(3)**	**(A-2)**	**(U-1)**	THF	30	95%	1.06	52
9	**(2)**	**(A-1)**	**(U-1)**	CH_2Cl_2	30	93.9%	1.08	70
10	**(2)**	**(A-2)**	**(U-1)**	THF	30	94%	1.06	43
11	**(4)**	**(A-2)**	**(U-1)**	THF	5 mins	88.0%	1.29	38
12	**(5)**	**(A-2)**	**(U-1)**	THF	30	94.0%	1.08	34
13	**(6)**	**(A-2)**	**(U-1)**	THF	30	92.0%	1.07	43
14	**(7)**	**(A-2)**	**(U-1)**	THF	30	91.0%	1.05	39
15	**(8)**	**(A-1)**	**(U-1)**	THF	30	86.0%	1.09	44
16	**(8)**	**(A-1)**	**(U-1)**	THF	10 mins	100%	1.14	52

Table 4.1: Batch polymerization experiments exploiting Urea and **(CPI)** catalyst system.

the PTMC OROP with DBU and ureas has already been proven [6, 25], yet **(CPI)** catalyst system yielded a living polymerization with first order kinetics, therefore confronting the polymerization time and the achieved conversion, it can be asserted that the **(CPI)** based catalyst system leads to higher activity as well.

Entry 3 of table 4.3 obtained from **(6)** with **(A-1)**, **(DBU)** and **(U-2)** catalyst system exhibited lower conversion 82% in a longer 80 s reaction time, with $Đ$ = 1.10 whereas

the same monomer in entry 13 of table 4.1 with the **(CPI)** catalyst system lead to 92% conversion in 30 s and $Đ$ = 1.07.

Entry 8 in table 4.1 obtained from **(3)** with **(CPI)** and the same monomer obtained with **(DBU)** in entry 6 of table 4.3 show the same trend of the previously mentioned case. Higher conversion was reached for the **(CPI)** catalysed synthesis at 95% within 30 s reaction time compared with the 91% in 90 s of the one where **(DBU)** was exploited in the synthesis. Contrarily to the higher activity of the **(CPI)** based catalyst system, the molecular weight distribution was finely controlled in both systems, which exhibited very small dispersity index $Đ$ = 1.05 for entry 6 of table 4.3 and $Đ$ = 1.06 for entry 8 of table 4.1. The same monomer was polymerised under $KOCH_3$ and **(U-4)** urea. The system activity was very high, reaching conversion of 76% in only 15 s, however the slow initiation rates combined with rapid propagation rates, leaded in this case to a quite broad molecular weight distribution with $Đ$ = 1.21, as shown in entry 8 of table 4.3.

Finally, the results of polymers synthesis, obtained from monomer **(2)**, are shown as entries 10 of table 4.1 and 7 of table 4.3, showing similar activity of the catalyst and rapid conversion. On the contrary, the molecular weight distribution control by the catalyst system widely differs. The one based on **(CPI)** catalyst synthesis system exhibits a narrower molecular weight distribution ($Đ$ = 1.06) compared to the one based on **(DBU)** ($Đ$ = 1.20), visible from the dispersity index, due to the catalyst system higher selectivity.

4.1.2 Polylactide synthesis, thermal and structural properties

PLA and PLLA samples were synthesised by Stanford colleagues with the same similar catalysts system exploited for the carbonate monomers and based on **(CPI)**, leading to the polymerization of a racemic lactide (rac-LA) mixture monomer **(16)** in only 2 seconds with nearly complete conversion and narrow molecular weight distribution

[21]. This synthesis result was achieved by choosing the correct **(CPI)** base paring with urea whose pK_a was similar to the base conjugate acid and exploiting the H-bonding promoting CH_2Cl_2 solvent, avoiding competitive enolization which results in broader molecular weight distribution and lower DP [62]. The main polymerization results obtained with this catalysis system for PLA are reported in table 4.2. Samples were also

Entry	Monomer	Catalysts	Solvent	time(s)	T(°C)	Conversion(^{1}H-NMR)	DP (^{1}H-NMR)	$Đ$ (GPC)	T_m(°C)	Pm
1	**(15)**	**(U-1) + (CPI)**	THF	10	RT	94%	98	1.04	168	1
2	**(16)**	**(U-3) + (CPI)**	THF	60	-15	97	101	1.04	169	0.85
3	**(16)**	**(U-3) + (CPI)**	THF	2 h	-36	>99	232	1.05	173	0.88

Table 4.2: PLLA and PLA obtained exploiting the **(CPI)** catalyst system.

analyzed with DSC in order to investigate the thermal properties of the PLA obtained with this catalyst system. An L-LA pure enantiomeric monomer **(15)** was polymerized to PLLA (entry 1 of table 4.2) and its thermal properties were compared with other two PLA obtained from **(16)** monomer. Their synthesis results and conditions are reported as entries 2 and 3 in table 4.2 for completeness. The DSC 2^{nd} heating spectra of entries 1-3 of table 4.2, in this order, are reported in Figures 29, 30 and 31.

A brief pause to delve deeper into the performance of this catalyst system for poly**(15)** and more generally PLA, is quite mandatory. Confronting entry 1 of table 4.2 with others of further sections, for example entry 2 of table 4.5 exploiting potassium methoxide and **(U-4)** highly active and selective catalyst, similar conversion of the **(CPI)** catalyst based system were achieved in half the time, with far greater control over the molecular weight distribution ($Đ$ = 1.04 against $Đ$ = 1.16). Similar consideration can be made for the flow polymerization made poly**(15)** in entry 1 of table 4.6. The potassium methoxide combined with a more reactive urea **(U-3)** catalyst system, delivered a broader molecular weight distributed polymer, with halved polymerization degree and slightly lower conversion. The performance of the **(CPI)** catalyst system

exploiting a well matched urea, is indeed astonishing in its performances for PLA synthesis.

DSC analyses were initially conducted following the method described by [63], upon which isothermal steps of 2 hours at T = 130 °C during cooling cycle to allow the material to crystallize were performed. In order to obtain a higher degree of crystallinity, the most promising candidates were sampled and a cooling cycle of low cooling rates mixed with isothermal steps were performed. The aforementioned method was carefully planned on the basis of previous performed analysis, with crystallization low cooling rate compatible with temperatures in which crystallization peaks were previously found, obtaining the displayed DSC spectra.

In particular, the candidates were chosen upon measuring the probability of finding mesodyads (two monomer units with same configuration) along the polymeric chain, calculated by homonuclear decoupled ^{1}H-NMR analysis, after deconvolution, where the calculations are based on Bernoulli statistics[21]. This probability is expressed by the Pm quantity present in table 4.2, the enantiopure based polymer exhibit a Pm = 1 value indeed.

The melting temperature of the polymerized rac-LA monomers mixtures resulted higher than the one of the enantiopure poly**(15)**. The DSC traces show the crystallization exothermic peaks for the poly**(15)** which is instead missing for the PLLA sample. The combination of high melting temperature highlighted during thermal cycles and the samples isotacticity, suggested the possibility of the presence of stereocomplexes, ascribing these properties to the low temperature synthesis condition. The former indeed, enhanced stereoregularity of the well matched **(CPI)**-**(U-2)** system catalyst, probably due to the lowering of the thermal energy noise and an increase in terms of stereo-selectivity of the catalyst. The presence of PDLA-b-PLLA stereocomplexes was proven to enhance the thermal property of the racemic polymer and ameliorate them, even surpassing its possible enantiopure forms ones [64] (reaction scheme in

Figure 4.1b). The stereocomplexes presence was indeed proved through wide angle x-ray scattering analysis (WAXS), reported in Figure 4.1c[21].

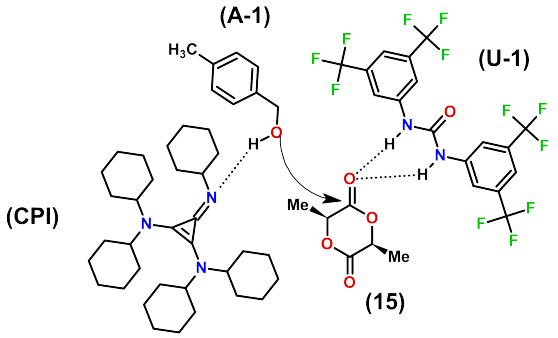

Figure 4.1a : Reaction pathway of **(15)** into PLLA with **(CPI)**, **(A-1)** and **(U-1)**.

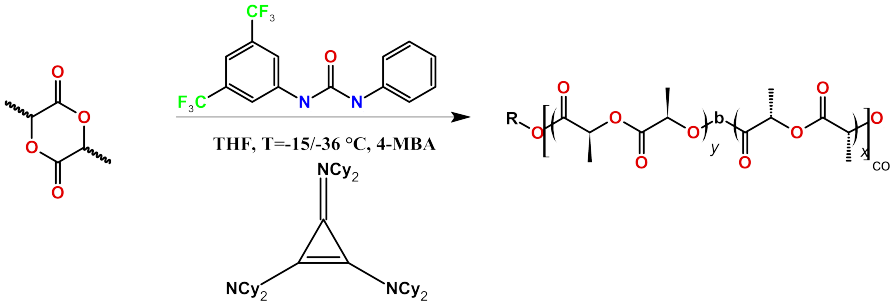

Figure 4.1b : Reaction scheme of PDLA-b-PLLA stereocomplexes formation from D,L-LA racemic monomer.

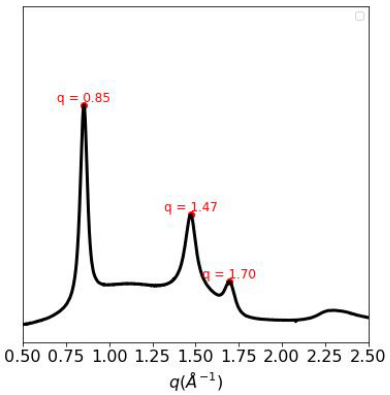

Figure 4.1c : Wide-angle X-ray scattering pattern of PLA obtained using a **(U-1)/(CPI)** organocatalytic system in THF at – 36 °C (presented as entry 3 of table 4.2) in q ($Å^{-1}$) which shows a scattering pattern identical to reported PLA stereocomplexes.
Literature data reports three peaks at 2θ = 12°, 21°, and 24° using an X-ray source with a wavelength of λ = 1.54 Å, [21, 30] which corresponds to q values of 0.85, 1.47, and 1.70 $Å^{-1}$ respectively. [65] Here, the X-ray source used has a wavelength of 0.976 Å.

4.2 Thermal assisted RCDEP and thermal degradation of polycarbonates

In this study, a series of thermal experiments were performed in order to investigate recycling and degradation properties of polycarbonates. To begin with, the results of synthesis experiments that led to the formation of the studied materials are listed below in table 4.3. Some materials obtained were already discussed in the previous section 4.1, in particular entry 1 of table 4.3 was obtained from monomer **(1)** and all the subsequent materials are realized as a result of substitutions to the 3-carbon atom of the 6 membered ring.

Entry 2 of table 4.3 was realised with a monomer presenting a largely increased degree of substitution, as well as entries 3, 6, 8 and 11 of table 4.3. Thanks to the Thorpe-Ingold effect these should lead to a lower T_c, but most importantly, favouring cyclization [66] and therefore RCDEP. This is particularly true for entries 9 and 10 of table 4.3 featuring the configuration of geminal di-methyl and di-ethyl substituents, respectively. Thorpe-Ingold effect was indeed firstly discovered thanks to a geminal dimethyl substituted carbon configuration and today is also known as geminal dimethyl substituent effect [66, 67]. These monomers were polymerized under low temperature conditions, as their polymer synthesis is extremely sensitive to temperature, affecting their ceiling temperature [68].

In order to polymerize entry 11 of table 4.3 a first attempt with the **(A-1)**, **(DBU)** and **(U-2)** catalyst system was performed unsuccessfully, a further attempt with more reactive **(U-4)** + $KOCH_3$ catalyst system with a low temperature synthesis condition, described in section 3.1.3, delivered the same result. Entries 9 and 10 of table 4.3, on the contrary, successfully delivered a polymer when the synthesis were performed in a low temperature system. Unfortunately, the synthesis corresponding to entry 9 of table 4.3 is lacking GPC analysis, however the synthesis experiment success is confirmed by

^{1}H-NMR analysis shown in Figure 13.

Entry	Monomer	Catalysts	Solvent	time(s)	Conversion (^{1}H-NMR)	DP (^{1}H-NMR)	$Đ$ (GPC)
1	**(1)**	**(U-2)** + **(DBU)**	THF	180	37%	24	1.07
2	**(9)**	**(U-2)** + **(DBU)**	THF	90	25%	18	1.15
3	**(6)**	**(U-2)** + **(DBU)**	THF	80	82%	43	1.10
4	**(10)**	**(U-2)** + **(DBU)**	THF	90	67%	33	1.06
5	**(11)**	**(U-2)** + **(DBU)**	THF	90	94%	45	1.07
6	**(3)**	**(U-2)** + **(DBU)**	THF	90	91%	50	1.05
7	**(2)**	**(U-2)** + **(DBU)**	THF	20	92%	44	1.20
8	**(3)**	**(U-4)** + $KOCH_3$	THF	15	76%	/	1.21
9	**(12)**	**(U-4)** + $KOCH_3$	THF	1 hr	>99%	/	/
10	**(13)**	**(U-4)** + $KOCH_3$	THF	2 h	>99%	/	1.30
11	**(14)**	**(U-4)** + $KOCH_3$	THF	50 mins	$\sim 0\%$	/	/

Table 4.3: Batch polymerization synthesis, at room temperature or low temperature, experiments results.

As a first step to investigate thermal degradability of the materials, thermogravimetric analysis (TGA) combined with in-situ mass spectroscopy (MS) were performed. A list of results is presented in the below table 4.4. Entries from table 4.4 match with entries from table 4.3 up to entry 10, entries 11-13 from table 4.4 refers to entries 8, 14 and 16 of table 4.1 respectively.

Most of the polymers nicely degraded with the relatively low maximum temperature of 400 °C, exceptions are made for entries 2, 3 and 13 of table 4.4, however further analyses (some of which presented in Figure 39 and in Figure 40 for entries 3 and 13 of table 4.4) with an heating cycle up to 600 °C confirmed their full degradation.

Entry	Monomer	$T_{d,max}$ [°C]	$T_{d,5\%}$ [°C]	Conditions	Residual weight[%]
1	**(1)**	284	237	N_2	0.3
2	**(9)**	290	196	N_2	23.5
3	**(6)**	228	218	N_2	31
4	**(10)**	341	298	N_2	6.9
5	**(11)**	196	192	Air	0.6
6	**(3)**	323	278	Air	0.2
7	**(2)**	326	267	N_2	0.3
8	**(3)**	227	218	Air	0.1
9	**(12)**	249	245	N_2	0.0
10	**(13)**	359	300	N_2	0.4
11	**(3)**	333	277	N_2	0.3
12	**(7)**	338	273	N_2	0.2
13	**(8)**	380	303	N_2	12.8

Table 4.4: TGA Analysis results for heating cycle up to 400 °C.

Neat degradation process was reported for entries 1, 6, 7, 9, 10, 11 and 12 of table 4.4, conversely to the other samples, which exhibited slower mass loss over broader temperature range. In some cases, possible water contamination caused low temperature initial mass loss and in others multiple relative maxima of mass loss over temperature were detected. The last, may be caused by the presence of hetero-atoms in the substituent [69, 70], or simply because of the substituent different nature [71] and subsequent different degradation mechanisms of its decomposed segments [72]. These behaviours are indeed more frequent for monomer with large substituent containing multiple different moieties. A more plausible explanation is the intrinsic onset of different degradation mechanisms, peculiar of the particular polymer.

In the case of entry 4, of table 4.4, the MS spectra for specific compound during TGA analysis confirmed the presence of water contamination. In particular in Figures 41, 42 and 43 are respectively presented the evolution in time of the partial pressure

of the ionized compound, whose related mass identify water, possible HF groups formed by the loss of F heteroatoms from the benzyl group and finally carbon dioxide, respectively. It is evident that water plays a role in the initial mass loss of the compound also because of the polycarbonates hygroscopicity [73]. Mass spectrum peaks of HF and F in first mass loss step, may as well suggest their elimination and their role in the overall sample mass loss.

Finally, insights of TGA analysis for entry 2 of table 4.4 is again further explored by the MS in-situ analysis. The multi-step degradation indicates that different degradation mechanisms are happening at different temperature. In Figure 44 the carbon dioxide partial pressure is presented, together with what could possibly look like cyclopropane or propene groups or equivalent molecular weight molecules in Figure 45 and finally, in Figure 46, large molecules, are present. The absence of CO_2 in the first degradation step may suggests the absence of random chain scission with decarboxylation of the polymer. This mechanism was indeed highlighted in literature, as one of the main thermal degradation mechanisms for poly**(1)** (whose substituted monomer unit deliver **(9)** related to the aforementioned polymer), together with chain unzipping depolymerization [74]. The latter indicates that alternative degradation mechanisms are happening. These could be partially due to the possible monomer large substituent side-group elimination mechanism [72, 75, 76]. These are often found to happen at lower temperatures compared to random chain scission mechanisms due to general higher strength of the polymer backbone bonds compared to its side groups bonds [77]. In particular, for this polymer substituent design, phenyl or benzyl groups and other sulphur containing particle of the substituent may be the cause of this initial degradation. Alternatively, depolymerization through unzipping mechanism, which is notoriously slower than random scission mechanism, compatible with the slow first degradation step [75], could be happening.

The degradation was further confirmed by DSC analysis conducted at the same

heating rate and maximum temperature of TGA analysis 400 °C, presented in Figure 32. In the previous analysis, mainly exothermic frequent peaks appear, from 130 °C to 260 °C, with minor events up to 300 °C. The hypothesis is that these peaks are related to chemical reaction, involved in the previously proposed unzipping and subsequent monomer degradation or/and side-groups elimination mechanisms. These could create smaller volatile molecule and phase transitions of weight fraction of the sample, catalysed by the thermal energy and resulting in the altering of the heat flux exchange. The neat large exothermic peak happening around 200 to 300 °C may be related to random chain scission, creating CO_2 molecules. Further investigations are required to inquire if the substituent groups through side-group elimination or unzipping depolymerization mechanisms are involved in creating the first degradation step and the overall degradation mechanisms of the sample.

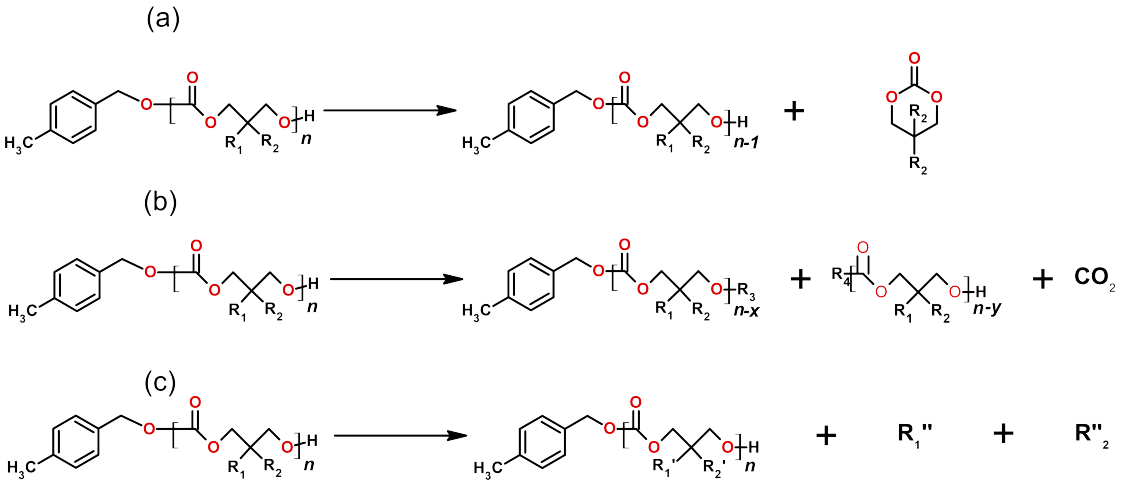

Figure 4.2: Possible decomposition mechanisms of investigated polymers, examples with **(A-1)** initiated polymer. Unzipping depolymerization mechanism (a), random chain scission with decarboxylation (b) and side-group elimination (c).

A particular study approach combining TGA, DSC analysis, ^{1}H-NMR and thermal depolymerization experiments staged through a hot plate heather, delivered some interesting results. TGA was performed on entry 5 of table 4.4, the results are visible in

Figure 47. The degradation of the polymer was slow and featuring multiple steps. The first degradation step is probably mainly due to thermal unzipping depolymerization, which is supported by a thermal depolymerization experiment, consisting of a 12 hours isothermal heating of bulk sample, in a capped vial, on a hotplate set at 230 °C (the sample equilibrium temperature with the environment is expected to lower the actual sample temperature) which delivered a 70.3% of monomer conversion and a remaining polymer with average DP = 12. The conversion and DP of the depolymerized polymer was estimated through a ^{1}H-NMR analysis of the sample presented in Figure 14 and Figure 15.

The sample contains minimal traces of water and other peaks that are not related to the polymer-monomer system. The previous confirm that degradation of polymer may happen through unzipping and subsequent monomer degradation with creation of water, CO_2, and other possible byproducts. Monomer degradation onset temperature in TGA is indeed usually lower than the polymer. Polymers enhanced thermal properties are related to their inter-molecular bonding, which makes them more thermally stable than their monomer unit [78]. Furthermore, the slow degradation confirmed by TGA is often a feature of unzipping depolymerization mechanisms, which is far slower than random chain scission [75]. Similar TGA behaviour are found with entry 9 of table 4.4, in which the same unzipping depolymerization behaviour was found as well.

The decrease of degradation rate may be explained by an initial higher concentration of monomer since unzipping depolymerization happens before the monomer degradation onset temperature, as highlighted by the ^{1}H-NMR analysis of the isothermal heating experiment sample. The initial monomer concentration could then be followed by the onset of monomer degradation and products volatilizing. The following sample degradation could be therefore driven by the slow unzipping of individual monomer units over time.

The CO_2 partial pressure trend detected during TGA-MS and presented in Figure

48 highlighted a second and third thermal degradation step. The two steps could be compatible with monomer unit multi step degradation. Monomers units degradation are indeed often found to onset at lower temperature and also presenting multi degradation steps on a large temperature span, often featuring slow degradation in temperature [78]. Alternatively, random chain scission with decarboxylation mechanism, side-group elimination, a combination of these, or a combination of these with unzipping mechanism as well could contribute and cause these phenomena, which is highly possible.

DSC analysis at the same heating rate of TGA, shown in Figure 33, a first endothermic melting peak at 82 °C is present, confirming that the polymer has a high degree of crystallinity. A subsequent analysis shown that fast cooling rate and re-heating transformed the polymer into an amorphous one, glass transition is visible in Figure 34 at 23 °C, the baseline slope of the spectrum was subtracted to show the transition. The melting process is no longer visible, probably requiring specific re-crystallization processes.

Several endothermic peaks are found in the DSC depolymerization experiments at temperatures 209 °C, 305 °C and a small, neat peak at 318 °C, similarly with the TGA multi-step degradation mechanism. In particular the endothermic peak onset at 195 °C, which coincides with the TGA degradation onset temperature, whereas the endothermic peak at 209 °C coincides with the small degradation rate increasing. Finally, the onset of the endothermic peak visible at 305 °C combined with the one at 318 °C are compatible with the degradation rate plateau and subsequent small increase visible in TGA analysis. The initial endothermic peak around 209 °C is compatible with the hypothesis of polymer unzipping depolymerization followed by monomer concentration increase with its subsequent abrupt degradation and slowing of degradation due to monomer concentration depletion. The other peaks related to higher temperature, followed by small and frequent heat flux variation may be related

to random chain scissions and other pyrolysis mechanisms.

An interesting case is to compare thermal analysis data for entries 1, 9 and 10 of table 4.4. TGA Analysis (with maximum temperature of 400 °C) spectra for entries 1, 9 and 10 of table 4.4 are available in Figures 49, 50, 51.

Entry 9 from table 4.4 is based on **(12)** unit, which presents the **(1)** monomer structure with a geminal di-methyl substituted carbon. Its polymer has a similar degradation temperature T_d to the one obtained in entry 1 from table 4.4 (whose monomer is **(1)**), however the degradation process happens at a much faster rate. Entry 10 from table 4.4, in the same fashion, presents a geminal di-ethyl substituted carbon, which appears to increase the T_d, which is an agreement with a recent study of similar configuration polycarbonates with increasing substitution degree of aromatic bulky rings and even of geminal configurations [79]. Indeed, entry 13 of table 4.4 composed by the bulkiest monomer unit **(8)** presents the highest thermal properties. This increases the curiosity toward this class of compounds which may present high thermal stability and the possibility to perform chemical recycling through their predisposition to cyclization.

The isothermal heating experiment on the hotplate heater was performed for entry 1 and 9 of table 4.4 in bulk at 230 °C, whereas for entry 10 of table 4.4 it was conducted at 170 °C with the addition of 10% weight of **(CPI)**, which was confirmed to be thermally unstable. Neither entry 1 nor 10 from table 4.4 showed appreciable polymer to monomer conversion, through monomer detection in the ^{1}H-NMR spectra of the samples. However, entry 1 from table 4.4 ^{1}H-NMR analysis revealed that the polymer DP averagely decreased of 4 units (combined with water, methyl and ethyl groups presence). This is in agreement with the demonstrated depolymerization mechanism through non-radical ester interchange reaction leading to the related cyclic monomer [80]. Entry 1 from table 4.4 DSC analysis with the same heating rate of TGA is shown in Figure 37, an endothermic melting peak is present at 35 °C, followed by

a large endothermic peak that onset at 225 °C and reaches its maximum at 307 °C, similarly with TGA decomposition results.

Entry 9 from table 4.4 was found to be able to convert into its monomer in high quantity. Its ^{1}H-NMR analysis in Figure 16 and Figure 17 demonstrated a 69% conversion of polymer into monomer. However, the presence of water and other peaks compatible with traces of acetone and acetaldehyde (or similar molecules), suggests possible oxidative pyrolysis may have taken place. DSC analysis with the same heating rate of TGA is shown in Figure 35 presenting a large endothermic degradation peak around 278 °C. Double melting peaks are found at T_{m1} = 91 °C T_{m2} = 109 °C which are ascribable to the material intrinsic polymorphic property [81]. The large endothermic peak is in direct correspondence with the variation of the degradation rate (observable in TGA) and onset of a different degradation mechanism. As stated in the case of entry 5 in table 4.4, this is compatible with monomer slow and multi-step degradation mechanisms, nevertheless, further studies should be made to investigate them.

Entry 10 of table 4.4 was found to be able to depolymerize through unzipping mechanisms, in agreement with past studies [68], confirmed by monomer traces in the ^{1}H-NMR analysis of DSC analysis up to 350 °C, with the same TGA analysis heating rate 5 °C min^{-1}, in Figures 36 and 18. ^{1}H-NMR analysis highlighted the unzipping depolymerization mechanism and oxidative pyrolysis due to high water formation. Depolymerization was probably not found in the isothermal heating experiment, due to the higher thermal property of this monomer, possibly requiring higher temperature than a hotplate heater set at 170 °C.

Entry 13 of table 4.4 delivered a 21% conversion to monomer thanks to the isothermal heating on the hotplate heater at 230 °C. ^{1}H-NMR spectra are available in Figure 19. The ^{1}H-NMR deconvoluted spectra confirmed that the only degradation mechanism is actually depolymerization unzipping, however, due to analogies to the case of poly**(13)**(entry 10 from table 4.4), the temperature was too low to obtain high

conversion, which could explain also the only presence unzipping depolymerization mechanism, similarly to other entries cases (such as poly**(1)**) [68, 80]. The DSC analysis performed with the same heating rate of TGA is presented in Figure 38. The spectrum highlights the presence of small degradation transition of the sample, which onset consistently around 337 °C, compatibly with TGA analysis and possibly indicating onset of multi-degradation mechanisms. This material is a promising candidate for high chemical recyclability, due to its α-tocopherol (vitamin-E) bulky substituent, which may also lead to biomedical application. Isothermal depolymerization experiment at more appropriate and controlled temperatures (as well as properly ensured inert environment) should be conducted. The exploiting of solvent, thermally stable catalyst or the combination of the two, could lead to serious high depolymerization conversion at relative low temperature.

Entries 6 and 8 from table 4.4, shows how the DP of the polymer determines its thermal properties [82]. However, entry 6 from table 4.4 synthesised with **(DBU)** + **(U-2)** + **(A-1)** and 11 from table 4.4 synthesised with **(CPI)** + **(U-1)** + **(A-2)** different catalysts, exhibiting comparable DP, shows minimal difference in terms of thermal properties. Both entries 6 and 12 from table 4.4 depolymerization properties were investigated with isothermal heating on the hotplate heater, leading to polymer conversion to monomer. In entry 11 from table 4.4, the conversion was minimal, but little to no degradation of the polymer-monomer system were observed, presented in Figures 20 and 20, with a 14.5% conversion. Entry 12 from table 4.4 on the contrary, exhibit degradation (possibly oxidative), with large amount of water.

4.3 Cyclopropenium salts as phase transfer catalyst Experiment

In this work, the class of cyclopropenium ions, were targeted and investigated as potential transfer phase catalysts (PTC) on the basis of previous results [11, 32, 83]. Their functionalization with dialkylamino and ethylamino (causing the gearing of the molecule and enhanced activity [11]) moieties **(S-1)** or bis-2-(methoxyethyl)amino moieties **(S-2)** combined with a chlorine anion, causes the formation of a salt, which possess an amphiphilic behaviour.

Polymerizations synthesis of **15** into PLLA were attempted under different conditions to investigate the properties of these possible PTC co-catalyst. Initial polymerization reactions with **(U-5)** or **(U-4)** combined with **(A-1)**, with or without **(S-1)**, and several different alkali metal bases such as KH, $KOCH_3$, KOtbut or NaOtbut or LiOtbut were exploited, in order to increase their solubility in THF through the PTC.

In the first case $KOCH_3$ base was exploited as a co-catalyst, together with **(U-4)**, **(A-1)**, with and without **(S-1)** in entries 1 and 2 respectively, from table 4.5. The presence of the supposed PTC **(S-1)** lead to a lower catalyst activity together with a broader molecular weight distribution. ^{1}H-NMR analyses for the two samples are respectively presented in Figures 22 and 23, whereas GPC analyses are presented respectively in Figures 6 and 7.

Similar results were obtained when the KH base with the more reactive **(U-5)** was exploited, in entries 3 and 4 from table 4.5.

When exploiting more sterically hindered bases such as lithium, sodium or potassium tert-butoxide the results worsened, resulting in little to no conversion at all, except for NaOtbut, which presented still broad molecular weight distribution. The results are presented in entries 5-16 from table 4.5 whereas the ^{1}H-NMR analysis of entry 5 from table 4.5 is presented in Figure 24, showing the minimal conversion.

Entry	Base	Urea	Salt	Time(s)	Conversion (^{1}H-NMR)	$Đ$ (GPC)
1	$KOCH_3$	**(U-4)**	**(S-1)**	20	45%	1.22
2	$KOCH_3$	**(U-4)**		20	98%	1.16
3	KH	**(U-5)**	**(S-1)**	30	98.5%	1.41
4	KH	**(U-5)**		30	98%	1.24
5	LiOtbut	**(U-5)**	**(S-1)**	30	2%	/
6	LiOtbut	**(U-5)**		30	98%	1.47
7	LiOtbut		**(S-1)**	30	4%	/
8	LiOtbut			30	85%	1.40
9	NaOtbut	**(U-5)**	**(S-1)**	30	100%	1.43
10	NaOtbut	**(U-5)**		30	98%	1.28
11	NaOtbut		**(S-1)**	30	77%	1.40
12	NaOtbut			30	99%	1.19
13	KOtbut	**(U-5)**	**(S-1)**	30	9%	/
14	KOtbut	**(U-5)**		30	98%	1.20
15	KOtbut		**(S-1)**	30	100%	1.28
16	KOtbut			30	98%	1.23
17	LiOtbut	**(U-5)**	**(S-4)**	30	97%	1.48
18	LiOtbut		**(S-4)**	30	87%	1.43
19	NaOtbut	**(U-5)**	**(S-4)**	30	97%	1.45
20	NaOtbut		**(S-4)**	30	98%	1.33
21	LiOtbut	**(U-5)**	**(S-3)**	30	93%	1.22

Table 4.5: Batch polymerization experiments exploiting cyclopropenium salts as transfer phase catalysts.

In comparison, benzyl-triethylammonium chloride **(S-3)**, a well known inexpensive PTC [84, 85], was substituted to **(S-1)**. The results are presented in entries 17-20 from table 4.5. Interestingly, when the LiOtbut base was employed, critical for **(S-1)**, better results were achieved, with slightly enhancement of catalyst activity and molecular weight distribution control. On the contrary, when LiOtbut was replaced with NaOtbut, the presence of **(S-4)** slightly worsened the results.

To inquire the possible causes of the failure, two new cyclopropenium chloride salts **(S-2)** and **(S-3)** with increasing number of bis(methoxy-diethylamino) functionalizing moieties were synthesised. The new functionalized moieties increased the solubility of

the salts in THF. Salt **(S-2)**, however, was reported to inhibit the synthesis of PLLA, delivering zero conversion when exploited with LiOtbut or NaOtbut, both in presence and absence of the urea **(U-1)**. Salt **(S-3)**, on the other hand, delivered a good result for system containing both the LiOtbut base and urea **(U-5)**, as reported in entry 21 from table 4.5, however when exploited without the presence of the urea, or alternatively substituting the LiOtbut with NaOtbut, no conversions were achieved.

Colour variations and transformation from clear to translucent liquid solution during synthesis reactions performed with **(S-1)**, **(S-2)** and **(S-3)** were visible, which could indicate some unwanted reactions happening, the reaction mixture vials in the case of salts **(S-2)** and **(S-3)** are shown in Figure 4.3. In order to investigate, salt **(S-1)** was mixed with **(A-1)** and with either LiOtbut or either NaOtbut, in CD_3CN (trideuteroacetonitrile). ^{1}H-NMR analyses were performed sequentially for multiple hours in order to detect reaction that could lead to the failure of the catalyst system. Some ^{1}H-NMR spectra, at different time steps, with LiOtbut and NaOtbut, are respectively presented in Figures 25 and 26. As evidenced by the ^{1}H-NMR spectra, no visible unexpected reaction could be detected, hence the reasons for which these catalyst systems failed to promote initiation during the polymer synthesis is still unclear and further investigation should be conducted to determine the failure of this experiment.

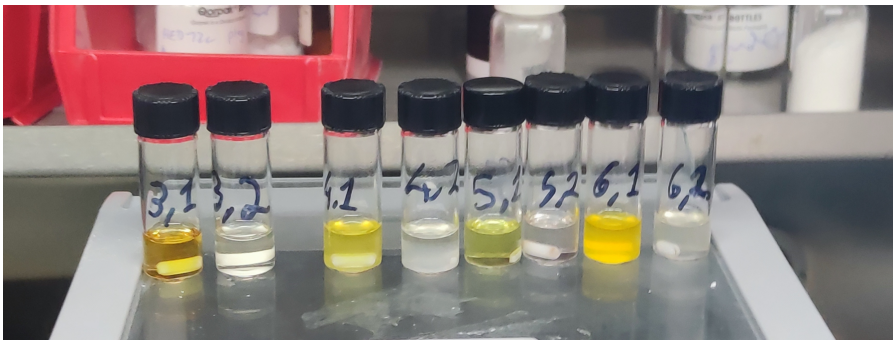

Figure 4.3: Optical properties changes of reaction mixtures containing salts **(S-2)** and **(S-3)**, in presence or absence of urea.

4.4 DSC analyses of PLLA library: data set creation for supervised ML predictive model training

DSC analyses of several PLLA (poly**(15)**) samples were conducted. These were synthesised with an automated reactor flow system, fastly delivering a large library of PLLA homopolymer synthesised under different combination of parameters such as reactor length, diameter, RT and flow rate. The analyses of these aimed at delivering a dataset for a machine learning model, in order to build an AI predictive model capable of understanding the QSPR between these parameters and the resulting polymer thermal properties.

The choice of automated flow reaction synthesis condition was based mainly on behalf of reliability and replicability of the experiments. Furthermore, the automated flow reactor provided a fast mean to obtain the polymer library, in a high-throughput fashion, however the DSC analysis to be performed still constituted a bottleneck in the process, yet it allowed to greatly speed up the overall process. An example of flow polymerization synthesis his herein reported, which is also the reproduction of an experiment reported in [38], in order to show the ability of this technique to reproduce experiment with high fidelity, a property which is further enhanced if the flow reactor is completely automated.

The synthesis of entry 1 from table 4.6, from monomer **(15)**, was performed exploiting a similar catalyst system to the one exploited in entry 2 of table 4.5. The difference among the two catalyst systems is that the one of entry 1 from table 4.6 is exploiting **(U-3)** which is less reactive than **(U-4)** exploited for entry 2 of table 4.5 [29]. However, the resulting synthesis required only a resident time of τ = 0.314 s, delivering a 92% monomer to polymer conversion, with equal molecular weight distribution broadening, therefore a higher control due to the higher conversion. ^{1}H-NMR analyses for entry 1 from table 4.6 are presented in Figure 27 (presenting the

^{1}H-NMR analysis of the reaction mixture and monomer to polymer conversion) and in Figure 28 (showing the purified polymer spectrum), GPC analysis is presented in Figure 8 showing the molecular weight distribution.

The process is at greatly higher scale, employing 720 mg of monomer and possibly further scalable to higher (or lower if needed) quantities, requiring only 50 s to deplete the reaction stock solutions and completing the reaction. The results of high activity and selectivity of the catalyst are ascribable to two main feature of flow polymerizations. One of the previously mentioned is the highly efficient mixing of the compounds in flow, enhanced by the T-mixer component that collects and mixes the two monomer and catalyst stock solutions. The last one is the finely controlled reaction time, which is controlled through the flow rate and resident time, after which the solution is ejected from the mixture in a solution containing the quenching agent.

In entry 2 of table 4.6, the original experiment, performed under the same conditions and instruments, reported in literature [38] is presented. Minimal variation arises in terms of conversion and dispersity, overall confirming the ability of this synthesis technique to deliver reliable and reproducible results.

Entry	Monomer	$[M_0]$	Base	Urea	τ(s)	Conversion (NMR)	$Đ$ (GPC)	Target DP	Conditions
1	**(15)**	0.5 M	$KOCH_3$	**(U-3)**	0.314	92%	1.16	25	Flow, RT
2	**(15)**	0.5 M	$KOCH_3$	**(U-3)**	0.314	96%	1.13	25	Flow, RT

Table 4.6: Flow-reaction polymerization experiment result.

The DSC spectra of the automated flow reaction condition synthesised PLA polymer library were processed, splitting the whole data into heating, cooling and reheating cycles, and possibly plotting them with heat flux peak detection or subtracting artifacts due to the DSC machine such as heat flux offset or slope. These were finally fed to the AI machine learning model separately. Hundreds of polymers were sampled and

analysed, DSC analyses of the first heating cycle of the analysed sample are shown in Figure 4.4.

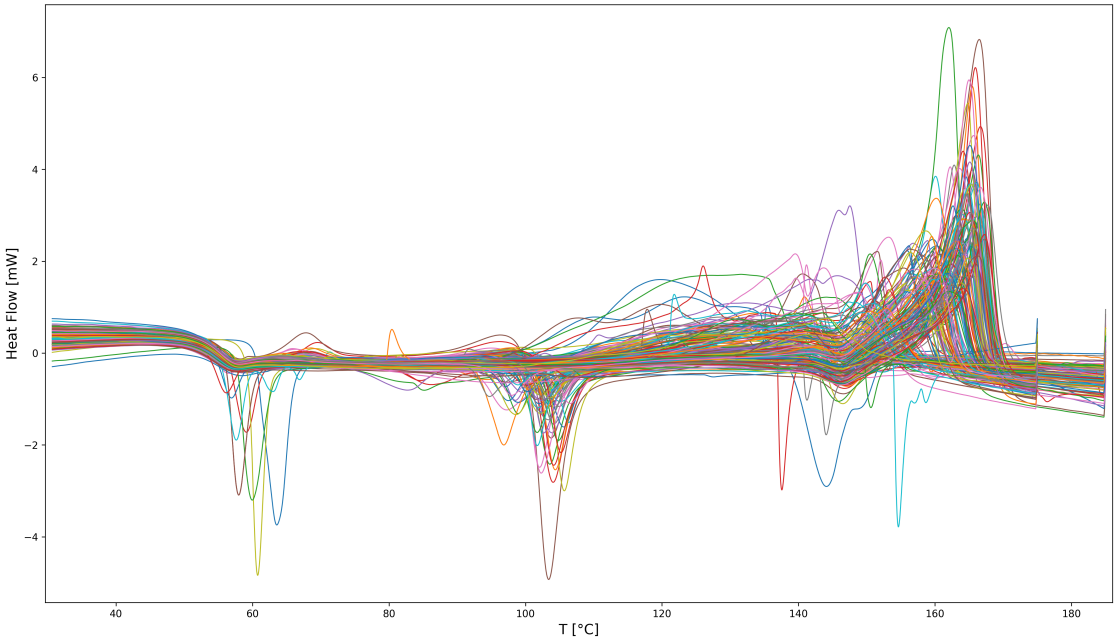

Figure 4.4: DSC analysis of PLLA (poly**(15)**) library obtained through an automated flow reactor, 1^{st} heating cycle, (endothermic peak upside).

Chapter 5

Conclusion and Future work

The results of the recently developed CPIs catalyst system have demonstrated the great potential of organocatalysis, reaching performances that can also surpass traditional inorganic catalyst systems when combined with co-catalysts such as (thio)ureas and alcohols. This approach has been shown to be highly effective in promoting the anionic ROP of cyclic monomers.

The system performances during the synthesis of polyesters and polycarbonates were particularly interesting, exhibiting high conversion rates and well-controlled polymerization processes, as well as living polymerization behaviour and high polymerization selectivity. In the particular case of rac-PLA synthesis at low temperature, the catalyst system also exhibited stereo-regularity resulting in high thermal performances and a subsequent increase in product lifetime.

This catalyst system has the potential to further promote the production of sustainable biodegradable and biocompatible polyesters and polycarbonates, which have a wide range of applications, including drug delivery systems and tissue engineering scaffolds. Nevertheless, the presence of PLA stereocomplexes were hypothesized according to DSC analysis which demonstrated enhanced thermal properties for low temperature reactions synthesised polymers, and the hypothesis was further corroborated by WAXS analysis technique. Therefore, possible new catalyst systems with equal or better performances, such as higher stereoselectivity could be seek, maybe even in the same CPIs class of compounds.

Thermal experiments and characterization demonstrated the possibility to perform chemical recycling of some of these particular polycarbonates, due to their intrinsic thermodynamic properties. The ability of some of these to undergo ring-closing depolymerization through means of solely thermal assisted unzipping mechanism, without requiring any solvent or catalyst and with simple bulk sample heating, is fascinating. Further experiments and the addition of GPC characterization analysis should be employed to further optimize the recycling of these polymers. The addition of an

eco-friendly solvent or thermally stable organocatalyst may increase the conversion efficiency and reduce the energy required to perform the chemical recycling process. Further experiments should be conducted to perform them with customized heating temperatures and times in order to find the optimal conditions for RCDEP, possibly combining also GPC characterization analysis for further knowledge of the reaction process results.

One of the main aspects of this research was to gain a comprehensive understanding of the quantitative structure-property relationships (QSPR) for the synthesized polymers. By correlating the synthesis conditions and monomer design with the properties of the polymers, it was possible to modify the recycling and thermal properties of the resulting polymers. Furthermore, the datasets generated through means of the DSC characterization of the PLA samples, obtained with an automated reaction flow during this research, will provide input to train the machine learning predictive model. This can further optimize polymer synthesis processes and deliver fundamental understanding on QSPR of PLA, also for the recycling aspects. The integration of machine learning models into the synthesis process could enable the rapid discovery and synthesis optimization of polymers with desired specific properties. It is anticipated that further development of the predictive model will occur, and that it will subsequently be applied to other materials, such as the polycarbonates developed under this study, which may deepen our related knowledge and ameliorate their specific properties for different applications.

The experiments related to the exploitation of cyclopropenium salts as PTC for anionic ROP of PLA essentially resulted in a failure of the catalyst system for causes that are yet to determine. Therefore, further investigation, should be performed in order to gain comprehension of the failure mechanism at the base of these results.

In conclusion, the 16 materials studied and synthesized in this thesis were developed using a holistic approach. This approach comprised their design selection, synthesis

procedures (which included approximately one hundred varied ROP-mediated syntheses to optimize processes and outcomes), characterizations, and analyses of their thermal recycling and degradation behaviors. The synthesis of materials with defined and controlled properties was achieved with an organocatalyst system whose performance are comparable and even better than many other less eco-friendly traditional catalyst systems. This can promote the exploitation of such materials for biomedical purposes, devoid of inorganic contaminants and residue, with well controlled molecular weight and degree of polymerization, which influence the bio-degradation properties of therapeutic agents based on such materials, for instance. These thermoplastic materials also offer modest mechanical properties that could find application in everyday life, supported by their important ability to biodegrade and being easily recyclable. Further studies for the applications of these materials should be conducted, which may reveal important properties for their intended use.

Appendix

GPC characterization data

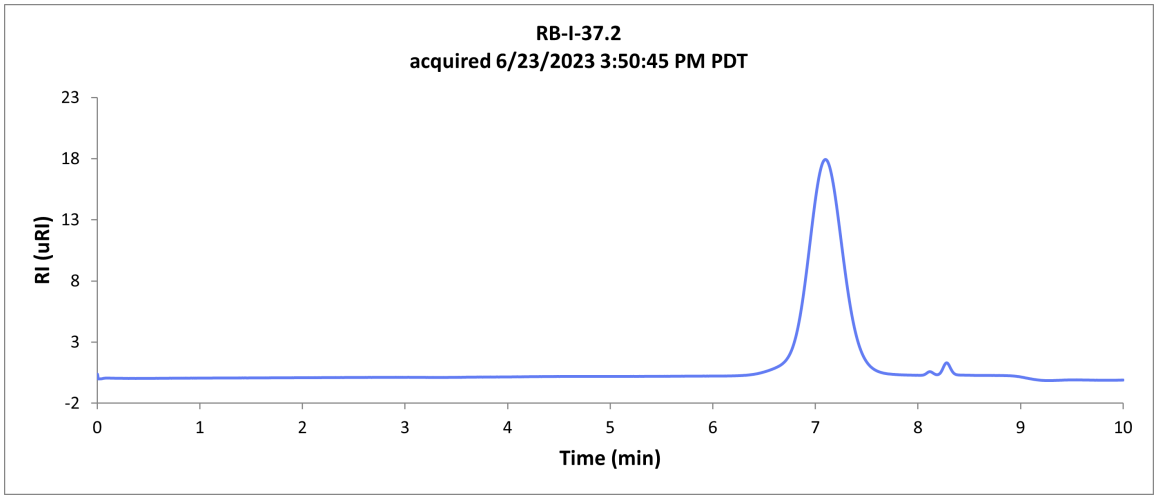

Figure 1: GPC analysis of PTMC, entry 1 from table 4.1.

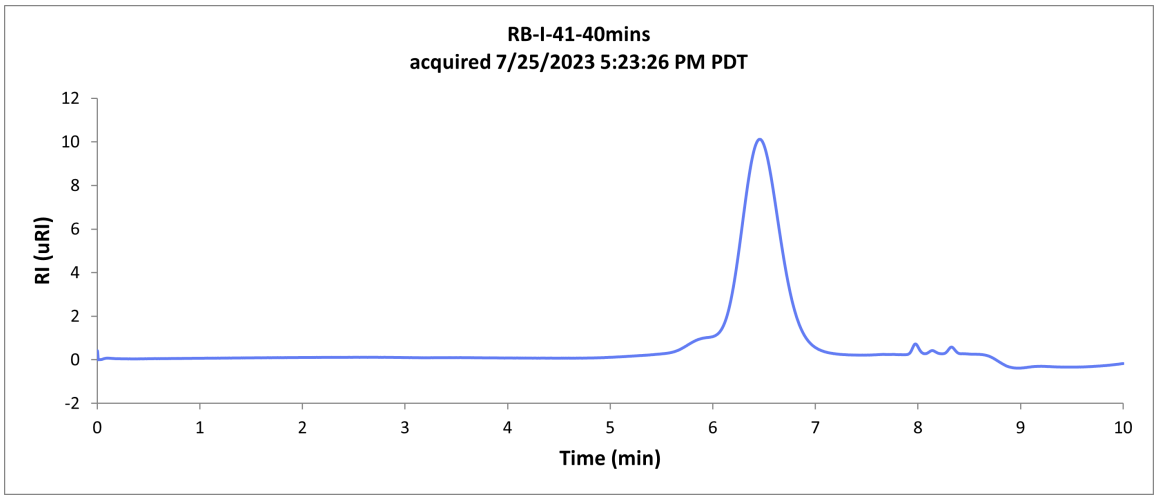

Figure 2: GPC analysis of entry 5 from table 4.1.

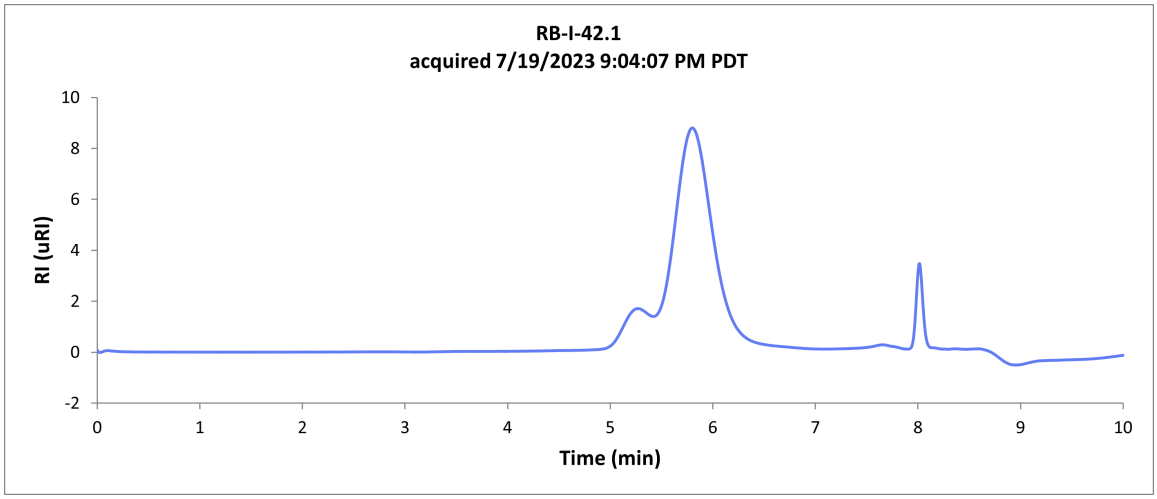

Figure 3: GPC analysis of entry 8 from table 4.1.

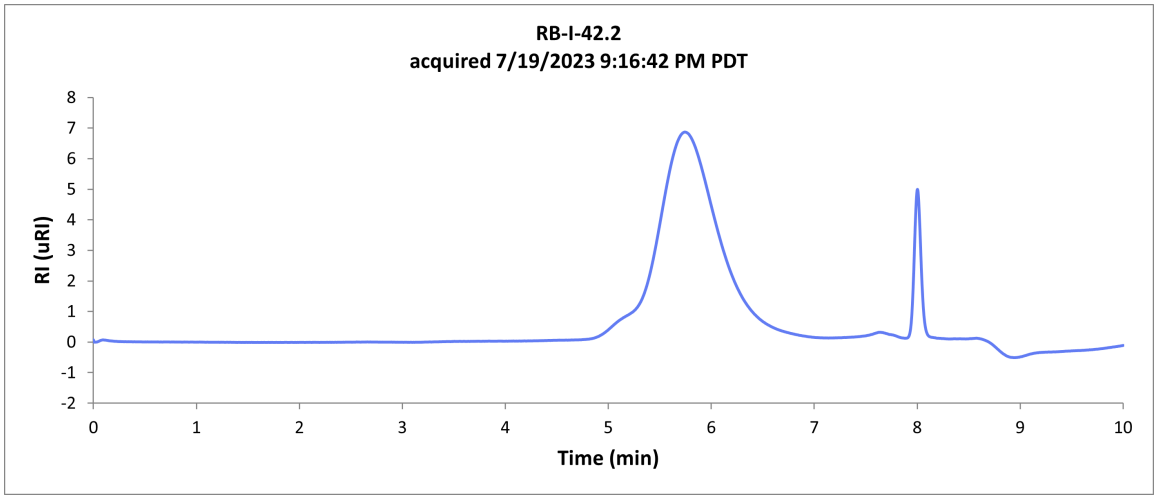

Figure 4: GPC analysis of entry 9 from table 4.1, synthesised in CH_2Cl_2 solvent.

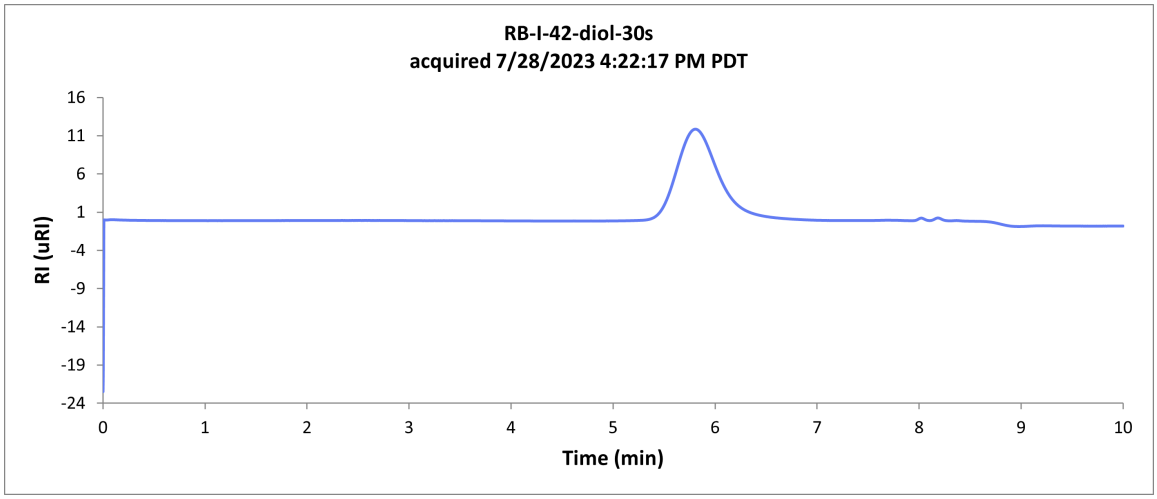

Figure 5: GPC analysis of entry 10 from table 4.1, with (A-2).

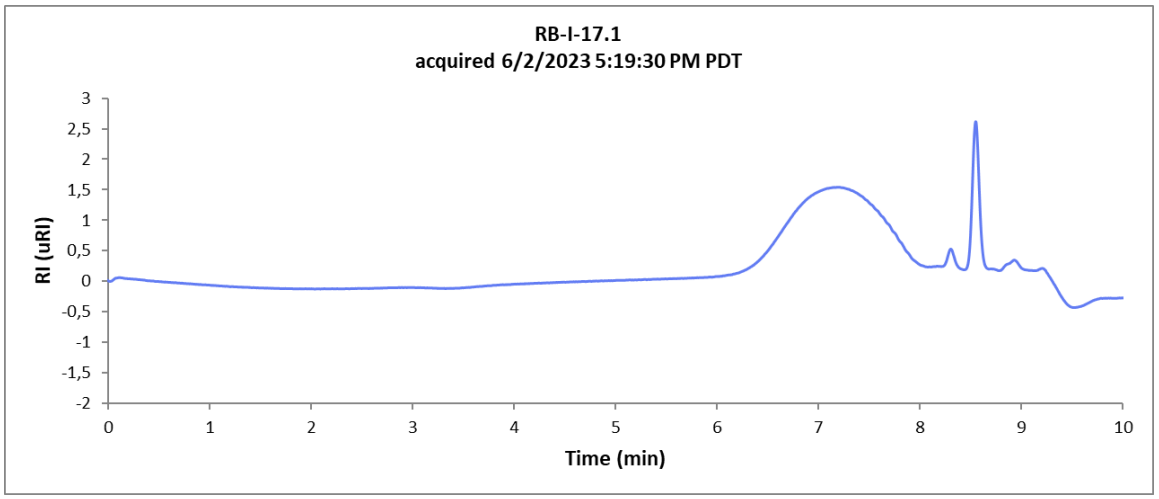

Figure 6: GPC analysis of entry 1 from table 4.5.

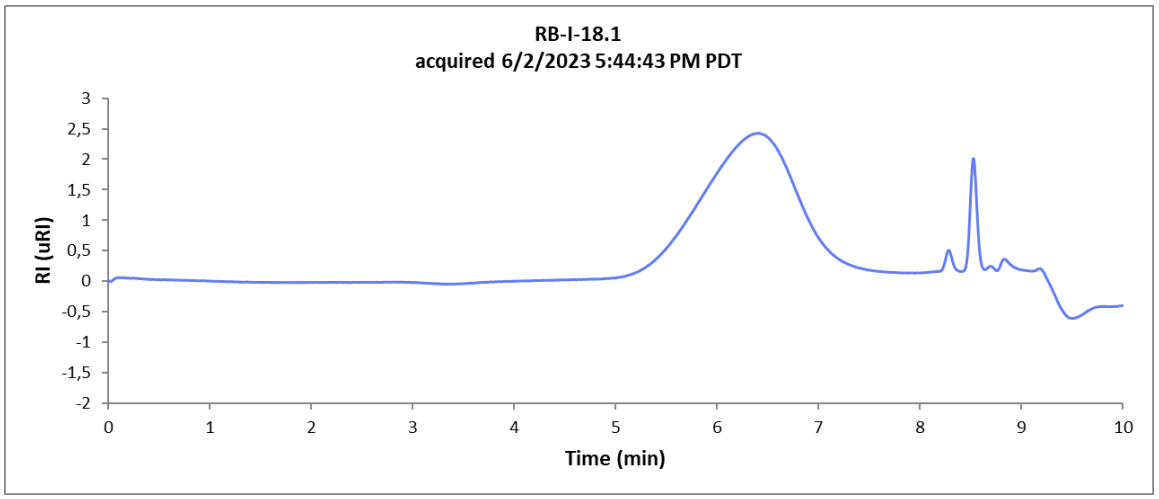

Figure 7: GPC analysis of entry 1 from table 4.5.

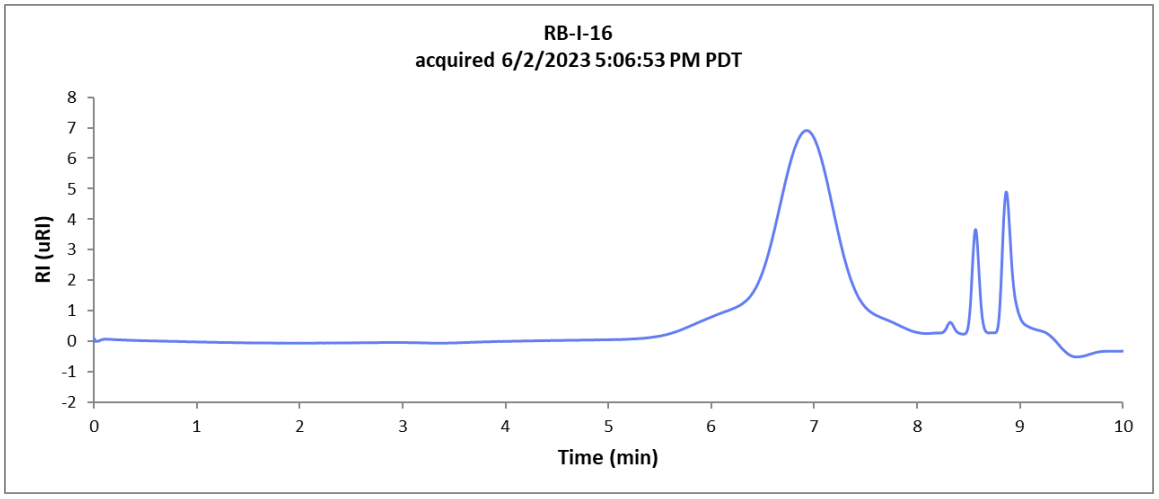

Figure 8: GPC analysis of entry 1 from table 4.6.

NMR characterization data

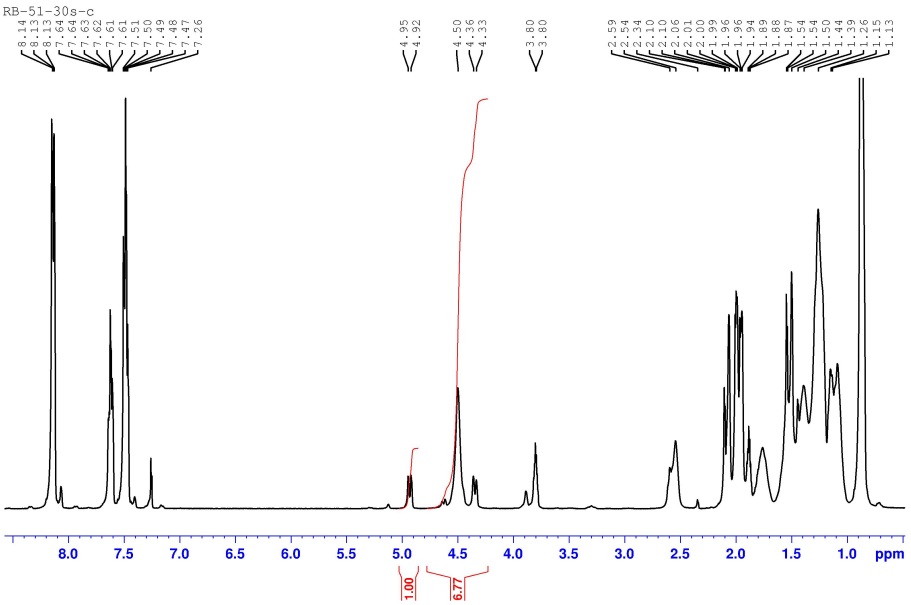

Figure 9: ^{1}H-NMR analysis of 15 from table 4.1, dried reaction mixture.

^{1}H-NMR ($CDCl_3$): poly**(8)** δ 4.48 (-CH2, s, 4H), **(8)** δ 4.92 (-CH2, d, 2H), δ 4.37 (-CH2, d, 2H) ppm.

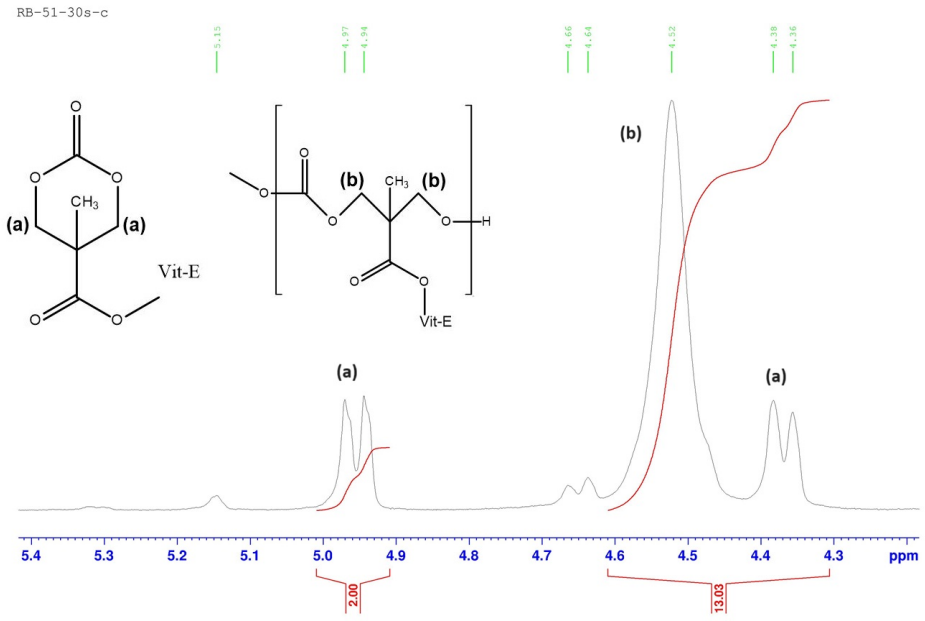

Figure 10: ^{1}H-NMR analysis of entry 15 from table 4.1, dried reaction mixture, detail.

^{1}H-NMR ($CDCl_3$): poly**(8)** δ 4.48 (-CH2, s, 4H), **(8)** δ 4.92 (-CH2, d, 2H), δ 4.37 (-CH2, d, 2H) ppm.

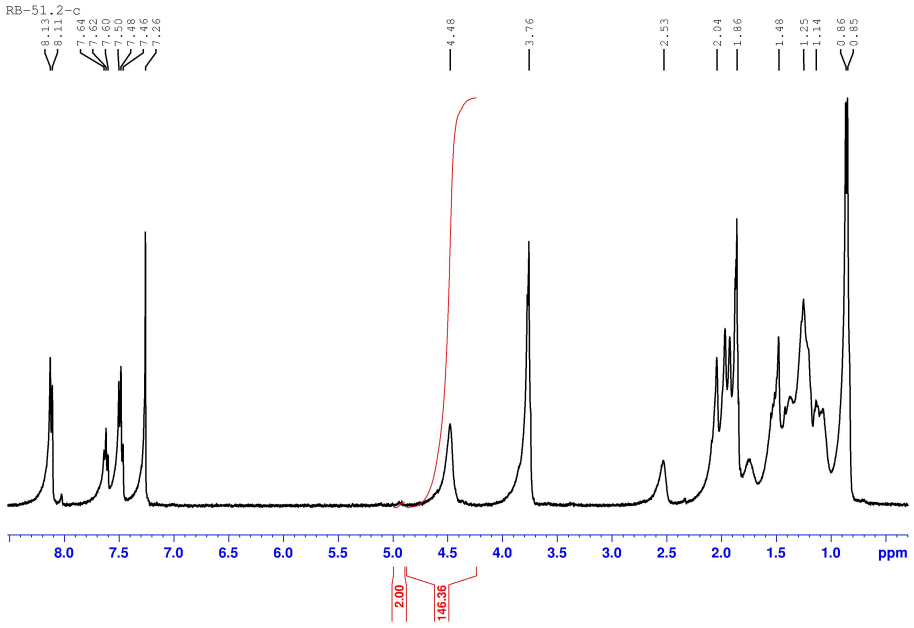

Figure 11: ^{1}H-NMR analysis of 16 from table 4.1, dried reaction mixture.

^{1}H-NMR ($CDCl_3$): poly**(8)** δ 4.48 (-CH2, s, 4H), **(8)** δ 4.92 (-CH2, d, 2H), δ 4.37 (-CH2, d, 2H) ppm.

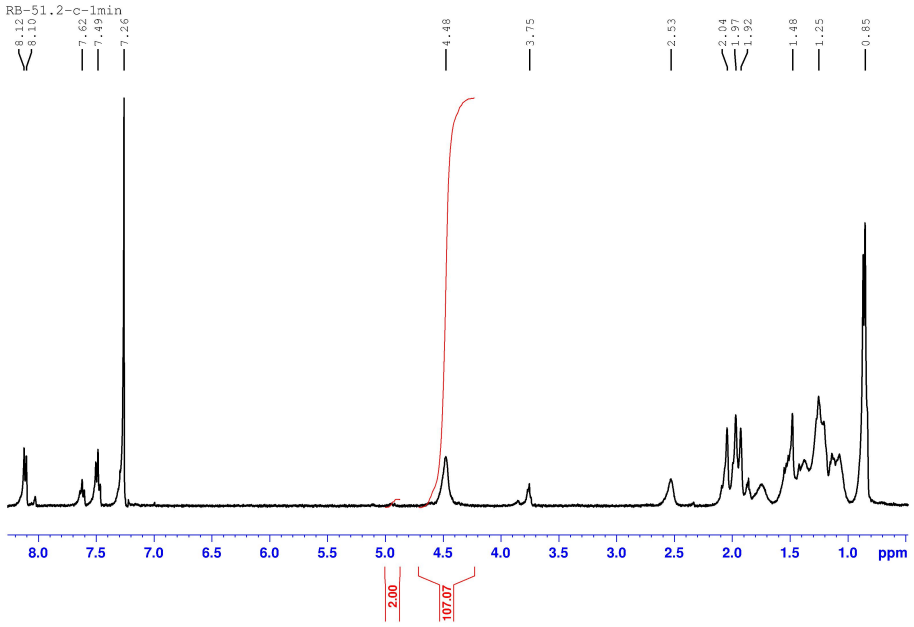

Figure 12: ^{1}H-NMR analysis of entry 16 from table 4.1, dried reaction mixture aliquot after 1 minute.

^{1}H-NMR ($CDCl_3$): poly**(8)** δ 4.48 (-CH2, s, 4H), **(8)** δ 4.92 (-CH2, d, 2H), δ 4.37 (-CH2, d, 2H) ppm.

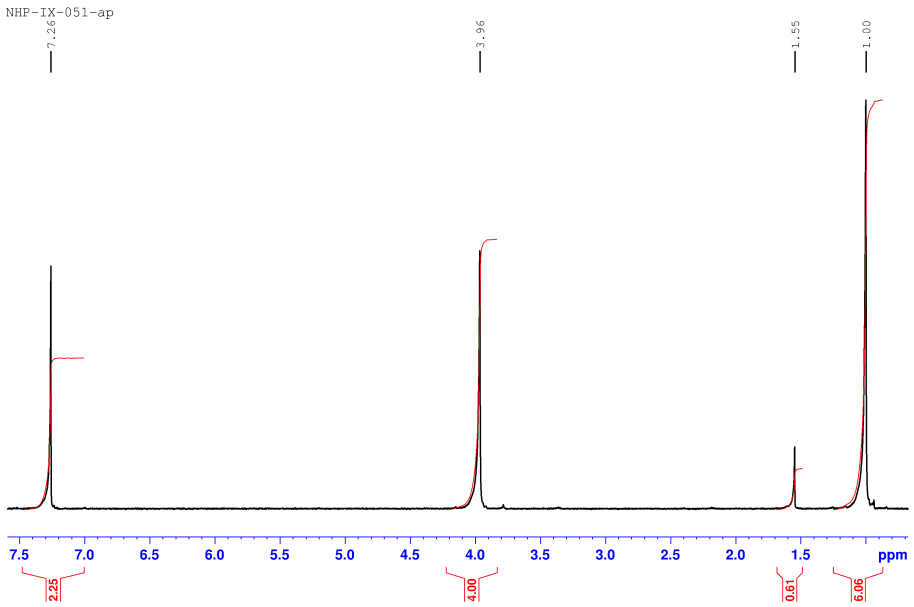

Figure 13: ^{1}H-NMR analysis of entry 9 from table 4.3, purified polymer.

^{1}H-NMR ($CDCl_3$): poly**(12)** δ 3.96 (-CH2, s, 4H), δ 1.00 (-CH3, s, 6H), $CDCl_3$ δ 7.26 (-CH, s, 1H), H_2O δ 1.55 (-CH, s, 2H) ppm.

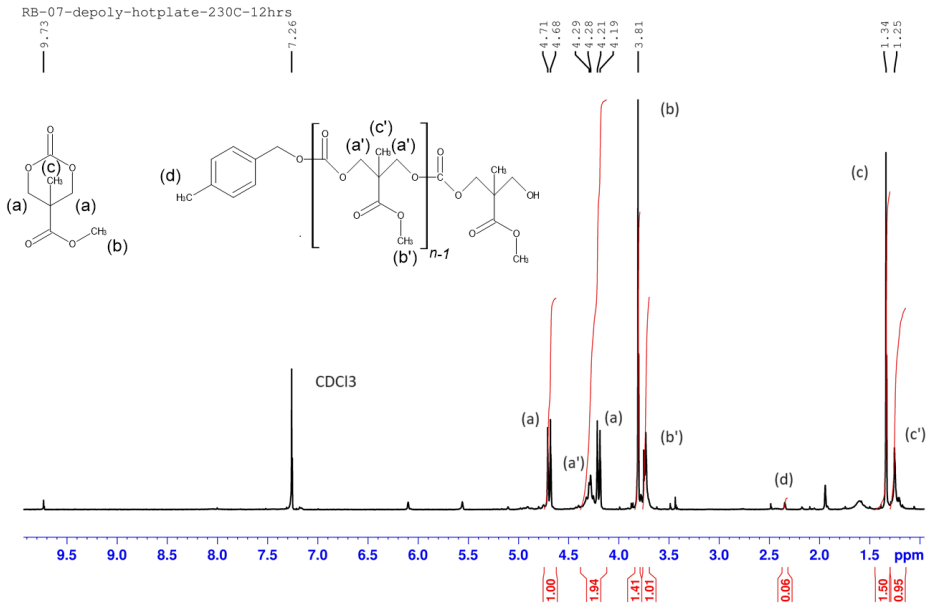

Figure 14: ^{1}H-NMR analysis of entry 5 from table 4.4, after bulk 12 h isothermal heating on hotplate heater at 230 °C, in a capped vial.

^{1}H-NMR ($CDCl_3$): poly**(11)** δ 4.28 (-CH2, s, 4H), δ 1.25 (-CH3, s, 3H), δ 3.74 (-CH3, s, 3H), **(11)** δ 4.18-4.21 (-CH2, d, 2H), δ 4.68-4.71 (-CH2, d, 2H), δ 1.34 (-CH3, s, 3H), δ 3.81 (-CH3, s, 3H), $CDCl_3$ δ 7.26 (-CH, s, 1H), H_2O δ 1.55 (-CH, s, 2H) ppm.

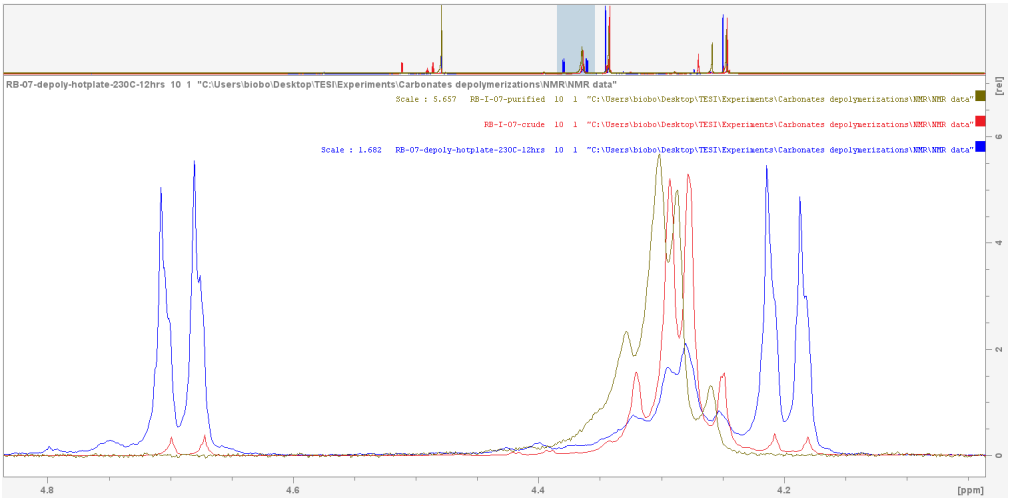

Figure 15: ^{1}H-NMR analysis of entry 5 from table 4.4, after bulk 12 h isothermal heating on hotplate heater at 230 °C, in a capped vial, conversion detail.

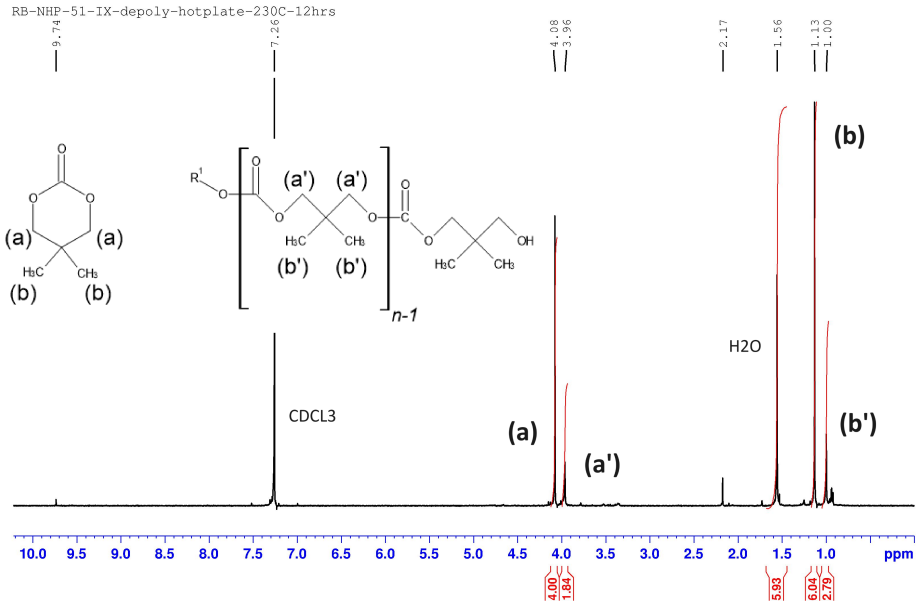

Figure 16: ^{1}H-NMR analysis of entry 9 from table 4.4, after bulk 12 hours isothermal heating on hotplate heater at 230 °C, in a capped vial.

^{1}H-NMR ($CDCl_3$): poly**(11)** δ 4.28 (-CH2, s, 4H), δ 1.25 (-CH3, s, 3H), δ 3.74 (-CH3, s, 3H), **(11)** δ 4.18-4.21 (-CH2, d, 2H), δ 4.68-4.71 (-CH2, d, 2H), δ 1.34 (-CH3, s, 3H), δ 3.81 (-CH3, s, 3H), $CDCl_3$ δ 7.26 (-CH, s, 1H), H_2O δ 1.55 (-CH, s, 2H) ppm.

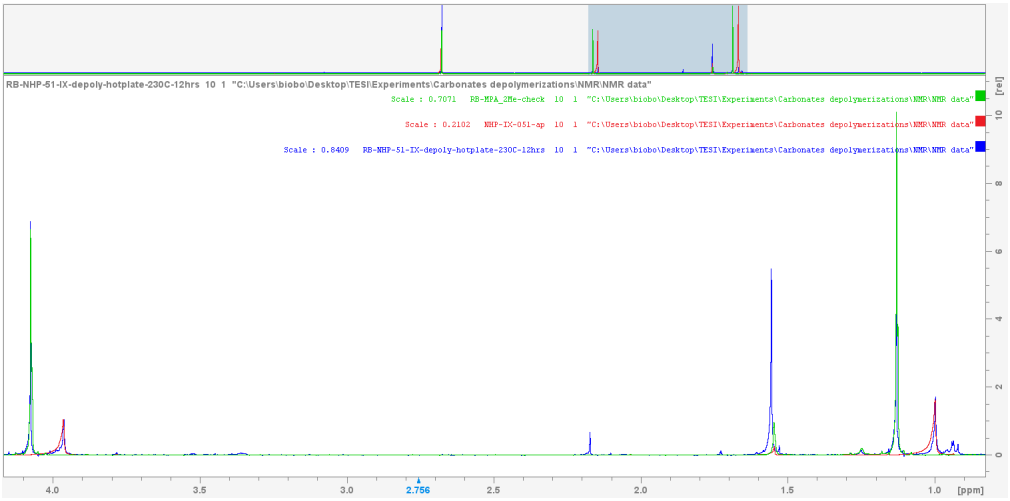

Figure 17: ^{1}H-NMR analysis of entry 9 from table 4.4, after bulk 12 hours isothermal heating on hotplate heater at 230 °C, in a capped vial, conversion detail.

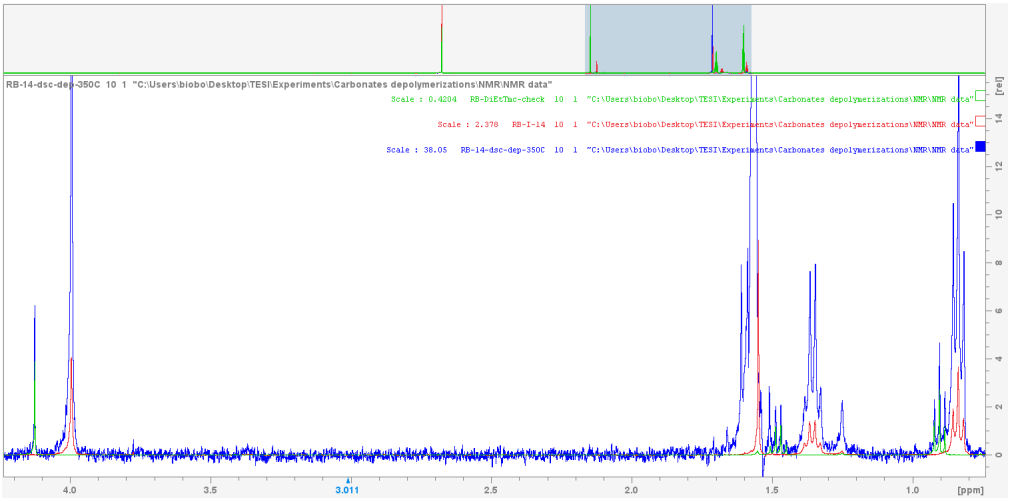

Figure 18: ^{1}H-NMR analysis of entry 10 from table 4.4, after DSC analysis from 20 °C to 350 °C, with 5 °C min^{-1} heating rate, conversion detail.

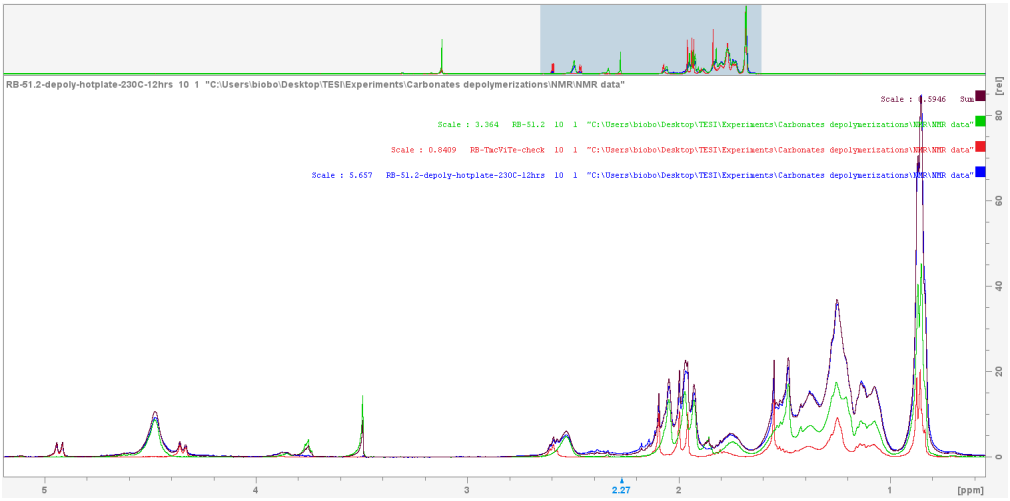

Figure 19: ^{1}H-NMR analysis of entry 13 from table 4.4, after bulk 12 hours isothermal heating on hotplate heater at 230 °C, in a capped vial, conversion detail.

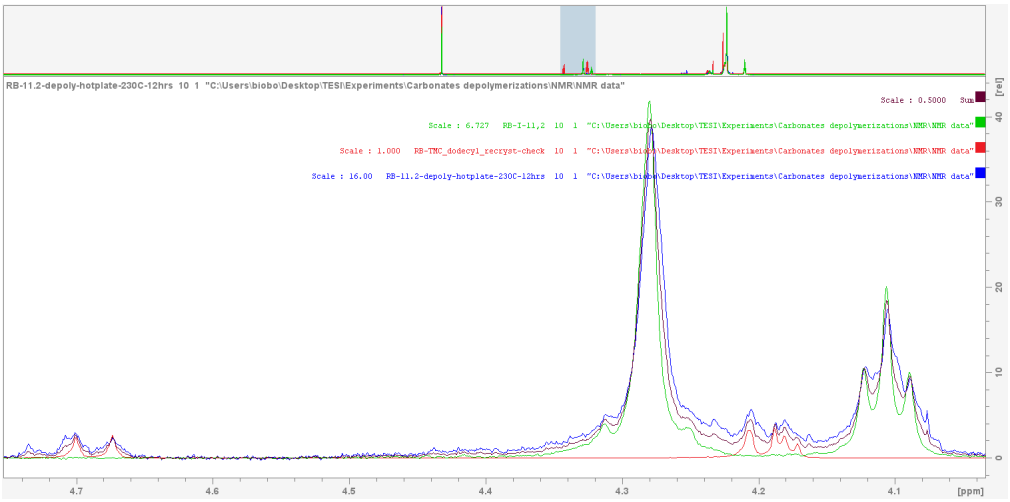

Figure 20: ^{1}H-NMR analysis of entry 6 from table 4.4, after bulk 12 hours isothermal heating on hotplate heater at 230 °C, in a capped vial, conversion detail.

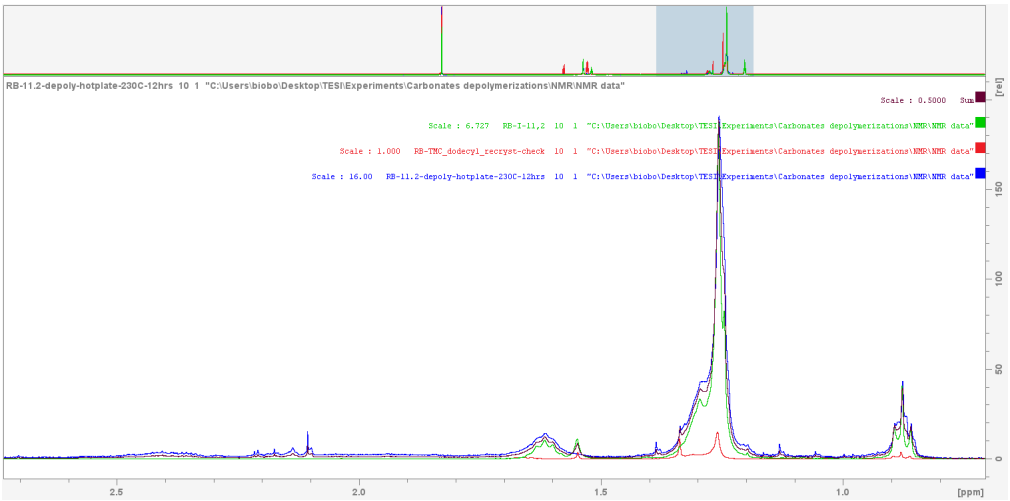

Figure 21: ^{1}H-NMR analysis of entry 6 from table 4.4, after bulk 12 hours isothermal heating on hotplate heater at 230 °C, in a capped vial, conversion detail.

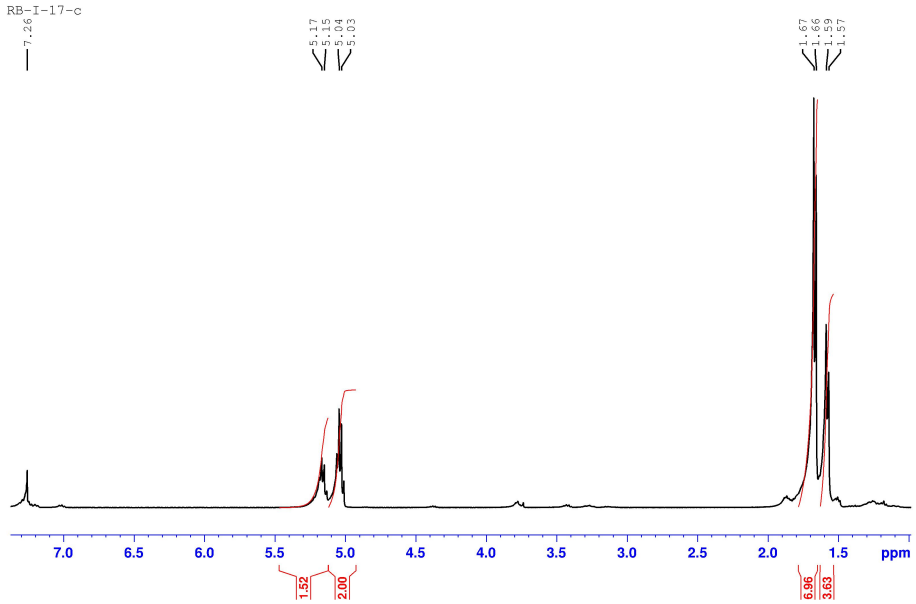

Figure 22: ^{1}H-NMR analysis of entry 1 reaction mixture from table 4.5.

^{1}H-NMR ($CDCl_3$): poly**(15)** δ 5.01-5.06 (-CH, q, 2H), δ 1.65-1.68 (-CH3, d, 3H), **(15)** δ 5.13-5.18 (-CH, q, 2H), δ 1.56-1.58 (-CH3, d, 3H), $CDCl_3$ δ 7.26 (-CH, s, 1H) ppm.

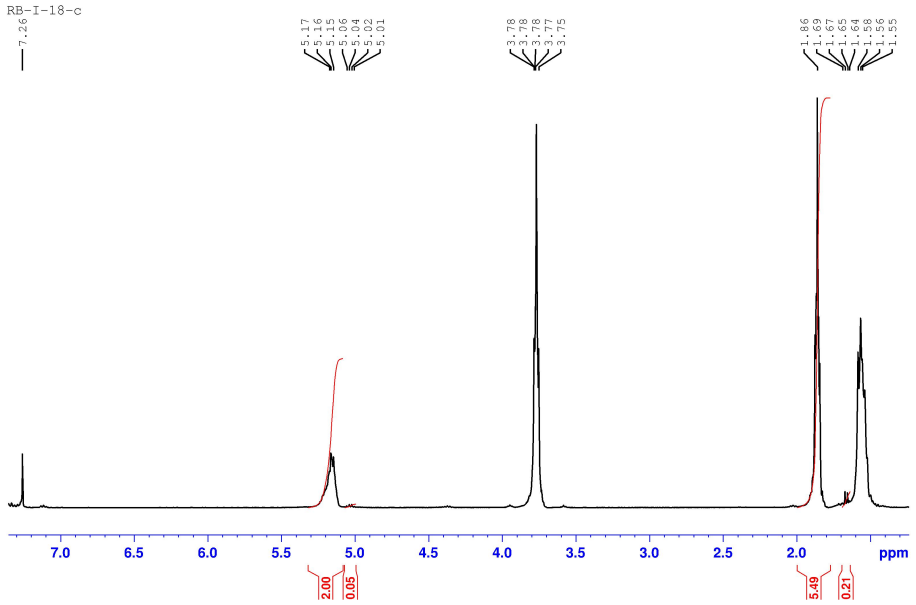

Figure 23: ^{1}H-NMR analysis of entry 2 reaction mixture from table 4.5.

^{1}H-NMR ($CDCl_3$): poly**(15)** δ 5.01-5.06 (-CH, q, 2H), δ 1.65-1.68 (-CH3, d, 3H), **(15)** δ 5.13-5.18 (-CH, q, 2H), δ 1.56-1.58 (-CH3, d, 3H), $CDCl_3$ δ 7.26 (-CH, s, 1H), H_2O δ 1.55 (-CH, s, 2H) , THF δ 3.78 (-CH2-O-, t, 4H), δ 1.88 (-CH2, t, 4H) ppm.

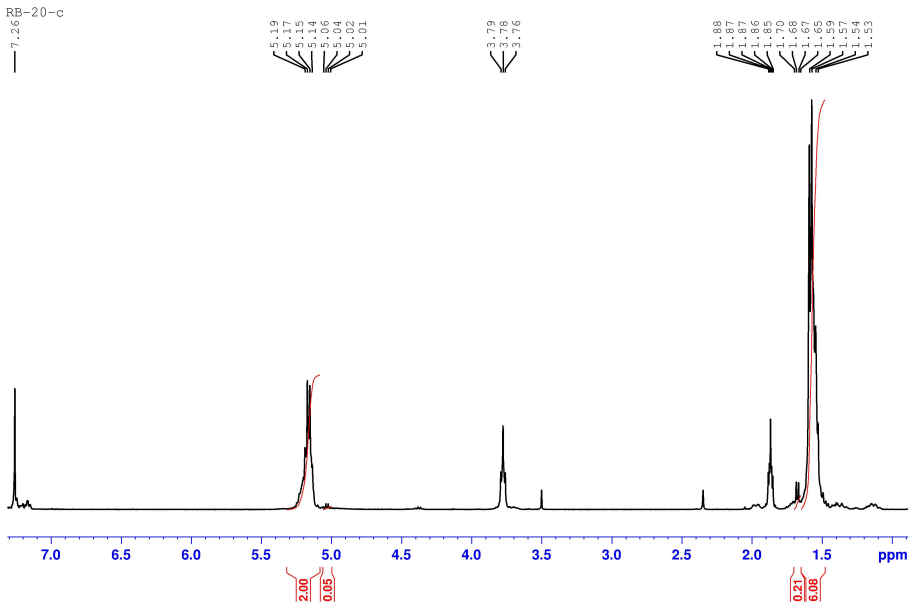

Figure 24: ^{1}H-NMR analysis of entry 5 reaction mixture from table 4.5.

^{1}H-NMR ($CDCl_3$): poly**(15)** δ 5.01-5.06 (-CH, q, 2H), δ 1.65-1.68 (-CH3, d, 3H), **(15)** δ 5.13-5.18 (-CH, q, 2H), δ 1.56-1.58 (-CH3, d, 3H), $CDCl_3$ δ 7.26 (-CH, s, 1H), H_2O δ 1.55 (-CH, s, 2H) , THF δ 3.78 (-CH2-O-, t, 4H), δ 1.88 (-CH2, t, 4H) ppm.

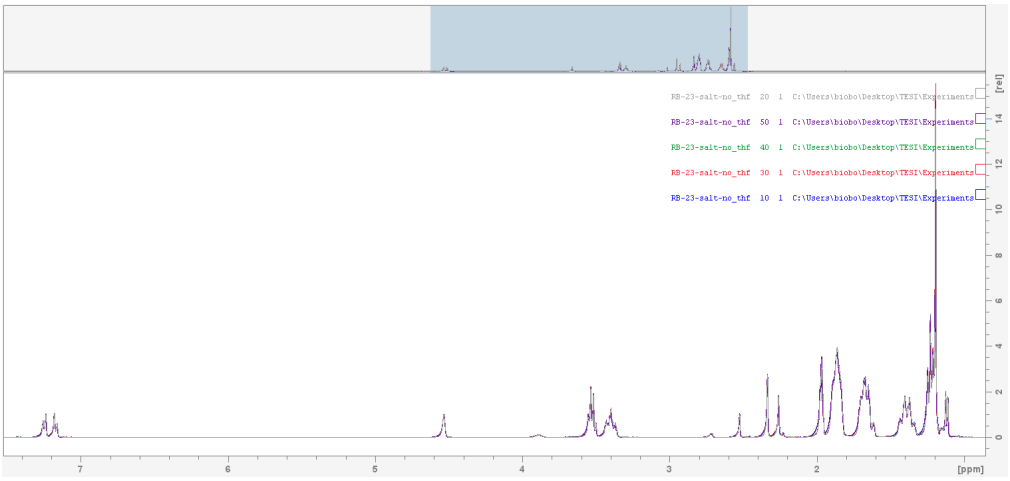

Figure 25: ^{1}H-NMR sequential multiple analysis of catalyst mixture composed of **(A-1)**, lithium tert-butoxide and **(S-1)** in CD_3CN. ^{1}H-NMR at 0, 28, 47, 74 and 101 minutes spectra.

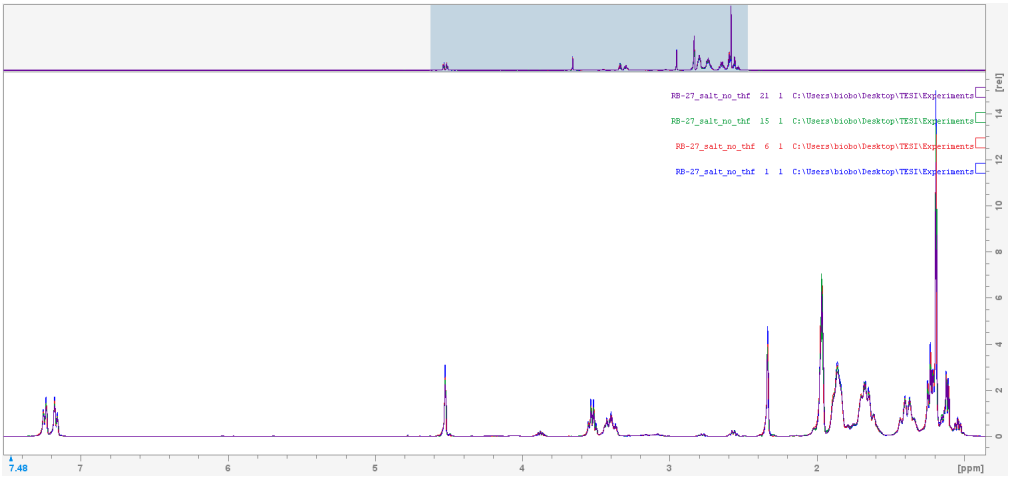

Figure 26: ^{1}H-NMR sequential multiple analysis of catalyst mixture composed of **(A-1)**, Sodium tert-butoxide and **(S-1)** in CD_3CN. ^{1}H-NMR at 0, 62, 131 and 205 minutes spectra.

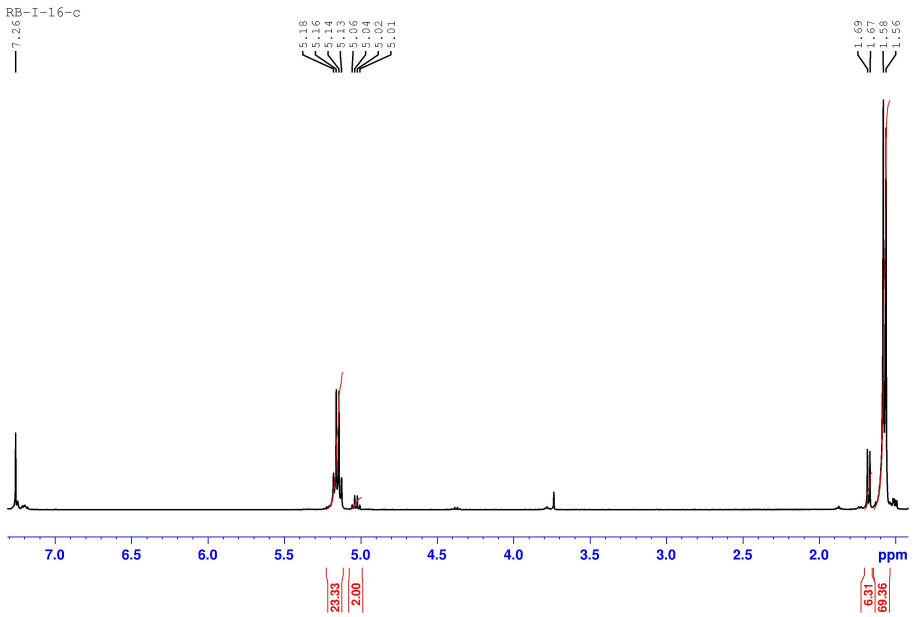

Figure 27: ^{1}H-NMR analysis of entry 1 reaction mixture from table 4.6.

^{1}H-NMR ($CDCl_3$): poly**(15)** δ 5.01-5.06 (-CH, q, 2H), δ 1.65-1.68 (-CH3, d, 3H), **(15)** δ 5.13-5.18 (-CH, q, 2H), δ 1.56-1.58 (-CH3, d, 3H), $CDCl_3$ δ 7.26 (-CH, s, 1H) ppm.

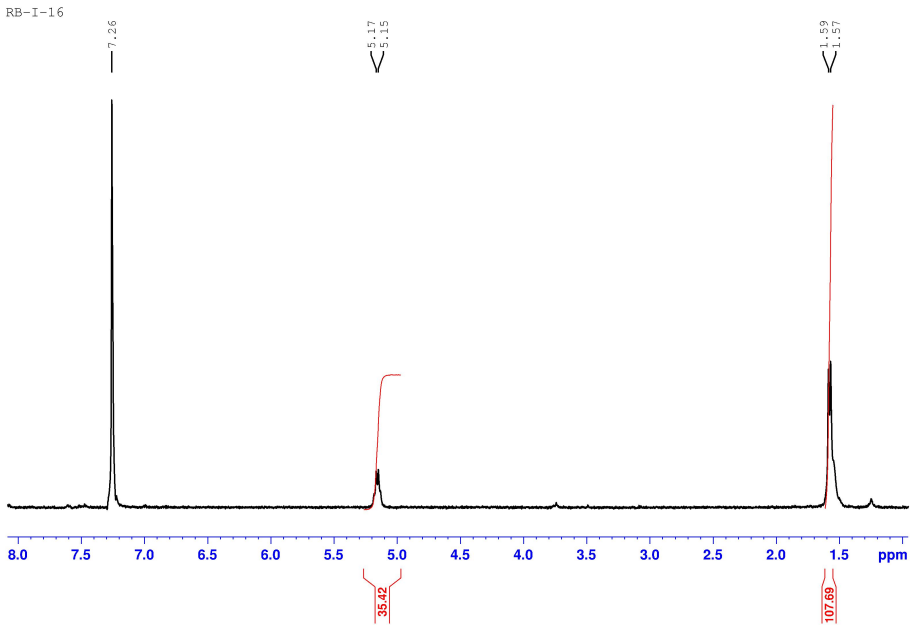

Figure 28: ^{1}H-NMR analysis of entry 1 reaction mixture from table 4.6.

^{1}H-NMR ($CDCl_3$): poly**(15)** δ 5.01-5.06 (-CH, q, 2H), δ 1.65-1.68 (-CH3, d, 3H), $CDCl_3$ δ 7.26 (-CH, s, 1H) ppm.

DSC characterization data

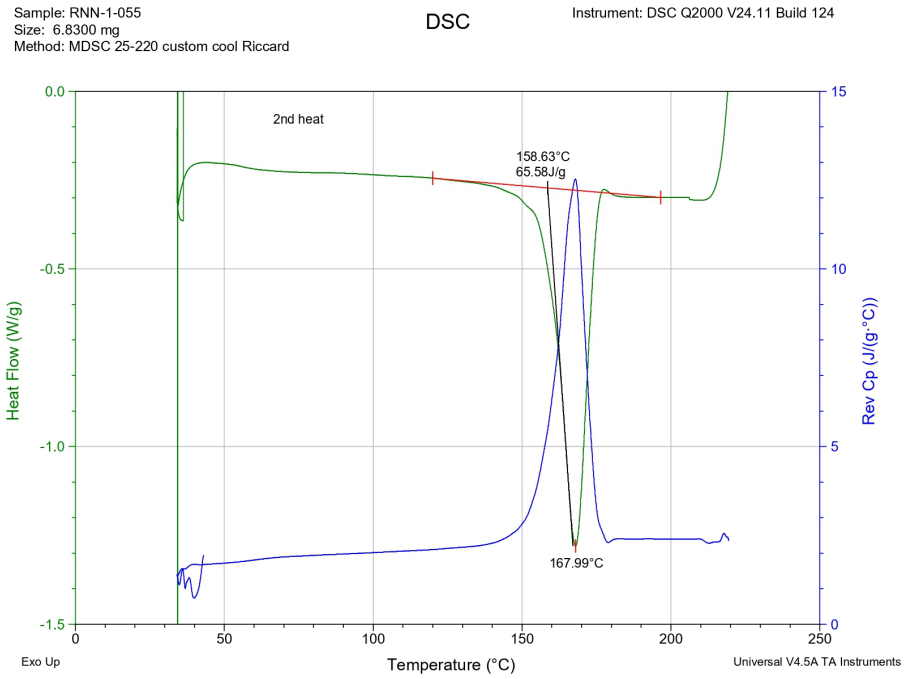

Figure 29: DSC analysis of poly**(15)** obtained at room temperature, entry 1 from table 4.2, 2^{nd} heating cycle, (endothermic peak downside).

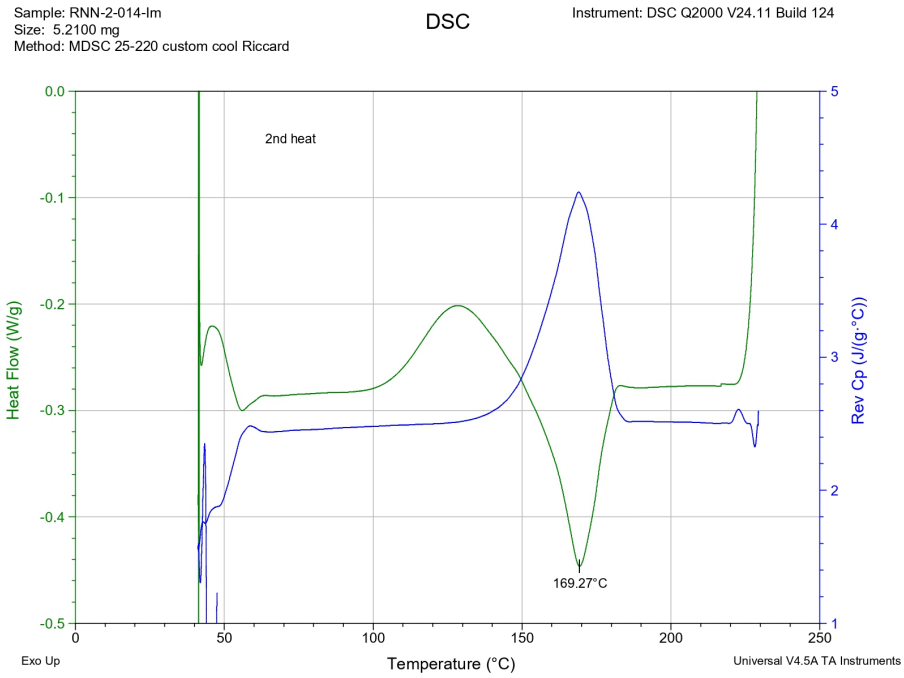

Figure 30: DSC analysis of poly**(16)** obtained at $-15\,^{\circ}C$, entry 2 from table 4.2, 2^{nd} heating cycle, (endothermic peak downside).

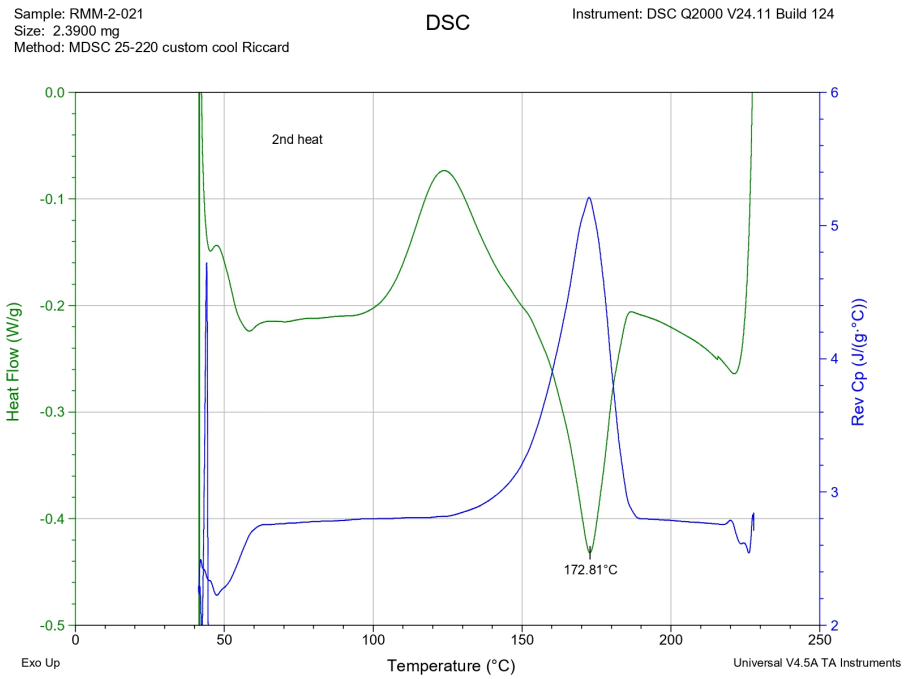

Figure 31: DSC analysis of poly**(16)** obtained at $-36\,^{\circ}\mathrm{C}$, entry 3 from table 4.2, 2^{nd} heating cycle, (endothermic peak downside).

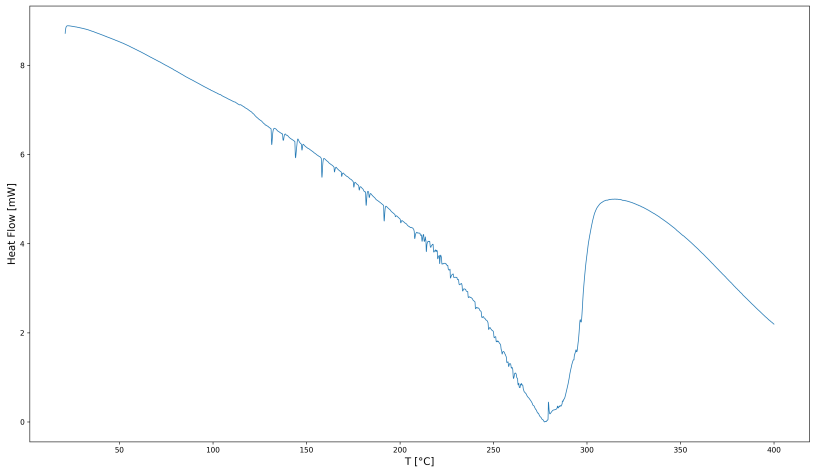

Figure 32: DSC analysis of decomposition experiment of poly**(9)**, entry 2 from table 4.4, single heating cycle, heating rate = $5\,^{\circ}\mathrm{C\,min^{-1}}$, (endothermic peak upside).

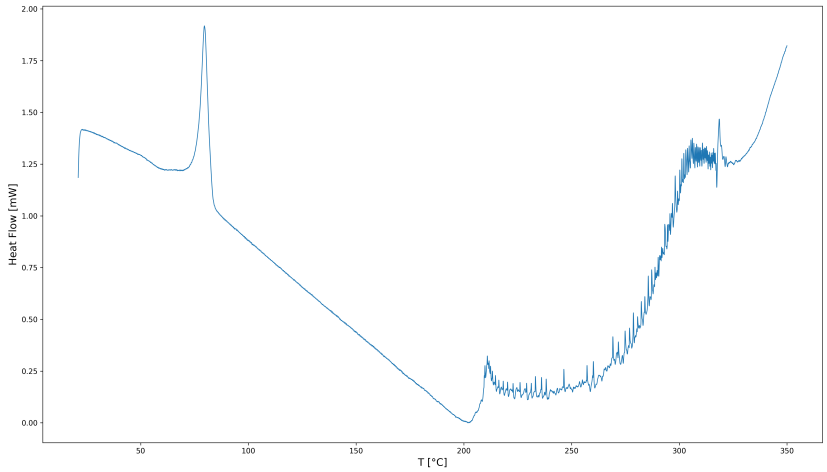

Figure 33: DSC analysis of decomposition experiment of poly**(11)**, entry 5 from table 4.4, single heating cycle, heating rate = 5 °C min^{-1}, (endothermic peak upside).

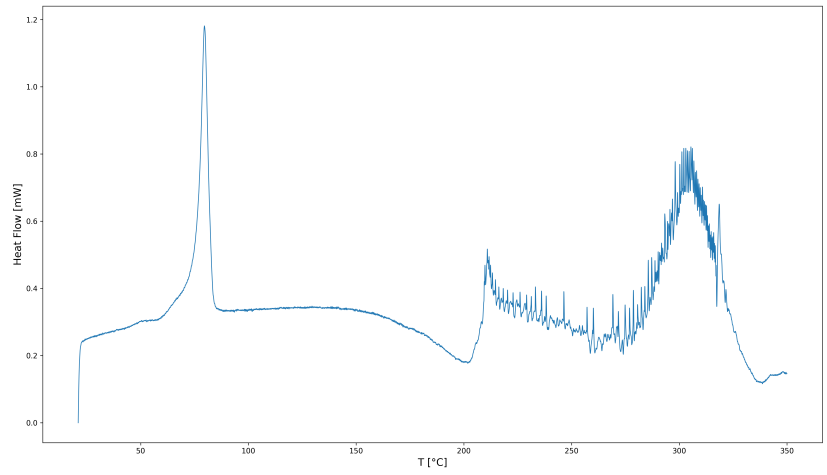

Figure 34: DSC analysis of poly**(11)**, entry 5 from table 4.4, second heating cycle, heating rate = 5 °C min^{-1}(1st heating cycle rate at 10 °C min^{-1} and cooling cycle rate at —10 °C min^{-1}). Third order interpolated curve subtracted, (endothermic peak upside).

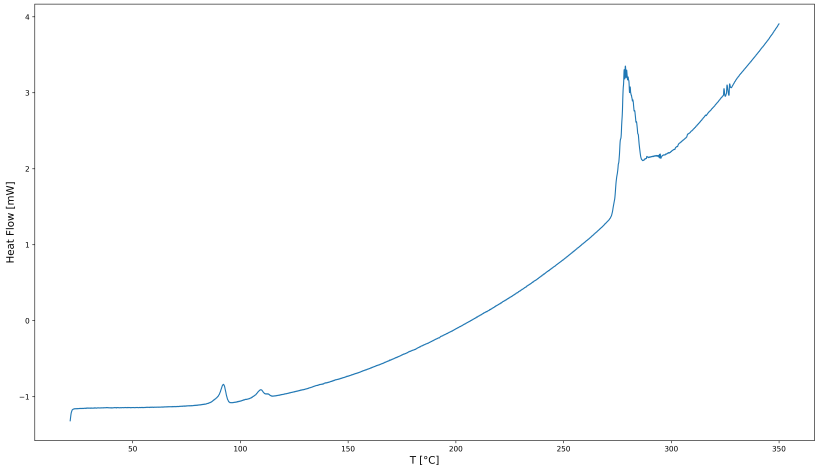

Figure 35: DSC analysis of decomposition experiment of poly**(12)**, entry 9 from table 4.4, single heating cycle, heating rate = 5 °C min^{-1}, (endothermic peak upside).

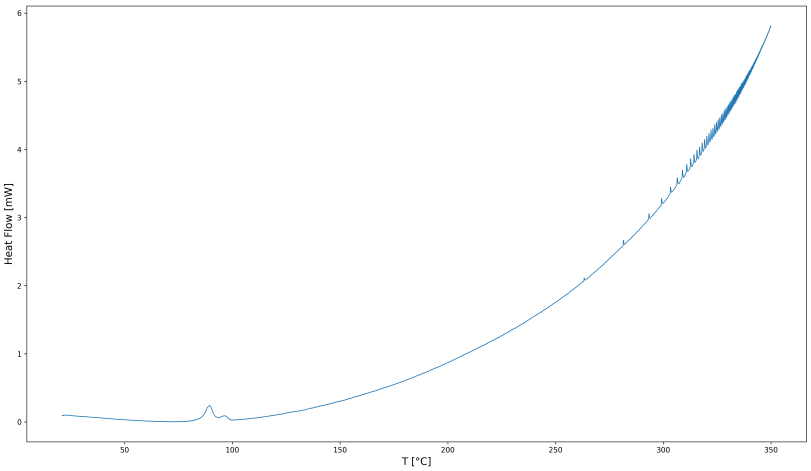

Figure 36: DSC analysis of decomposition experiment of poly**(13)**, entry 10 from table 4.4, single heating cycle, heating rate = 5 °C min^{-1}, (endothermic peak upside).

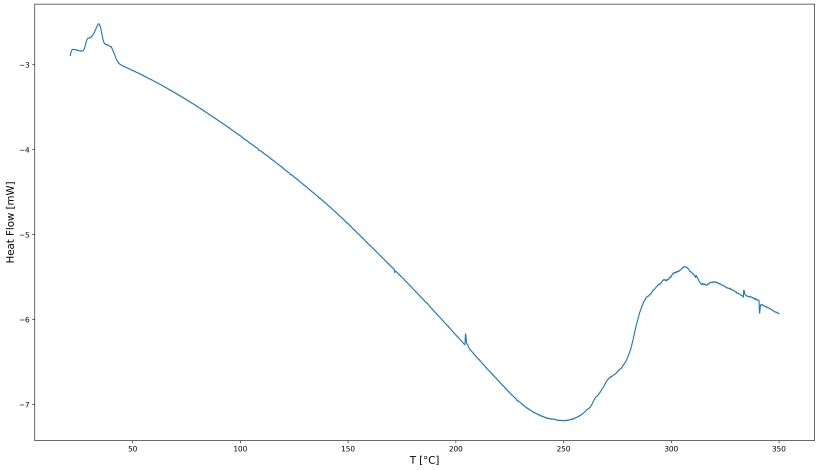

Figure 37: DSC analysis of decomposition experiment of poly**(1)**, entry 1 from table 4.4, single heating cycle, heating rate = 5 °C min^{-1}, (endothermic peak upside).

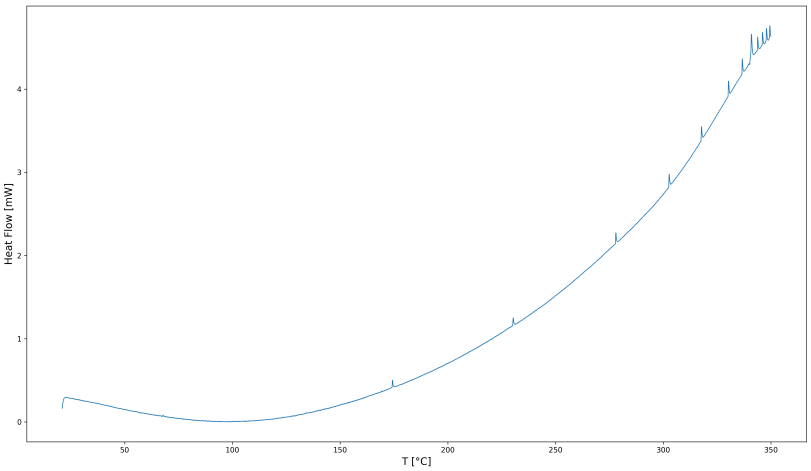

Figure 38: DSC analysis of decomposition experiment of poly**(8)**, entry 13 from table 4.4, single heating cycle, heating rate = 5 °C min^{-1}, (endothermic peak upside).

TGA-MS characterization data

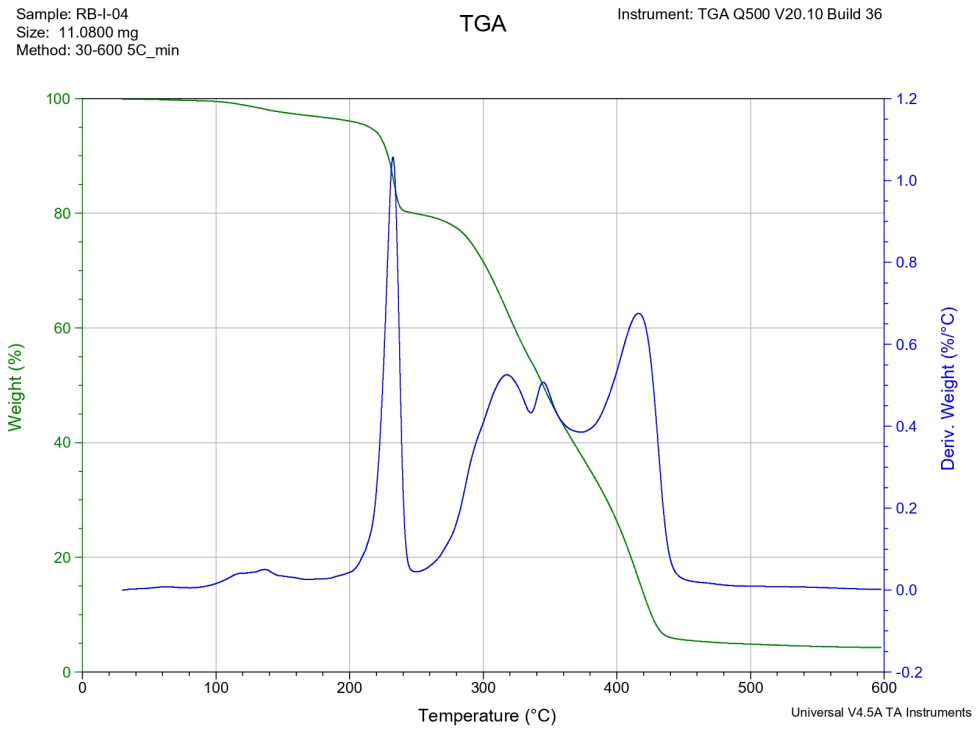

Figure 39: TGA analysis of poly**(6)**, entry 3 from table 4.4.

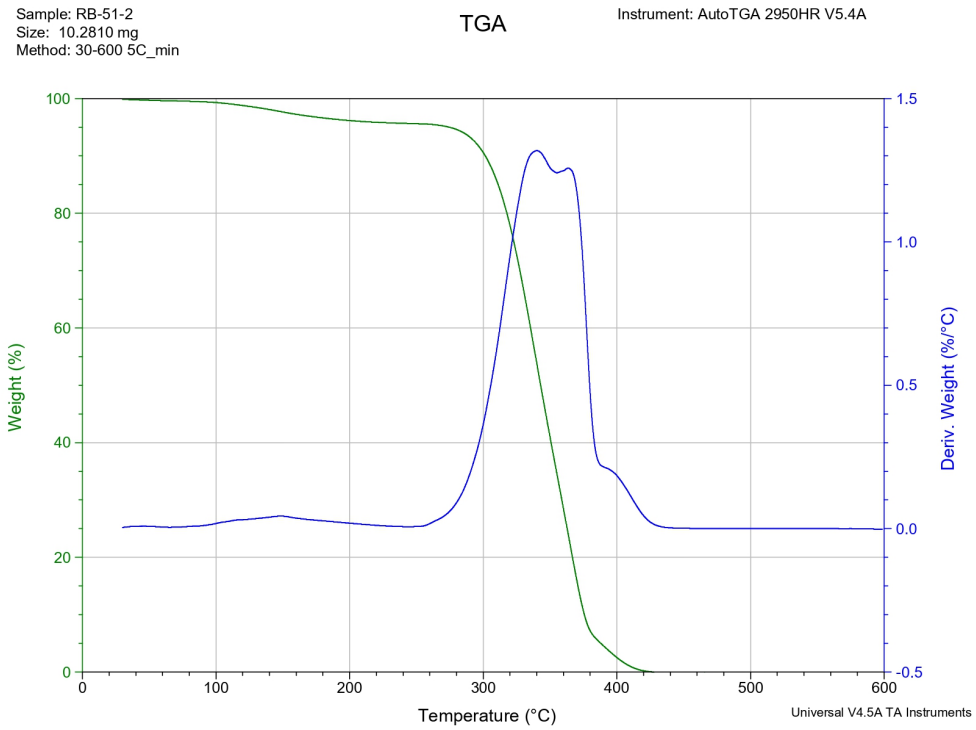

Figure 40: TGA analysis of poly**(8)**, entry 13 from table 4.4.

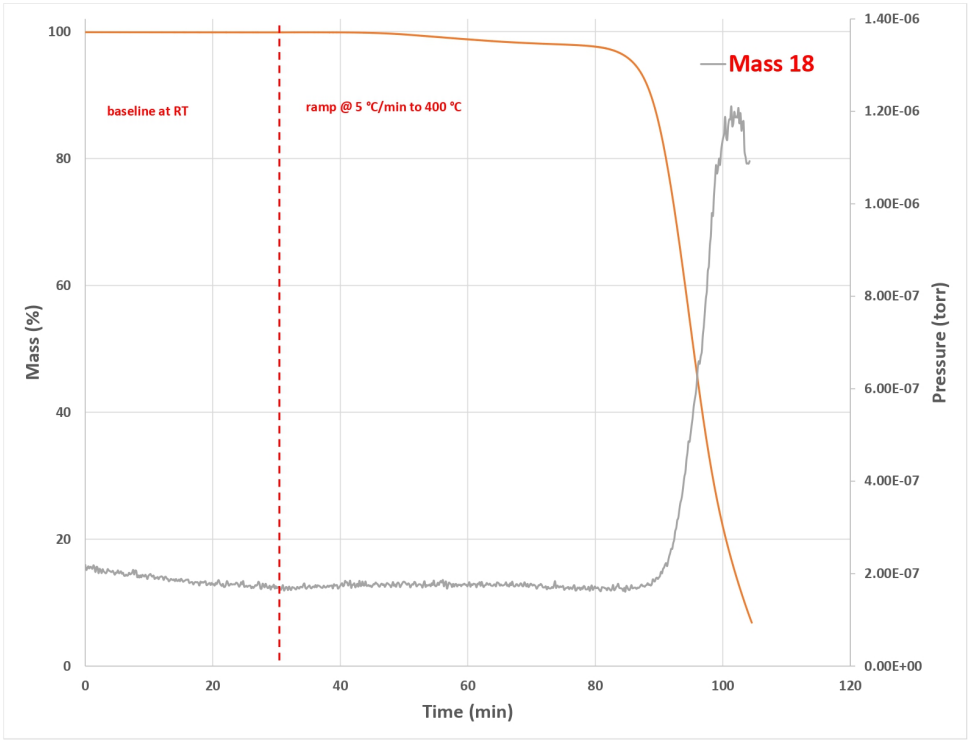

Figure 41: In situ MS analysis during TGA of poly**(10)**, entry 4 from table 4.4. Water partial pressure detection.

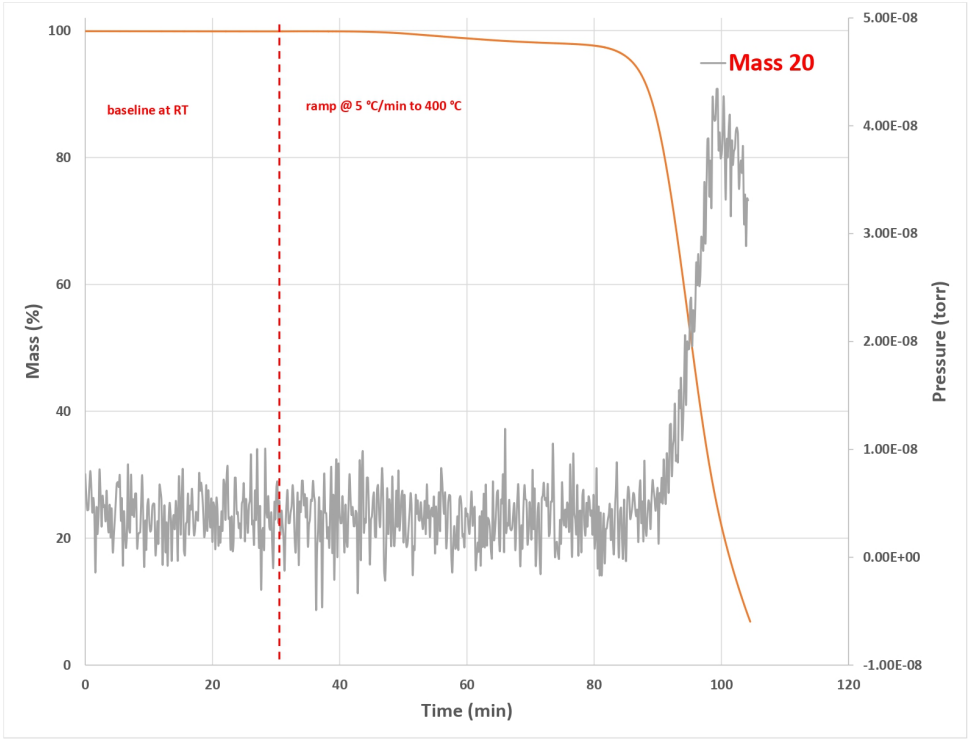

Figure 42: In situ MS analysis during TGA of poly**(10)**, entry 4 from table 4.4. Possible HF partial pressure detection.

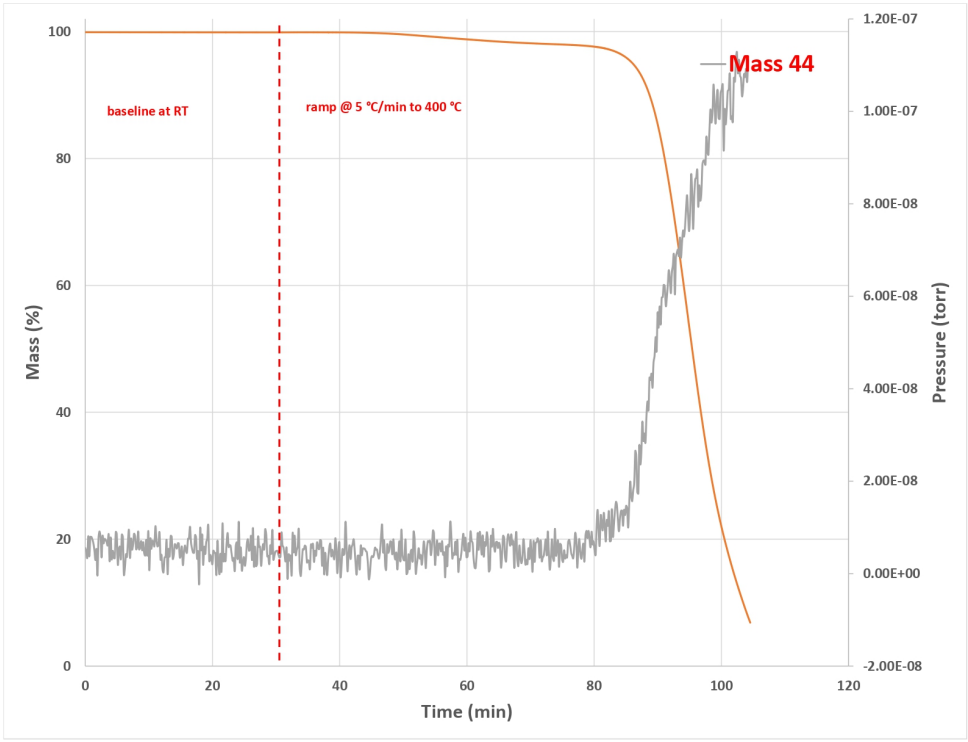

Figure 43: In situ MS analysis during TGA of poly**(10)**, entry 4 from table 4.4. Carbon dioxide partial pressure detection.

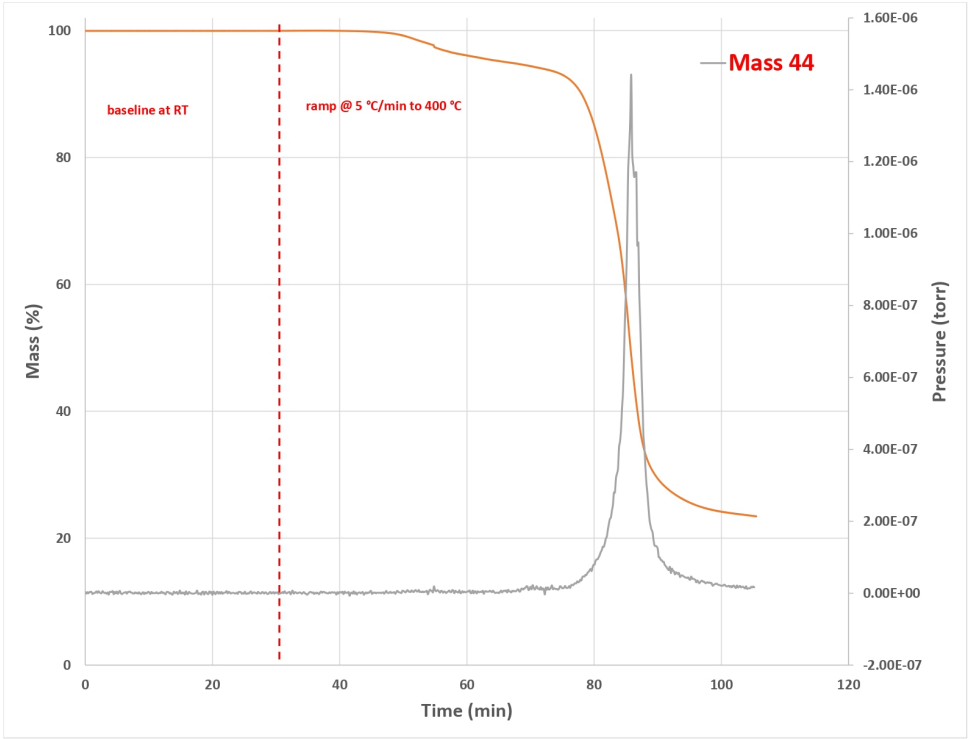

Figure 44: In situ MS analysis during TGA of poly**(9)**, entry 2 from table 4.4. Carbon dioxide partial pressure detection.

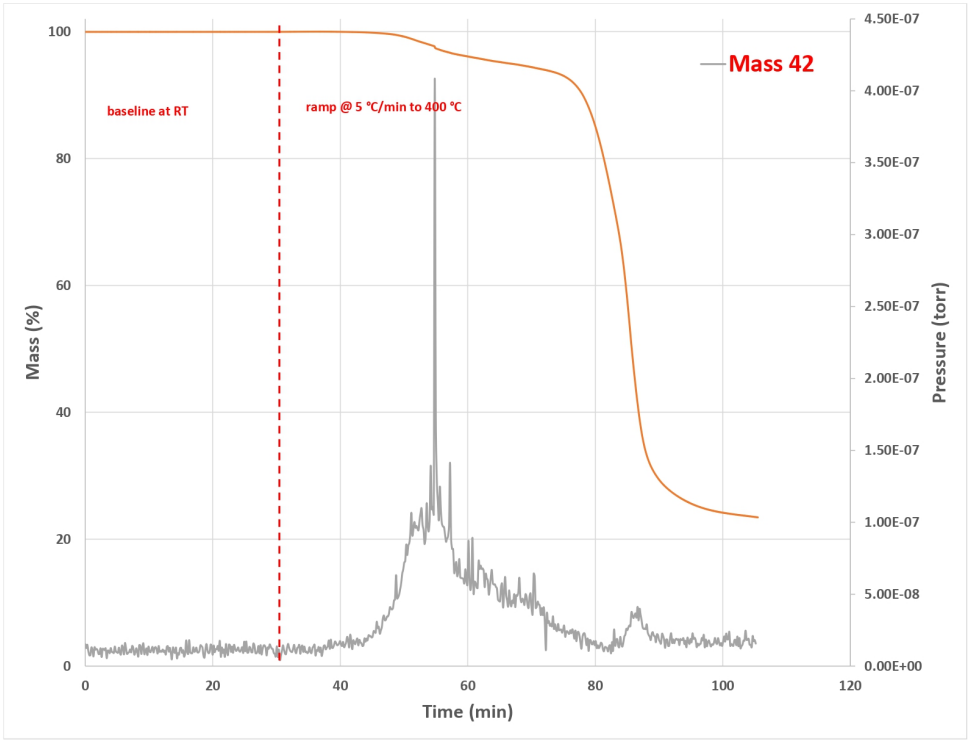

Figure 45: In situ MS of TGA analysis of poly**(9)**, entry 2 from table 4.4. Not identified partial pressure detection.

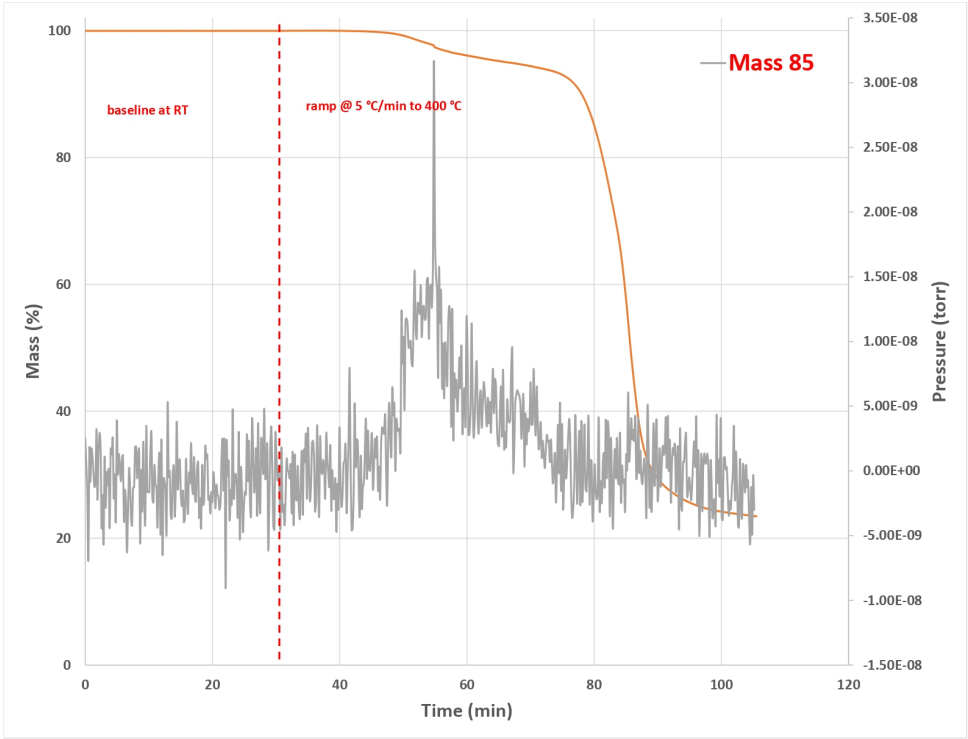

Figure 46: In situ MS analysis during TGA of poly**(9)**, entry 2 from table 4.4. Not identified partial pressure detection.

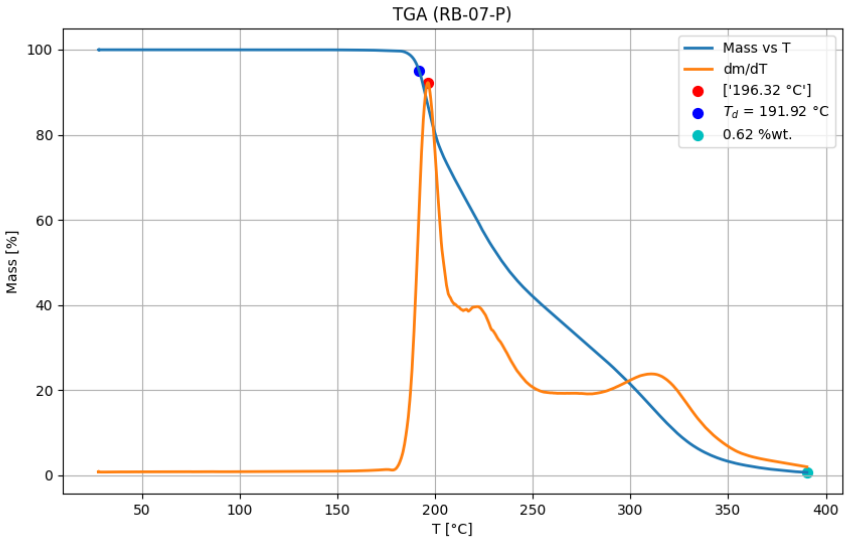

Figure 47: TGA analysis of poly**(11)**, entry 5 from table 4.4.

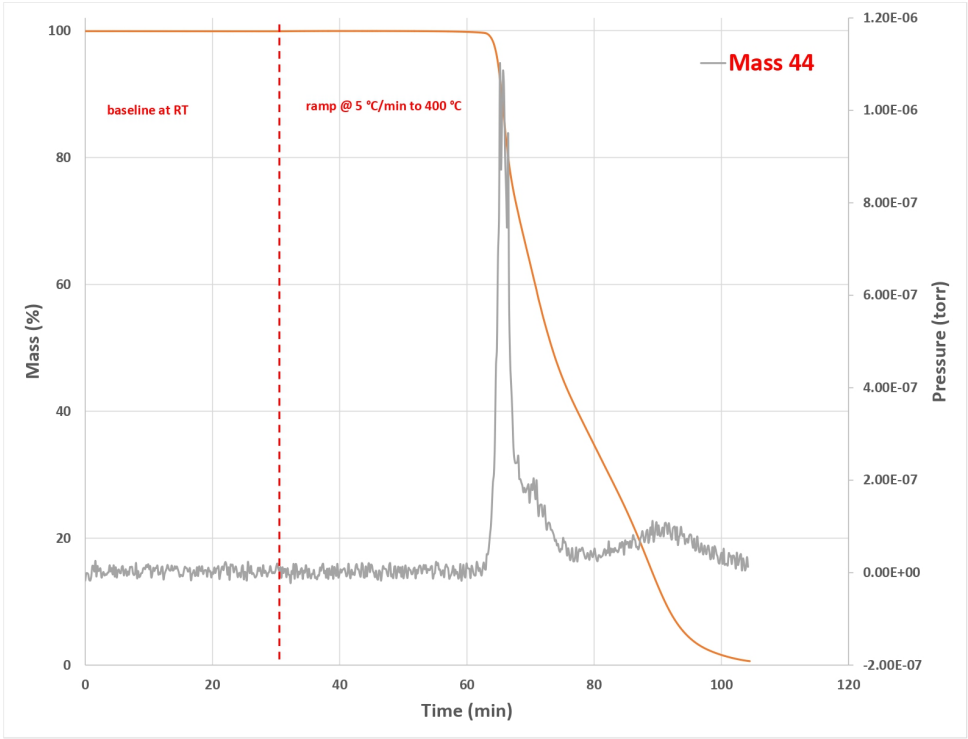

Figure 48: In situ MS analysis of poly**(11)**, entry 5 from table 4.4. Carbon dioxide partial pressure detection.

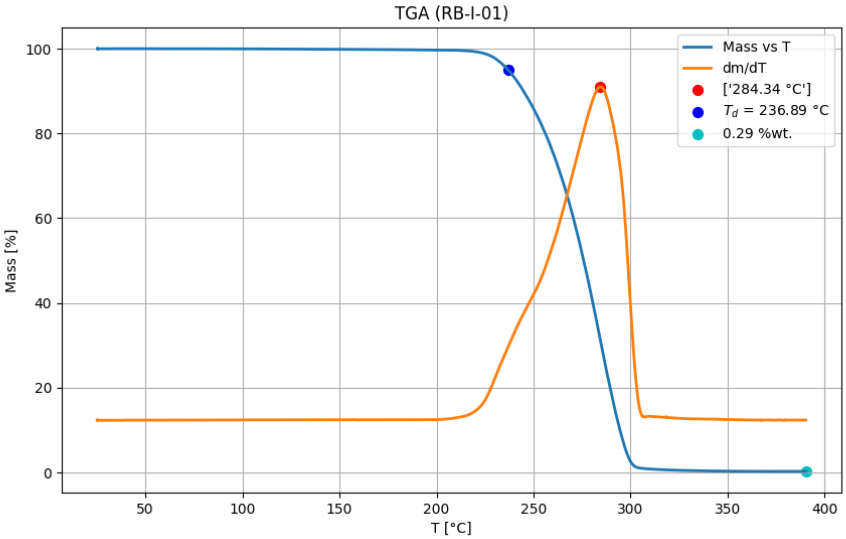

Figure 49: TGA analysis of poly**(1)**, entry 1 from table 4.4.

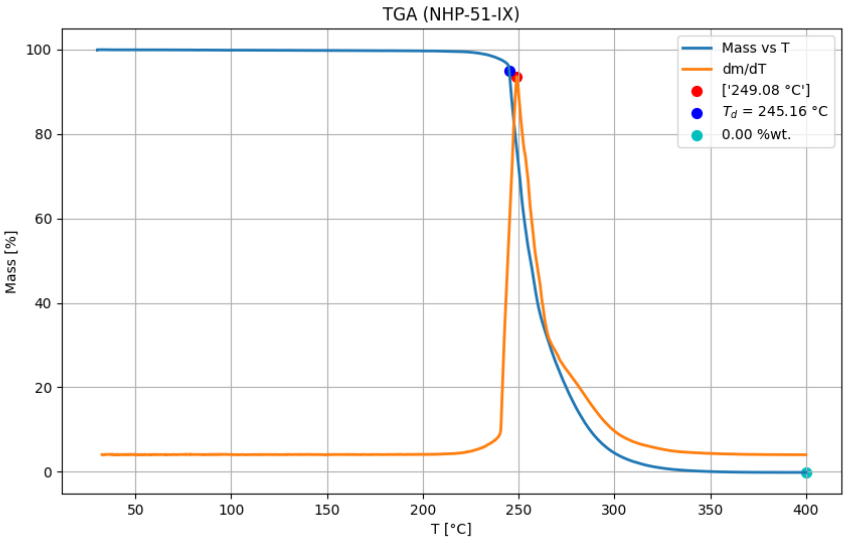

Figure 50: TGA analysis of poly**(12)**, entry 9 from table 4.4.

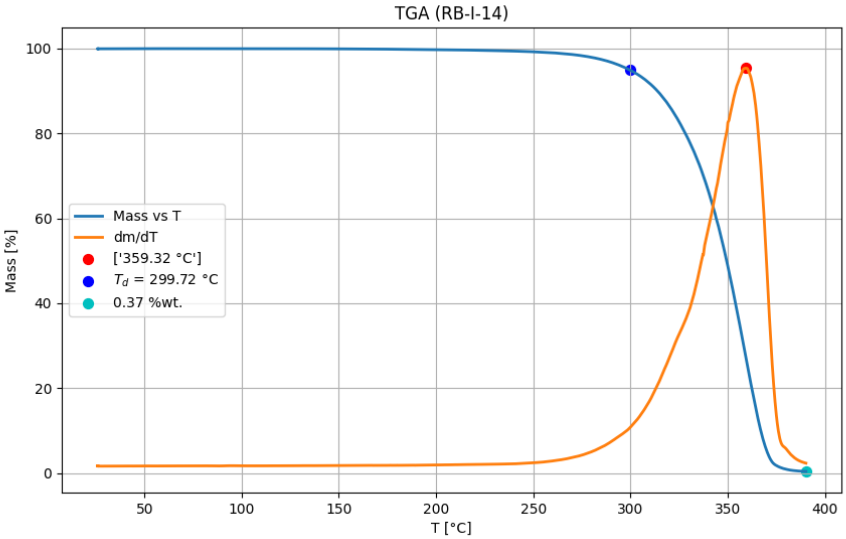

Figure 51: TGA analysis of poly**(13)**, entry 10 from table 4.4.

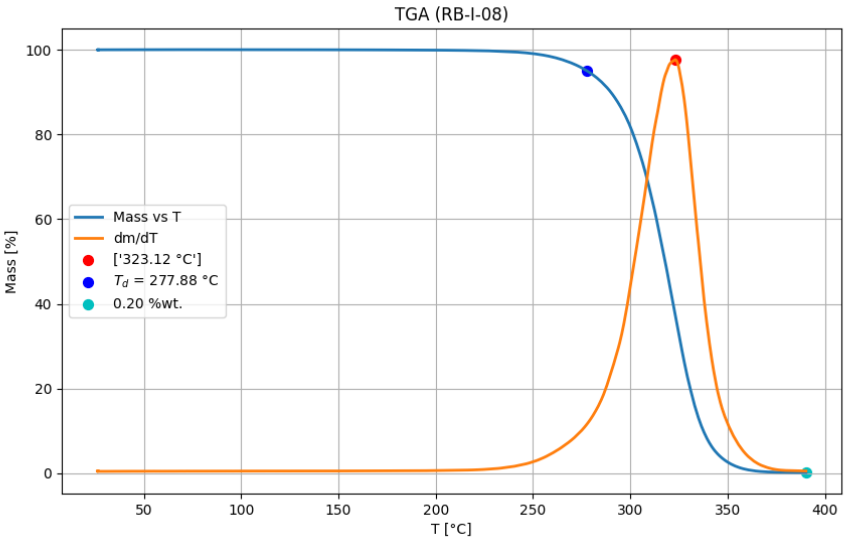

Figure 52: TGA analysis of poly**(3)**, entry 6 from table 4.4.

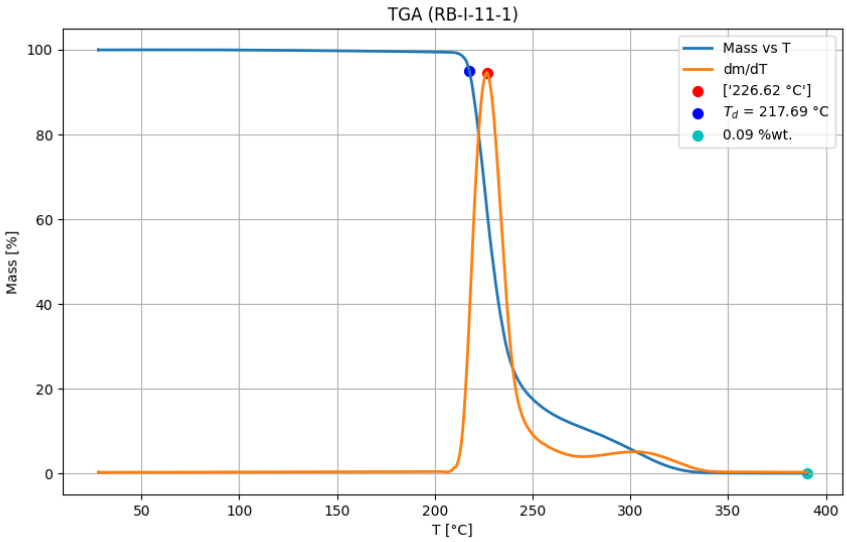

Figure 53: TGA analysis of poly**(3)**, entry 8 from table 4.4.

Bibliography

[1] Xiangyi Zhang, Mareva Fevre, Gavin O. Jones, and Robert M. Waymouth. «Catalysis as an Enabling Science for Sustainable Polymers». In: *Chemical Reviews* 118.2 (2018), pp. 839–885. doi: 10.1021/acs.chemrev.7b00329. url: https://doi.org/10.1021/acs.chemrev.7b00329 (cit. on pp. 2, 14, 16, 26, 30).

[2] Andrzej Duda and Adam Kowalski. «Thermodynamics and Kinetics of Ring-Opening Polymerization». In: *Handbook of Ring-Opening Polymerization*. John Wiley & Sons, Ltd, 2009, pp. 1–51. isbn: 978-3-527-62840-7. url: https://www.onlinelibrary.wiley.com/doi/abs/10.1002/9783527628407.ch1 (cit. on pp. 2, 4–8, 10–16, 27, 30).

[3] Peter Olsén, Karin Odelius, and Ann-Christine Albertsson. «Thermodynamic Presynthetic Considerations for Ring-Opening Polymerization». In: *Biomacromolecules* 17.3 (2016), pp. 699–709. doi: 10.1021/acs.biomac.5b01698. url: https://doi.org/10.1021/acs.biomac.5b01698 (cit. on pp. 2, 4, 5, 8–13, 15, 27–30, 77).

[4] Rahul Upadhya, Shashank Kosuri, Matthew Tamasi, Travis A. Meyer, Supriya Atta, Michael A. Webb, and Adam J. Gormley. «Automation and data-driven design of polymer therapeutics». In: *Advanced Drug Delivery Reviews* 171 (2021), pp. 1–28. doi: 10.1016/j.addr.2020.11.009. url: https://www.sciencedirect.com/science/article/pii/S0169409X20302180 (cit. on pp. 2, 3, 31–34).

[5] Jiaru Bai, Liwei Cao, Sebastian Mosbach, Jethro Akroyd, Alexei A. Lapkin, and Markus Kraft. «From Platform to Knowledge Graph: Evolution of Laboratory Automation». In: *JACS Au* 2.2 (2022), pp. 292–309. doi: 10.1021/jacsau.1c00438. url: https://doi.org/10.1021/jacsau.1c00438 (cit. on pp. 2, 31–33).

[6] Matthew K. Kiesewetter, Eun Ji Shin, James L. Hedrick, and Robert M. Waymouth. «Organocatalysis: Opportunities and Challenges for Polymer Synthesis». In: *Macromolecules* 43.5 (2010), pp. 2093–2107. doi: 10.1021/ma9025948. url: https://doi.org/10.1021/ma9025948 (cit. on pp. 2, 12, 14–17, 78).

[7] G. Crotts and Tae Gwan Park. «Protein delivery from poly(lactic-co-glycolic acid) biodegradable microspheres: Release kinetics and stability issues». In: *Journal of Microencapsulation* 15.6 (1998). PMID: 9818948, pp. 699–713. doi: 10.3109/02652049809008253. url: https://doi.org/10.3109/02652049809008253 (cit. on p. 2).

[8] Vincent Pavot, Morgane Berthet, Julien Rességuier, Sophie Legaz, Sarah C Gilbert Nadège Handké, Stéphane Paul, and Bernard Verrier. «Poly(Lactic Acid) and Poly(Lactic-Co-Glycolic Acid) Particles as Versatile Carrier Platforms for Vaccine Delivery». In: *Nanomedicine* 9.17 (2014). PMID: 25529572, pp. 2703–2718. doi: 10.2217/nnm.14.156. url: https://doi.org/10.2217/nnm.14.156 (cit. on p. 2).

[9] Marcus Reis, Filipp Gusev, Nicholas G. Taylor, Sang Hun Chung, Matthew D. Verber, Yueh Z. Lee, Olexandr Isayev, and Frank A. Leibfarth. «Machine-Learning-Guided Discovery of 19F MRI Agents Enabled by Automated Copolymer Synthesis». In: *Journal of the American Chemical Society* 143.42 (2021), pp. 17677–17689. doi: 10.1021/jacs.1c08181. url: https://doi.org/10.1021/jacs.1c08181 (cit. on pp. 2, 32, 33, 35).

[10] Christopher M. Plummer, Le Li, and Yongming Chen. «Ring-Opening Polymerization for the Goal of Chemically Recyclable Polymers». In: *Macromolecules* 56.3 (2023), pp. 731–750. doi: 10.1021/acs.macromol.2c01694. url: https://doi.org/10.1021/acs.macromol.2c01694 (cit. on pp. 2, 6, 26–30).

[11] Rebecca M. Wilson and Tristan H. Lambert. «Cyclopropenium Ions in Catalysis». In: *Accounts of Chemical Research* 55.20 (2022), pp. 3057–3069. doi: 10.1021/acs.accounts.2c00546. url: https://doi.org/10.1021/acs.accounts.2c00546 (cit. on pp. 3, 20, 21, 93).

[12] Michael Breulmann, Johannes Becker, Sabine Philipp, Valentine Reimer, Sebastian Koltzenburg, Gabriel Skupin, Michael Bernhard Schick, Katharina Schlegel,

Carsten Sinkel, and Motonori Yamamoto. *Polymers, Biodegradable*. English. Copyright © 2016 Wiley-VCH Verlag GmbH & Co. KGaA. All rights reserved. Weinheim, Germany, 2009 (cit. on p. 3).

[13] Xiangyi Zhang, Gavin O. Jones, James L. Hedrick, and Robert M. Waymouth. «Fast and selective ring-opening polymerizations by alkoxides and thioureas». In: *Nature Chemistry* 8.11 (2016), pp. 1047–1053. doi: 10.1038/nchem.2574. url: https://www.nature.com/articles/nchem.2574 (cit. on pp. 3, 12, 14–16, 19).

[14] Eddy W. P Tan, James L Hedrick, Pedro L Arrechea, Tim Erdmann, Vivien Kiyek, Simon Lottier, Yi Yan Yang, and Nathaniel H Park. «Overcoming Barriers in Polycarbonate Synthesis: A Streamlined Approach for the Synthesis of Cyclic Carbonate Monomers». eng. In: *Macromolecules* 54.4 (2021), pp. 1767–1774. issn: 0024-9297 (cit. on p. 3).

[15] Benjamín Rodríguez Hernández and Antje Lieske. «Widening the Application Range of PLA-Based Thermoplastic Materials through the Synthesis of PLA-Polyether Block Copolymers: Thermal, Tensile, and Rheological Properties». eng. In: *Macromolecular materials and engineering* 309.3 (2024). issn: 1438-7492 (cit. on p. 3).

[16] K. Fukushima. «Poly(trimethylene carbonate)-based polymers engineered for biodegradable functional biomaterials». In: *Biomater. Sci.* 4 (1 2016), pp. 9–24. doi: 10.1039/C5BM00123D. url: http://dx.doi.org/10.1039/C5BM00123D (cit. on p. 3).

[17] Andrzej Duda, Adam Kowalski, Jan Libiszowski, and Stanislaw Penczek. «Thermodynamic and Kinetic Polymerizability of Cyclic Esters». In: *Macromolecular Symposia* 224.1 (2005), pp. 71–84. doi: 10.1002/masy.200550607. url: https://onlinelibrary.wiley.com/doi/abs/10.1002/masy.200550607 (cit. on pp. 3, 5, 7).

[18] Rohit Batra, Le Song, and Rampi Ramprasad. «Emerging materials intelligence ecosystems propelled by machine learning». In: *Nature Reviews Materials* (2020), pp. 1–24. doi: 10.1038/s41578-020-00255-y. url: https://www.nature.com/articles/s41578-020-00255-y (cit. on pp. 3, 11, 33–35).

[19] Tarak K. Patra. «Data-Driven Methods for Accelerating Polymer Design». In: *ACS Polymers Au* 2.1 (2022), pp. 8–26. doi: 10.1021/acspolymersau.1c00035. url: https://doi.org/10.1021/acspolymersau.1c00035 (cit. on pp. 3, 33, 34).

[20] Kan Hatakeyama-Sato. «Recent advances and challenges in experiment-oriented polymer informatics». In: *Polymer Journal* (2022), pp. 1–15. doi: 10.1038/s41428-022-00734-9. url: https://www.nature.com/articles/s41428-022-00734-9 (cit. on pp. 3, 33, 34).

[21] Romain Morodo, David M. Dumas, Jia Zhang, Kai H. Lui, Paul J. Hurst, Riccardo Bosio, Luis M. Campos, Nathaniel H. Park, Robert M. Waymouth, and James L. Hedrick. «Ring-Opening Polymerization of Cyclic Esters and Carbonates with (Thio)urea/Cyclopropenimine Organocatalytic Systems». eng. In: *ACS macro letters* 13.2 (2024), pp. 181–188. issn: 2161-1653 (cit. on pp. 4, 12, 14–16, 18, 74, 75, 80–82).

[22] Thierry Hamaide, Yves Holl, Laurent Fontaine, Jean-luc Six, and Armand Soldera. «Teaching Polymer Chemistry: Revisiting the Syllabus». In: *Open Journal of Polymer Chemsitry* 2 (Nov. 2012), p. 132. doi: 10.4236/ojpchem.2012.24018 (cit. on p. 5).

[23] Changxia Shi, Liam T. Reilly, V. Sai Phani Kumar, Matthew W. Coile, Scott R. Nicholson, Linda J. Broadbelt, Gregg T. Beckham, and Eugene Y.-X. Chen. «Design principles for intrinsically circular polymers with tunable properties». In: *Chem* 7.11 (2021), pp. 2896–2912. issn: 2451-9294. doi: https://doi.org/10.1016/j.chempr.2021.10.004. url: https://www.sciencedirect.com/science/article/pii/S2451929421004824 (cit. on pp. 5–8, 15, 28–30).

[24] Peter Olsén, Jenny Undin, Karin Odelius, Helmut Keul, and Ann-Christine Albertsson. «Switching from Controlled Ring-Opening Polymerization (cROP) to Controlled Ring-Closing Depolymerization (cRCDP) by Adjusting the Reaction Parameters That Determine the Ceiling Temperature». In: *Biomacromolecules* 17.12 (2016), pp. 3995–4002. doi: 10.1021/acs.biomac.6b01375. url: https://doi.org/10.1021/acs.biomac.6b01375 (cit. on pp. 6, 8, 10, 28, 30).

[25] Nahrain E. Kamber, Wonhee Jeong, Robert M. Waymouth, Russell C. Pratt, Bas G. G. Lohmeijer, and James L. Hedrick. «Organocatalytic Ring-Opening Polymerization». In: *Chemical Reviews* 107.12 (2007), pp. 5813–5840. doi: 10.1021/cr068415b. url: https://doi.org/10.1021/cr068415b (cit. on pp. 6, 12–17, 78).

[26] Immanuel Charles David. «Principles of Polymerization-Fourth Edition By George Odian». eng. In: *AIChE Journal* 54.11 (2008), pp. 3029–3029. issn: 0001-1541 (cit. on pp. 7, 8, 12).

[27] Penczek and Stanislaw. «Terminology of kinetics and thermodynamics and mechanisms of polymerization». eng. In: *Journal of polymer science. Part A and Polymer chemistry* 40.11 (2002), pp. 1665–1676. issn: 0887-624X (cit. on p. 9).

[28] Junpeng Zhao and Nikos Hadjichristidis. «Polymerization of 5-alkyl δ -lactones catalyzed by diphenyl phosphate and their sequential organocatalytic polymerization with monosubstituted epoxides». In: *Polym. Chem.* 6 (14 2015), pp. 2659–2668. doi: 10.1039/C5PY00019J. url: http://dx.doi.org/10.1039/C5PY00019J (cit. on p. 10).

[29] Binhong Lin and Robert M. Waymouth. «Urea Anions: Simple, Fast, and Selective Catalysts for Ring-Opening Polymerizations». In: *Journal of the American Chemical Society* 139.4 (2017), pp. 1645–1652. doi: 10.1021/jacs.6b11864. url: https://doi.org/10.1021/jacs.6b11864 (cit. on pp. 12, 14–19, 23, 96).

[30] Caleb N. Jadrich, Vince E. Pane, Binhong Lin, Gavin O. Jones, James L. Hedrick, Nathaniel H. Park, and Robert M. Waymouth. «A Cation-Dependent Dual Activation Motif for Anionic Ring-Opening Polymerization of Cyclic Esters». In: *Journal of the American Chemical Society* 144.19 (2022), pp. 8439–8443. doi: 10.1021/jacs.2c01436. url: https://doi.org/10.1021/jacs.2c01436 (cit. on pp. 14, 16, 20, 82).

[31] Caleb N. Jadrich, Vince E. Pane, Binhong Lin, Gavin O. Jones, James L. Hedrick, Nathaniel H. Park, and Robert M. Waymouth. «A Cation-Dependent Dual Activation Motif for Anionic Ring-Opening Polymerization of Cyclic Esters». In: *Journal of the American Chemical Society* 144.19 (2022), pp. 8439–8443. doi: 10.1021/jacs.2c01436. url: https://doi.org/10.1021/jacs.2c01436 (cit. on p. 15).

[32] Jeffrey S. Bandar, Anont Tanaset, and Tristan H. Lambert. «Phase-transfer and other types of catalysis with cyclopropenium ions». In: *Chemistry* 21.20 (2015), pp. 7365–8. doi: 10.1002/chem.201500124. url: https://doi.org/10.1002/chem.201500124 (cit. on pp. 20, 93).

[33] Marcus H. Reis, Frank A. Leibfarth, and Louis M. Pitet. «Polymerizations in Continuous Flow: Recent Advances in the Synthesis of Diverse Polymeric Materials». In:

ACS Macro Letters 9.1 (2020), pp. 123–133. doi: 10.1021/acsmacrolett.9b00933. url: https://doi.org/10.1021/acsmacrolett.9b00933 (cit. on pp. 21, 22, 24).

[34] Porta Riccardo, Benaglia Maurizio, and Puglisi Alessandra. «Flow Chemistry: Recent Developments in the Synthesis of Pharmaceutical Products». eng. In: *Organic process research & development* 20.1 (2016), pp. 2–25. issn: 1083-6160 (cit. on p. 21).

[35] Tonhauser Christoph, Natalello Adrian, Löwe Holger, and Frey Holger. «Microflow Technology in Polymer Synthesis». eng. In: *Macromolecules* 45.24 (2012), pp. 9551–9570. issn: 0024-9297 (cit. on p. 21).

[36] Mastan Erlita and He Junpo. «Continuous Production of Multiblock Copolymers in a Loop Reactor: When Living Polymerization Meets Flow Chemistry». eng. In: *Macromolecules* 50.23 (2017), pp. 9173–9187. issn: 0024-9297 (cit. on p. 21).

[37] Binhong Lin, Caleb N. Jadrich, Vince E. Pane, Pedro L. Arrechea, Tim Erdmann, Charles Dausse, James L. Hedrick, Nathaniel H. Park, and Robert M. Waymouth. «Ultrafast and Controlled Ring-Opening Polymerization with Sterically Hindered Strong Bases». In: *Macromolecules* 53.20 (2020), pp. 9000–9007. doi: 10.1021/acs.macromol.0c01571. url: https://doi.org/10.1021/acs.macromol.0c01571 (cit. on pp. 21, 22).

[38] Binhong Lin, James L Hedrick, Nathaniel H Park, and Robert M Waymouth. «Programmable High-Throughput Platform for the Rapid and Scalable Synthesis of Polyester and Polycarbonate Libraries». eng. In: *Journal of the American Chemical Society* 141.22 (2019), pp. 8921–8927. issn: 0002-7863 (cit. on pp. 21–23, 31, 96, 97).

[39] Nagaki Aiichiro, Tomida Yutaka, and Yoshida Jun-ichi. «Microflow-System-Controlled Anionic Polymerization of Styrenes». eng. In: *Macromolecules* 41.17 (2008), pp. 6322–6330. issn: 0024-9297 (cit. on p. 22).

[40] Morsbach Jan, Müller Axel H. E, Berger-Nicoletti Elena, and Frey Holger. «Living Polymer Chains with Predictable Molecular Weight and Dispersity via Carbanionic Polymerization in Continuous Flow: Mixing Rate as a Key Parameter». eng. In: *Macromolecules* 49.14 (2016), pp. 5043–5050. issn: 0024-9297 (cit. on p. 22).

[41] Jedlinski Z, Kowalczuk M, and Kurcok P. «What is the real mechanism of anionic polymerization of β-lactones by potassium alkoxides? A critical approach». eng. In: *Macromolecules* 24.5 (1991), pp. 1218–1219. issn: 0024-9297 (cit. on p. 22).

[42] Jincai Wu, Te-Liang Yu, Chi-Tien Chen, and Chu-Chieh Lin. «Recent developments in main group metal complexes catalyzed/initiated polymerization of lactides and related cyclic esters». In: *Coordination Chemistry Reviews* 250 (2006), pp. 602–626. url: https://api.semanticscholar.org/CorpusID:97871299 (cit. on p. 22).

[43] Ito Koichi, Hashizuka Yutaka, and Yamashita Yuya. «Equilibrium Cyclic Oligomer Formation in the Anionic Polymerization of iϵ-Caprolactone». eng. In: *Macromolecules* 10.4 (1977), pp. 821–824. issn: 0024-9297 (cit. on p. 22).

[44] Sanda Fumio, Kamatani Jun, and Endo Takeshi. «Synthesis and Anionic Ring-Opening Polymerization Behavior of Amino Acid-Derived Cyclic Carbonates». eng. In: *Macromolecules* 34.6 (2001), pp. 1564–1569. issn: 0024-9297 (cit. on p. 22).

[45] Haba Osamu, Tomizuka Haruka, and Endo Takeshi. «Anionic Ring-Opening Polymerization of Methyl 4,6-O-Benzylidene-2 and 3-O- carbonyl-α-d-glucopyranoside¦ A First Example of Anionic Ring-Opening Polymerization of Five-Membered Cyclic Carbonate without Elimination of CO2». eng. In: *Macromolecules* 38.9 (2005), pp. 3562–3563. issn: 0024-9297 (cit. on p. 22).

[46] B.E. Rapp. *Microfluidics: Modeling, Mechanics and Mathematics*. Micro and Nano Technologies. Elsevier Science, 2022. isbn: 9780128240236. url: https://books.google.it/books?id=yaRXEAAAQBAJ (cit. on p. 24).

[47] Russum James P., Jones Christopher W., and Schork F. Joseph. «Impact of flow regime on polydispersity in tubular RAFT miniemulsion polymerization». eng. In: *AIChE journal* 52.4 (2006), pp. 1566–1576. issn: 0001-1541 (cit. on p. 24).

[48] Zhou Yang, Gu Yu, Jiang Kunming, and Chen Mao. «Droplet-Flow Photopolymerization Aided by Computer: Overcoming the Challenges of Viscosity and Facilitating the Generation of Copolymer Libraries». eng. In: *Macromolecules* 52.15 (2019), pp. 5611–5617. issn: 0024-9297 (cit. on p. 24).

[49] Stephan Klutz, Safa Kutup Kurt, Martin Lobedann, and Norbert Kockmann. «Narrow residence time distribution in tubular reactor concept for Reynolds number range of 10–100». In: *Chemical Engineering Research and Design* 95 (2015), pp. 22–33. issn: 0263-8762. doi: https://doi.org/10.1016/j.cherd.2015.

01.003. url: https://www.sciencedirect.com/science/article/pii/S0263876215000106 (cit. on p. 24).

[50] Dambarudhar Parida, Christophe A. Serra, Dhiraj K. Garg, Yannick Hoarau, Florence Bally, Rene M Muller, and Michel Bouquey. «Coil Flow Inversion as a Route To Control Polymerization in Microreactors». In: *Macromolecules* 47 (2014), pp. 3282–3287. url: https://api.semanticscholar.org/CorpusID:101082129 (cit. on p. 24).

[51] Chhotu Ram, Amit Kumar, and Pushpa Rani. «Municipal Solid Waste Management: A Review of Waste to Energy (WtE) Approaches». In: *Bioresources* 16 (Feb. 2021), pp. 1–47. doi: 10.15376/biores.16.2.Ram (cit. on p. 26).

[52] Bozell Joseph J. and Petersen Gene R. «Technology development for the production of biobased products from biorefinery carbohydrates—the US Department of Energy's 'Top 10' revisited». In: *Green Chem.* 12 (4 2010), pp. 539–554. doi: 10.1039/B922014C. url: http://dx.doi.org/10.1039/B922014C (cit. on p. 26).

[53] Jan P. Eubeler, Sabine Zok, Marco Bernhard, and Thomas P. Knepper. «Environmental biodegradation of synthetic polymers I. Test methodologies and procedures». In: *TrAC Trends in Analytical Chemistry* 28.9 (2009), pp. 1057–1072. issn: 0165-9936. doi: https://doi.org/10.1016/j.trac.2009.06.007. url: https://www.sciencedirect.com/science/article/pii/S016599360900137X (cit. on p. 26).

[54] I.C. McNeill and H.A. Leiper. «Degradation studies of some polyesters and polycarbonates—1. Polylactide: General features of the degradation under programmed heating conditions». In: *Polymer Degradation and Stability* 11.3 (1985), pp. 267–285. issn: 0141-3910. doi: https://doi.org/10.1016/0141-3910(85)90050-3. url: https://www.sciencedirect.com/science/article/pii/0141391085900503 (cit. on p. 27).

[55] I.C. McNeill and H.A. Leiper. «Degradation studies of some polyesters and polycarbonates—2. Polylactide: Degradation under isothermal conditions, thermal degradation mechanism and photolysis of the polymer». In: *Polymer Degradation and Stability* 11.4 (1985), pp. 309–326. issn: 0141-3910. doi: https://doi.org/10.1016/0141-3910(85)90035-7. url: https://www.sciencedirect.com/science/article/pii/0141391085900357 (cit. on p. 27).

[56] F.-D. Kopinke, M. Remmler, K. Mackenzie, M. Möder, and O. Wachsen. «Thermal decomposition of biodegradable polyesters—II. Poly(lactic acid)». In: *Polymer Degradation and Stability* 53.3 (1996), pp. 329–342. issn: 0141-3910. doi: https://doi.org/10.1016/0141-3910(96)00102-4. url: https://www.sciencedirect.com/science/article/pii/0141391096001024 (cit. on p. 27).

[57] Haruo Nishida, Tomokazu Mori, Shinya Hoshihara, Yujiang Fan, Yoshihito Shirai, and Takeshi Endo. «Effect of tin on poly(l-lactic acid) pyrolysis». In: *Polymer Degradation and Stability* 81.3 (2003), pp. 515–523. issn: 0141-3910. doi: https://doi.org/10.1016/S0141-3910(03)00152-6. url: https://www.sciencedirect.com/science/article/pii/S0141391003001526 (cit. on p. 27).

[58] Peter Olsén, Karin Odelius, and Ann-Christine Albertsson. «Ring-Closing Depolymerization: A Powerful Tool for Synthesizing the Allyloxy-Functionalized Six-Membered Aliphatic Carbonate Monomer 2-Allyloxymethyl-2-ethyltri- methylene Carbonate». In: *Macromolecules* 47.18 (2014), pp. 6189–6195. doi: 10.1021/ma5012304. url: https://doi.org/10.1021/ma5012304 (cit. on pp. 27, 28, 30).

[59] Bingyang Yan et al. «PLGA-PTMC-Cultured Bone Mesenchymal Stem Cell Scaffold Enhances Cartilage Regeneration in Tissue-Engineered Tracheal Transplantation». In: *Artificial Organs* 41.5 (2017), pp. 461–469. doi: 10.1111/aor.12805. url: https://doi.org/10.1111/aor.12805 (cit. on p. 75).

[60] Binhong Lin and Robert Waymouth. «Organic Ring-Opening Polymerization Catalysts: Reactivity Control by Balancing Acidity». In: *Macromolecules* 51 (2018), pp. 2932–2938. doi: 10.1021/acs.macromol.8b00540 (cit. on p. 75).

[61] Viktor Gutmann. «Solvent effects on the reactivities of organometallic compounds». In: *Coordination Chemistry Reviews* 18.2 (1976), pp. 225–255. issn: 0010-8545. doi: https://doi.org/10.1016/S0010-8545(00)82045-7. url: https://www.sciencedirect.com/science/article/pii/S0010854500820457 (cit. on p. 76).

[62] Tyler S Stukenbroeker, Jeffrey S Bandar, Xiangyi Zhang, Tristan H Lambert, and Robert M Waymouth. «Cyclopropenimine Superbases: Competitive Initiation Processes in Lactide Polymerization». eng. In: *ACS macro letters* 4.8 (2015), pp. 853–856. issn: 2161-1653 (cit. on p. 80).

[63] Daniele Battegazzore, Silvia Bocchini, and Alberto Frache. «Crystallization kinetics of poly(lactic acid)-talc composites». In: *EXPRESS Polymer Letters* 5.10 (2011), pp. 865–880 (cit. on p. 81).

[64] Hye-Seon Park and Chang-Kook Hong. «Relationship between the Stereocomplex Crystallization Behavior and Mechanical Properties of PLLA/PDLA Blends». In: *Polymers* 13.11 (2021), p. 1851. issn: 2073-4360. doi: 10.3390/polym13111851. url: https://doi.org/10.3390/polym13111851 (cit. on p. 81).

[65] Tsao Yi-Yun Timothy and Wooley Karen L. «Correction to "Synthetic, Functional Thymidine-Derived Polydeoxyribonucleotide Analogues from a Six-Membered Cyclic Phosphoester"». eng. In: *Journal of the American Chemical Society* 140.11 (2018), pp. 4182–4184. issn: 0002-7863 (cit. on p. 82).

[66] Michael E. Jung and Grazia Piizzi. «gem-Disubstituent Effect: Theoretical Basis and Synthetic Applications». In: *Chemical Reviews* 105.5 (2005), pp. 1735–1766. issn: 0009-2665. doi: 10.1021/cr940337h. url: https://doi.org/10.1021/cr940337h (cit. on p. 83).

[67] Tien-Yau Luh, Chih-Hsien Chen, and Guo-Qiao Lai. «Thorpe-Ingold Effect on Polymer Conformations. Photophysical Behavior as a Probe for Folding of Alt-Dialkylsilylene-divinylarene Copolymers». In: *Bulletin of the Chemical Society of Japan* 94.2 (2020), pp. 490–501. issn: 0009-2673. doi: 10.1246/bcsj.20200289. url: https://doi.org/10.1246/bcsj.20200289 (cit. on p. 83).

[68] Jyuhou Matsuo, Kazutaka Aoki, Fumio Sanda, and Takeshi Endo. «Substituent Effect on the Anionic Equilibrium Polymerization of Six-Membered Cyclic Carbonates». In: *Macromolecules* 31.14 (1998), pp. 4432–4438. doi: 10.1002/(SICI)1521-3935(19981101)199:11<2489::AID-MACP2489>3.0.CO;2-V (cit. on pp. 83, 91, 92).

[69] Jiaxi Xu and Nikos Hadjichristidis. «Heteroatom-containing degradable polymers by ring-opening metathesis polymerization». In: *Progress in Polymer Science* 139 (2023), p. 101656. doi: https://doi.org/10.1016/j.progpolymsci.2023.101656. url: https://www.sciencedirect.com/science/article/pii/S0079670023000114 (cit. on p. 85).

[70] Krzysztof Górski, Krzysztof Noworyta, and Justyna Mech-Piskorz. «Influence of the heteroatom introduction on the physicochemical properties of 5-heterotruxenes

containing nitrogen, oxygen and sulfur atom». In: *RSC Adv.* 10.69 (2020), pp. 42363–42377. doi: 10.1039/D0RA07483G. url: http://dx.doi.org/10.1039/D0RA07483G (cit. on p. 85).

[71] Yi-Min Tu, Fu-Long Gong, Yan-Chen Wu, Zhongzheng Cai, and Jian-Bo Zhu. «Insights into substitution strategy towards thermodynamic and property regulation of chemically recyclable polymers». In: *Nature Communications* 14.1 (2023), p. 3198. doi: 10.1038/s41467-023-38916-5. url: https://doi.org/10.1038/s41467-023-38916-5 (cit. on p. 85).

[72] Yves Martelé, Veronique Van Speybroeck, Michel Waroquier, and Etienne Schacht. «Thermodegradable polycarbonates: Effect of substituents on the degradation temperature». In: *e-Polymers* 2.1 (2002), p. 048. doi: 10.1515/epoly.2002.2.1.701. url: https://doi.org/10.1515/epoly.2002.2.1.701 (cit. on pp. 85, 86).

[73] M. Gracia García-Martín, Rocío Ruiz Pérez, Elena Benito Hernández, José Luis Espartero, Sebastián Muñoz-Guerra, and Juan A. Galbis. «Carbohydrate-Based Polycarbonates. Synthesis, Structure, and Biodegradation Studies». In: *Macromolecules* 38.21 (2005), pp. 8664–8670. issn: 0024-9297. doi: 10.1021/ma050676k. url: https://doi.org/10.1021/ma050676k (cit. on p. 86).

[74] Elena Díaz-Celorio, Lourdes Franco, Yolanda Márquez, Alfonso Rodríguez-Galán, and Jordi Puiggalí. «Thermal degradation studies on homopolymers and copolymers based on trimethylene carbonate and glycolide units». In: *Thermochimica Acta* 528 (2012), pp. 23–31. issn: 0040-6031. doi: https://doi.org/10.1016/j.tca.2011.11.006. url: https://www.sciencedirect.com/science/article/pii/S004060311100548X (cit. on p. 86).

[75] K. Pielichowski, J. Njuguna, and Rapra Technology Limited. *Thermal Degradation of Polymeric Materials*. Rapra Technology, 2005. isbn: 9781859574980. url: https://books.google.it/books?id=bo8MVDXVy9kC (cit. on pp. 86, 88).

[76] Jose James, Pramoda Kumari. Pallathadka, and Sabu. Thomas. *Polymers and multicomponent polymeric systems: thermal, thermo-mechanical and dielectric analysis*. eng. 1st ed. Boca Raton, FL: CRC Press, 2020. isbn: 0-429-94346-6 (cit. on p. 86).

[77] Fatih Biryan and Kadir Demirelli. «Characterization, thermal behavior, and electrical measurements of poly[4-(2-bromoisobutyroyl methyl)styrene]». eng. In: *Advances in polymer technology* 37.6 (2018), pp. 1994–2012. issn: 0730-6679 (cit. on p. 86).

[78] Gülbanu Koyundereli Çılgı and Metin Ak. «Thermal degradation kinetics and thermodynamics of maleimide-sytrene based alternating copolymer: A comparative investigation of monomer and polymer structures». In: *Journal of Molecular Structure* 1221 (2020), p. 128879. issn: 0022-2860. doi: https://doi.org/10.1016/j.molstruc.2020.128879. url: https://www.sciencedirect.com/science/article/pii/S0022286020312047 (cit. on pp. 88, 89).

[79] Rikyu Miyake and Hiroharu Ajiro. «Investigation of the mechanical properties and degradation of ester-free poly(trimethylene carbonate) derivatives bearing various bulky aromatic groups». In: *Polymer Journal* 56.4 (2024), pp. 319–333. doi: 10.1038/s41428-023-00848-8. url: https://doi.org/10.1038/s41428-023-00848-8 (cit. on p. 90).

[80] Wei Liu, Wenxiang Zhu, Chuncheng Li, Guohu Guan, Dong Zhang, Yaonan Xiao, and Liuchun Zheng. «Thermal degradation mechanism of poly(hexamethylene carbonate)». In: *Polymer Degradation and Stability* 112 (2015), pp. 70–77. issn: 0141-3910. doi: https://doi.org/10.1016/j.polymdegradstab.2014.12.013. url: https://www.sciencedirect.com/science/article/pii/S0141391014004467 (cit. on pp. 90, 92).

[81] Giancarlo Sidoti, Silvia Capelli, Stefano V. Meille, and Giovanni C. Alfonso. «The polymorphic behaviour of poly(2,2-dimethyltrimethylenecarbonate) and of its cyclic monomer. Evidence for a high entropy, conformationally disordered modification». In: *Polymer* 39.1 (1998), pp. 165–172. issn: 0032-3861. doi: https://doi.org/10.1016/S0032-3861(97)00224-3. url: https://www.sciencedirect.com/science/article/pii/S0032386197002243 (cit. on p. 91).

[82] Zhipeng Hou, Siwen Chen, Zhongcun Li, Zhangpei Chen, Jianshe Hu, Jing Guo, Peng Li, and Liqun Yang. «Controllable Degradation of Poly (trimethylene carbonate) via Self-blending with Different Molecular Weights». In: *Polymer Degradation and Stability* 189 (2021), p. 109596. issn: 0141-3910. doi: https://doi.org/10.1016/j.polymdegradstab.2021.109596. url: https://www.sciencedirect.com/science/article/pii/S0141391021001166 (cit. on p. 92).

[83] Roya Mir and Travis Dudding. «Phase-Transfer Catalyzed O-Silyl Ether Deprotection Mediated by a Cyclopropenium Cation». eng ; jpn. In: *Journal of organic chemistry* 82.1 (2017), pp. 709–714. issn: 0022-3263 (cit. on p. 93).

[84] Chahinez Aouf, Sofia Benyahya, Antoine Esnouf, Sylvain Caillol, Bernard Boutevin, and Hélène Fulcrand. «Tara tannins as phenolic precursors of thermosetting epoxy resins». eng. In: *European polymer journal* 55 (2014), pp. 186–198. issn: 0014-3057 (cit. on p. 94).

[85] Gaukhar K. Bishimbayeva, Nina K. Gusarova, Arailym M. Nalibayeva, Svetlana I. Verkhoturova, Amangul Bold, Natalya A. Chernysheva, Assem K. Zhangabayeva, Svetlana N. Arbuzova, Yerlan N. Abdikalykov, and Dinara S. Zhumabayeva. «Synthesis and Properties of Sulfur-Containing Organophosphorus Extractants Based on Red Phosphorus, Alkyl Bromides, and Elemental Sulfur». In: *Materials* 16.9 (2023). issn: 1996-1944. url: https://www.mdpi.com/1996-1944/16/9/3394 (cit. on p. 94).